# EFFECTIVENESS OF PRIMECAST® AND POLY (METHYL METHACRYLATE) ADDITIVE MANUFACTURING PROCESSES TO PRODUCE PATTERNS FOR INVESTMENT CASTING

**NTHATENG PATRICIA NKHASI**

Dissertation submitted in fulfilment of the requirements for the degree

**MASTER OF ENGINEERING IN MECHANICAL ENGINEERING**

in the

Department of Mechanical and Mechatronics Engineering
Faculty of Engineering and Information Technology

at

Central University of Technology, Free State

Supervisor: Prof Willie du Preez
Co-supervisor: Dr Kobus van der Walt

BLOEMFONTEIN
2018

# Declaration

I, **Nthateng Patricia Nkhasi**, passport number and student number , do hereby declare that this research project submitted to Central University of Technology, Free State for the Degree of **Master of Engineering in Mechanical Engineering** is my own independent work. This work complies with the code of Academic Integrity, as well as other relevant policies, procedures, rules and regulations of Central University of Technology, Free State; and has not been submitted before to any institution by myself or any other person for the attainment of a qualification.

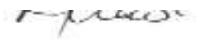

18 October 2018

Nthateng Patricia Nkhasi — Date

# Acknowledgements

I would like to offer my special thanks to the following people or organizations:

1. Prof Willie du Preez and Dr Kobus van der Walt; they inspired me with the concept and guided me to the completion of this research dissertation.
2. Pierre Rossouw; Senior Researcher at CSIR, Materials Science and Manufacturing, who is an expert in investment casting.
3. South African Department of Science and Technology is gratefully acknowledged for their financial support through the Collaborative Program in Additive Manufacturing (Contract № CSIR-NLC-CPAM-15-MOA-CUT-01).
4. The Centre for Rapid Prototyping and Manufacturing (CRPM) is also acknowledged for facilitating in redesigning of the PrimeCast® pattern.

Thank you all.

# Dedication

This dissertation is dedicated to my son, Emmanuel Nkhasi, and my fiancé, Pule Mohlouoa, for their support and encouragement during the study of this project.

My God, thank you for providing me with the strength and determination in the completion of this study.

# Abstract

Investment casting is known as a “near net shape” process as it can produce parts that need very little secondary machining operations. The investment casting process is one of several metal casting processes and it has an advantage in that very complex designs can be produced with good accuracy and surface finish. The investment casting process begins with the fabrication of a sacrificial pattern, typically made of foundry wax, with the same basic geometrical shape as the finished cast part. Normally, the sacrificial wax patterns are produced by injection moulding where hot wax is injected into the desired patterns. Runner and gates systems are assembled and attached onto the completed fabricated wax patterns. Next, the wax patterns with runners and gates are repeatedly dipped into a ceramic slurry, with a drying period in between dipping, to form layers that create a shell. Investment casting sacrifices a pattern and ceramic shell mould for each metal part that is made. The investment casting process suffers long lead times when a new part is designed, due to the fabrication of initial tooling. Cost and lead-time to produce tooling can be prohibitively high and complexity is limited by what is possible with injection moulding in the chosen time. These factors have lead investment casting foundries as well as the companies purchasing the castings to explore alternate methods to create investment cast parts without the cost and time burden associated with permanent tooling.

Additive manufacturing patterns provides an alternative method for producing investment casting patterns that can provide dramatic time and cost savings. It also gives the designers freedom to rapidly modify and redesign a product without significant increase in the total development time and cost. Nowadays, the foundries are able to play around with different designs, test them, and reach the optimum design very quickly. It is relatively expensive and time-consuming to do this using conventional investment casting. Furthermore, by using additive manufacturing, patterns can be made as complex as needed without any impact on the cost. This study determined the difference in dimensional accuracy between PrimeCast® and PMMA patterns produced for

investment casting by two different additive manufacturing technologies as well as their corresponding castings.

PrimeCast® and PMMA patterns were built at the same time at Central University of Technology, Free State and Vaal University of Technology, respectively. Metrology was performed on all patterns just after manufacturing using a micro-computed X-ray tomography scanner to compare dimensional accuracies of different features of the patterns. Aluminium alloy A356 was cast in the moulds made from both types of patterns. Similar metrology was performed on all the castings to compare dimensional accuracies of different features of the castings from the two types of patterns. The patterns had features such as thin walls, cavities and angles that pose challenges to these additive manufacturing technologies and the investment casting process.

From the results of this study, it was found that both technologies provided good dimensional results on simpler shapes. The PrimeCast® pattern had a better dimensional accuracy than the PMMA pattern. However, the casting from the PMMA pattern had relatively better dimensional accuracy than the casting from the PrimeCast® pattern.

# Table of Contents

# List of Figures

# List of Tables

# List of acronyms and abbreviations

| | |
|---|---|
| 2D | Two-Dimensional |
| 3D | Three-Dimensional |
| 3DP | Three-Dimensional Printing |
| AM | Additive Manufacturing |
| ASTM | American Society for Testing and Materials |
| BJ | Binder Jetting |
| CAD | Computer Aided Design |
| CMM | Coordinate Measuring Machine |
| CRPM | Centre for Rapid Prototyping and Manufacturing |
| CSIR | Council for Scientific and Industrial Research |
| CT | Computed Tomography |
| CUT | Central University of Technology, Free State |
| DLP | Digital Light Processing |
| DMLS | Direct Metal Laser Sintering |
| EBM | Electron Beam Melting |
| EDM | Electrical Discharge Machining |
| EOS | Electro Optical Systems GmbH |
| FDM | Fused Deposition Modelling |
| IC | Investment Casting |
| LMD | Multi-jet modelling (MJM) |
| LOM | Laminated Object Manufacturing |
| LS | Laser Sintering |
| MIT | Massachusetts Institute of Technology |
| MJM | Multi-Jet Modelling |
| PBIH | Powder Bed And Inkjet Heat |
| PC1 | Casting from PrimeCast® pattern 1 |
| PC2 | Casting from PrimeCast® pattern 2 |
| PMMA | Poly(methyl methacrylate) |
| PMMA1 | Casting from Poly(methyl methacrylate) pattern 1 |
| PMMA2 | Casting from Poly(methyl methacrylate) pattern 2 |
| PP | Plaster-based 3D Printing (PP) |

| | |
|---|---|
| RIC | Rapid Investment Casting |
| SHS | Selective Heat Sintering |
| SLA | Stereolithography |
| SLS | Selective Laser Sintering |
| STL | Standard Tessellation Language |
| UC | Ultrasonic Consolidation |
| USA | United States of America |
| VUT | Vaal University of Technology |

# Publications Emanating from this Research

1. **Nkhasi, N., du Preez, W. & van der Walt, J.G.** "Effectiveness of PrimeCast® and PMMA additive manufacturing processes to produce patterns for investment casting," *Proceedings of the* 18*th Annual RAPDASA International Conference*, ISBN Number 978-0-620-77329-4, Durban ICC, 07–10 November 2017*,* pp. 62–64, 2017.

2. **Nkhasi, N., du Preez, W. & van der Walt, J.G.** "Investment casting of Aluminium alloy A356 using Primecast® and PMMA additive manufacturing materials for sacrificial patterns," *Proceedings of the* 19*th Annual RAPDASA International Conference*, ISBN Number 978-0-620-80987-0, University of Johannesburg and Resolution Circle, 06–09 November 2018, pp 22-31,2018.

# Chapter 1: Introduction

## 1.1 Background

Producing a near-net shape product by pouring metal into a mould is a manufacturing process that can be traced back thousands of years [1]. When more complex designs were required, the process was altered slightly by building moulds using a wax model that could be burned out before the metal was poured into the mould; the process is known as investment casting (IC) or lost-wax casting [2]. With time, as the designs became even more complex, the cost associated with IC rose and the lead times increased. A short run of IC using traditional manufacturing methods can raise the production costs to near unacceptable levels. Production of the wax patterns requires expensive injection-moulding tools and wax presses. When used in short runs the tooling costs can be extremely expensive and time consuming. Additive manufacturing offers a faster, less expensive alternative to creating IC moulds [3].

Worldwide, additive-layer manufacturing, now formally known as additive manufacturing (AM) and popularly called three-dimensional printing (3DP), is a technology that is rapidly growing in usefulness and capability, and South Africa is no exception [4]. Back in the 1980s, this technology was originally known as rapid prototyping [5], a process by which components are produced directly from computer models by selectively curing, depositing or joining materials in successive layers. These technologies have traditionally been limited to the manufacture of models suitable for product conception but, over the past decade, have quickly developed into a new standard called AM. The main advantage of this process is its ability to create almost any possible shape, which is made possible by layer-upon-layer manufacturing [6]. Among the major advances that are presented by this process in product development is time and cost reduction. Moving from one technology to another in the production process, the manufacturing direction, the model

orientation and material behaviour are important to get an accurate model and efficient production [7].

The use of AM parts as sacrificial patterns for IC is generally referred to as rapid investment casting (RIC) [8]. Most AM technologies can produce patterns directly with polymers that have the same ability as wax patterns used for the IC process. Designers can transfer the 3D CAD data to casting very easily and efficiently when merging IC with AM patterns [3]. RIC could dramatically reduce the lead-time and production cost and give the designers freedom to rapidly modify and redesign a product without a significant increase in the total development time and cost. The use of AM patterns is only applicable to low-production- and process-development applications [9], when only a few patterns of parts are required for testing and to ensure that the design is correct before making larger investment in a wax pattern tooling.

From literature it was found that there has been significant work done on poly(methyl methacrylate) (PMMA) [10], [11], [12], [13] and PrimeCast® [3], [9], [14], [15] trying to show that they can be used to replace the lost-wax process in IC. While the Council for Scientific and Industrial Research (CSIR) and Vaal University of Technology (VUT) have done work on PMMA, this has not been published.

## 1.2 Problem statement

IC is known as a “near-net shape” process because it can produce parts that need very little secondary machining operations. Parts produced using IC display a high degree of accuracy and precise dimensions. They may have very complex geometries and high quality surface finish and detail in the final components. These parts are often used for aerospace, automotive industries and military applications. Nowadays the world is moving from the conventional method of IC to using AM patterns for IC especially on the development stage; hence, the need for this study. However, there are many different AM technologies using different materials. The two AM technologies (laser sintering and binder jetting) used in this study are available in South Africa and there was no research found on direct comparisons between PrimeCast®

and PMMA for use as sacrificial patterns for IC. Comparison of the two types of AM patterns will provide information on the advantages and limitations of these two types of patterns which should enable the foundry industry to select the most appropriate technology for their IC needs.

## 1.3 Aim of study

The aim of this research was to investigate the advantages and limitations of two different AM technologies, each using a specific AM material, to produce sacrificial patterns for IC and to compare the dimensional accuracy of both sacrificial patterns and resulting castings.

## 1.4 Objectives

- To produce sacrificial patterns for IC in PrimeCast® and PMMA AM materials from the computer-aided design (CAD) of an internationally recognised test part.
- To use these patterns for casting the test part in A356 aluminium alloy.
- To determine the deviations from the CAD model of the castings produced from these two AM technologies.
- To determine and document the advantages and limitations of using PrimeCast® and PMMA patterns produced by AM for IC.

## 1.5 Delineations and limitations

The focus of this study is on the determination of the difference in dimensional accuracy of the two AM technologies used to generate IC patterns as determined through micro-computed X-ray tomography (micro-CT). Observations regarding the surface roughness of the IC patterns were based on the results of this technique as well as visual observations.

The manufacturing lead times for producing the two types of patterns were not compared in this study as both manufacturing processes are automated and the patterns can be built overnight. Therefore, the delivery time is merely dependent on the efficiency of the service provider.

## 1.6 Research approach

An IC sacrificial pattern geometry that could be built in both PMMA and PrimeCast® was selected and built in both AM materials through the two types of AM technology. The IC patterns that were built in PrimeCast® were manufactured using an Electro Optical Systems (EOS) AM machine at Central University of Technology (CUT), while those that were built in PMMA were manufactured at VUT using Voxeljet 3D printing technology. Immediately after manufacturing the patterns, micro-CT metrology was performed on two of the patterns, one from each AM material to compare its correlation with the CAD design. Subsequently, the same mould-making, burnout and casting processes were executed on patterns from both AM materials. The micro-CT metrology was also performed on the castings based on the two types of patterns to compare different features of these castings.

The standard part used had features such as cubes, rectangular protrusion, pyramid, half-sphere, cone, freeform (conical and sinkhole), wedges, rectangular hole, hollow cylinder, triangular hole, flat thin walls and a square base that pose challenges to these AM technologies.

## 1.7 Layout of the dissertation

The layout of the dissertation is presented schematically in Figure 1.1.

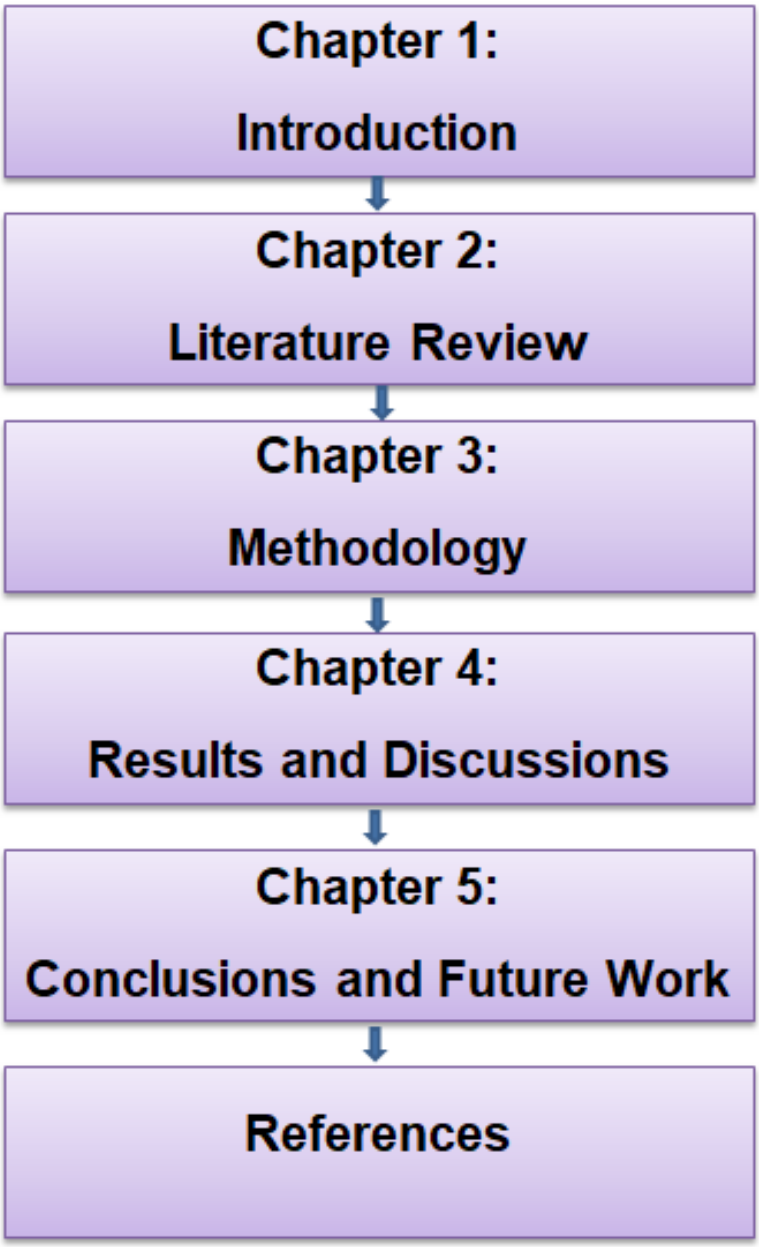


**Figure 1.1. Layout of the dissertation**

# Chapter 2: Literature Review

## 2.1 Introduction

This chapter describes the study of the existing knowledge in the field and discusses what other authors have discovered in their research on related topics. The flow diagram in Figure 2.1 summarises the highlights of this chapter.

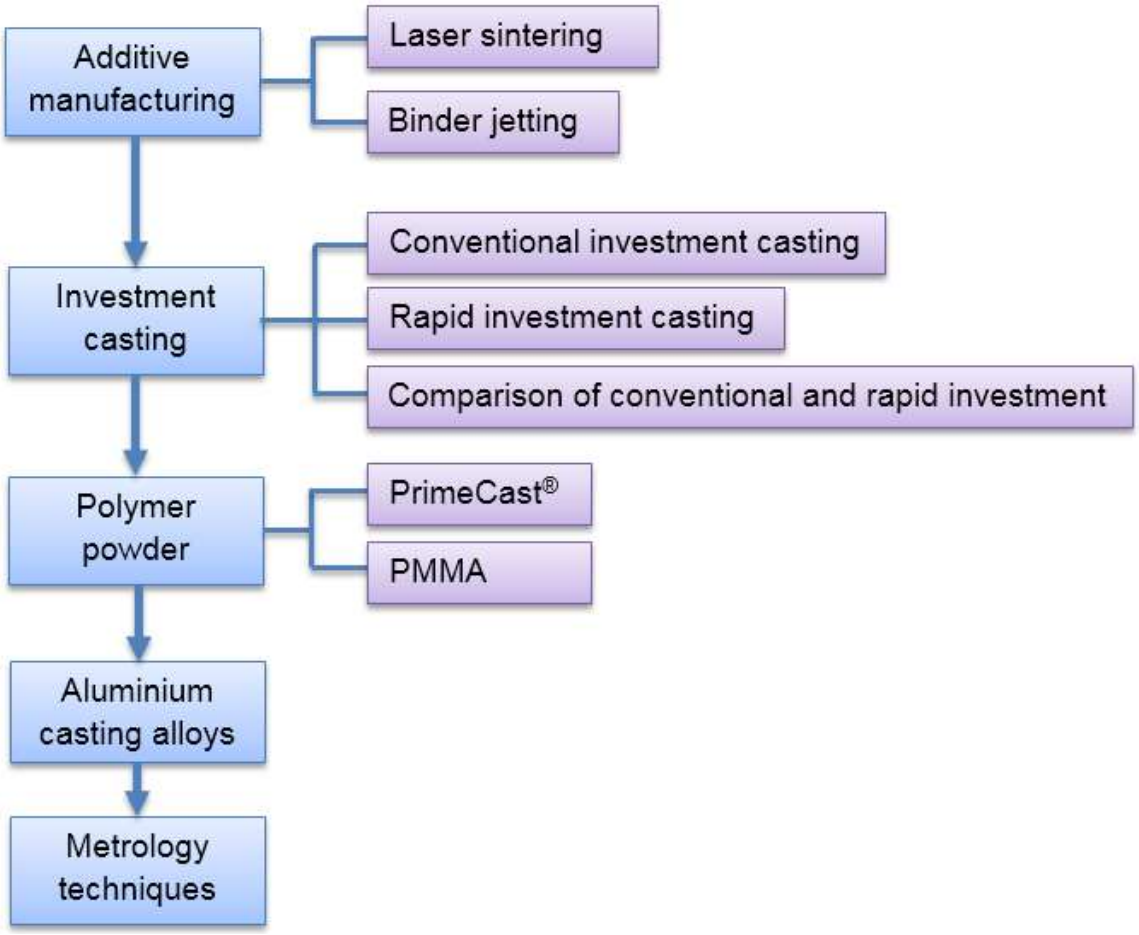


**Figure 2.1. Flow diagram of chapter 2**

## 2.2 Additive manufacturing

AM has been defined as “a process of joining materials to make objects from 3D model data, usually layer upon layer, as opposed to subtractive manufacturing methodologies” by the American Society for Testing and Materials (ASTM) [16]. The traditional metal removal processes, such as milling, turning, grinding and electrical discharge machining (EDM), are examples of subtractive manufacturing. AM is the opposite of subtractive

manufacturing approaches that remove material to form the shape of a work piece, since it only deposits material where needed. AM is more accurate in that it describes a professional production technique which is clearly distinguishable from conventional methods of material forming or removal. AM manufactures components directly from 3D computer models by selectively depositing, curing or fusing materials one layer upon the next. Each layer represents a cross-sectional geometry of the component at a given height [17].

The demand of AM machines has been increasingly growing since the 1990s [18]. We are now beginning to see AM used for the construction of a range of functional end-use components [4]. In the aerospace industry, components often have complex geometries and are usually made from advanced materials that are difficult, costly and time-consuming to manufacture. Some of these components can be more easily manufactured through AM technologies. AM is transforming the medical sector, as now it is possible to have a precise model of skeletal features of a patient before surgery and an accurate implant can be created prior to the operation. The automotive industry is now using AM technologies in design and development of automotive components as it can shorten the development cycle and reduce manufacturing and product costs. AM is easing the work of architects by enabling then to print 3D models of any complex shape for civil projects. Although extensive research and development continues to be done and needs to be done, the technology is now being used for commercial manufacturing purposes, although still only in certain niches [7].

In South Africa, the Department of Science and Technology commissioned the development of a roadmap for AM in this country. This involved a survey of the capabilities already existing in South Africa and of the active participants in the sector [4]. The aim was to identify niches the country could exploit and make a difference, and which would benefit from investment [19]. It soon became clear that the production of qualified parts for the aerospace and medical industries had to be focus areas, as should the use of AM to support the traditional manufacturing sector, particularly with regard to tooling

and refurbishment [20]. The outcome of the road mapping process was the publication of the South African Additive Manufacturing Strategy.

AM processes have shown significant potential for innovative, rapid, concept-to-part competence for making high-value, complex and individually customized parts. In addition, by using AM technology parts can be produced that are difficult or impossible to manufacture with conventional manufacturing techniques. AM technologies give the industry new design flexibility, reduce energy use and shorten time to market [21]. Furthermore, AM techniques are also increasingly becoming standard tools in product design and manufacturing. With revolutionary capabilities to rapidly fabricate 3D parts for design verification or to serve as functional prototypes and short-run production tooling, AM has become an essential tool for shortening product design and development time cycles [7].

Figure 2.2 shows a simple process sequence for producing an AM part.


**Figure 2.2. Typical AM process chain, adapted from** [6]

The process begins with the designing of a 3D model in CAD software. Thereafter, the CAD model is converted to standard tessellation language (STL) file format. This file is processed by AM technology specific software, and the AM system computer then slices the STL files into cross-sectional two-dimensional (2D) layers of a specified thickness [17]. The slicing process introduces inaccuracy to the file because the algorithm replaces the continuous contour with discrete stair steps. The AM machine then fabricates the part by adding the 2D cross-sections layer upon layer and repeating the layer building until the full 3D part is produced. After fabricating the part, it is post-processed. This includes cleaning, hardening and finishing the model and removing supporting structures, if any [22]. The whole build process is fully automated in the AM machine. The build time of the part is estimated by the machine based on the height of the build from the building platform. To minimize the build time, the part should be oriented in a way that the height from the building platform is minimized [23].

The process categories provided by ASTM International in the ASTM F2792 standard [16] allows for the discussion of a category of the technology without having to explain the wide list of commercial machine variations of a particular AM process. Each process category has distinct operating principles, production characteristics, and compatible material types. These characteristics affect the cost, quality and sometimes the colour and scale of parts that can be produced, and therefore can considerably influence design decisions. The categories, as defined in ASTM F2792-12a, are as follows;

**Table 2.1. AM process categories by ASTM F2792-12a** [16]**.**

| ***Process type*** | ***Description*** | ***Related technologies*** | ***Companies*** | ***Materials*** |
|---|---|---|---|---|
| Powder bed fusion | Thermal energy selectively fuses regions of powder bed | Electron beam melting (EBM), selective laser sintering (SLS), selective heat sintering (SHS), and | EOS (Germany), 3D Systems (US), Arcam (Sweden) | Metals, polymers |

| | | | | |
|---|---|---|---|---|
| | | direct metal laser sintering (DMLS) | | |
| Direct Energy Deposition | Focused thermal energy is used to fuse materials by melting as they are being deposited | Laser metal deposition (LMD) | Optomec (US), POM (US) | Metals |
| Material Extrusion | Material is selectively dispensed through a nozzle or orifice | Fused deposition modelling (FDM) | Stratasys (Israel), Bits from Bytes (UK) | Polymers |
| Vat photopoly-merization | Liquid photopolymer in a vat is selectively cured by light-activated polymerization | Stereolithography (SLA), Digital light processing (DLP) | 3D Systems (US), Envisiontec (Germany) | Photo-polymers |
| Binder jetting | A liquid bonding agent is selectively deposited to join powder materials | Powder bed and inkjet heat (PBIH), plaster-based 3D printing (PP) | 3D Systems (US), ExOne (US) | Polymers, foundry sand, metals |
| Material jetting | Droplets of build material are selectively deposited | Multi-jet modelling (MJM) | Object (Israel), 3D Systems (US) | Polymers, waxes |
| Sheet lamination | Sheets of material are bonded to form an object | Laminated object manufacturing (LOM), ultrasonic consolidation (UC) | Fabrisonic (US), Mcor (Ireland) | Paper, metals |

The AM process categories that this study focused on are powder bed fusion, (namely laser sintering (LS)) and binder jetting (BJ).

**Benefits of AM technologies over subtractive manufacturing methodologies** [7]**,** [12]**,** [24]**.**

- Lower energy consumption: AM eliminates production steps, uses substantially less material, allows reuse of by-product, and produces lighter products.
- Less waste: The object is built up layer by layer instead of subtractive processes that cut away material.
- Reduced production time: Once the design is completed, the manufacturing process can start without the need for expensive and time-consuming part tooling.
- Innovation: The objects that were previously difficult or even impossible to manufacture can now be fabricated using AM technology. Geometries enabled by AM technologies can lead to performance and environmental benefits in a component's product applications.
- Part consolidation: AM can build a part as a whole, thus reducing the number of parts in an assembly. This cuts the overhead cost associated with documentation and production planning and control.
- Lightweight parts: Elimination of tooling and ability to produce complex shapes. AM allows the production of parts that have the same functional specifications as the conventional parts, but with reduced weight.

**Technical challenges of AM technologies** [11]**,** [25]**,** [26]**.**

- Process control: Feedback control systems and metrics are needed to improve the precision and reliability of the manufacturing process and to increase throughput, while maintaining consistent quality.
- Tolerances: Some potential applications would require micrometer-scale accuracy in printing.
- Finish: The surface finishes of products manufactured using additive technology require further refinement. With improved geometric accuracy, finishes may impart corrosion and wear resistance or unique sets of desired properties.
- Validation and demonstration: Manufacturers, standards' organizations, and others maintain high standards for critical structural materials, such as

those used in aerospace applications. Providing a high level of confidence in the structural integrity of components built with AM technology may require extensive testing, demonstration, and data collection.

- Conventional manufacturing bias: Industry designers know the traditional manufacturing methods and use them at a high level, so learning a new system faces resistance. Additionally, many parts are optimized for conventional manufacturing and facilities would need to slow down production while installing AM systems.

### 2.2.1 Laser sintering

LS is a typical AM process based on the layer-by-layer powder spreading and successive laser sintering. Dr. Carl Robert Deckard invented the process in 1988 [5] and the major commercial manufacturers of LS equipment include 3D Systems and EOS [27]. Main advantages of this process are the ability to use a variety of materials; a number of polymer materials rendered into a powder form of appropriate size and morphology can be used, and the fact that unused powder can be largely recycled. The LS process does not require support structures because the part being fabricated is surrounded by unsintered powder [28]. The disadvantages are that the accuracy is limited by the size of the material particles, oxidation needs to be avoided by executing the process in an inert gas atmosphere and the process must occur at a constant temperature near the melting point [29]. The LS system normally consists of a laser, an automatic powder layering apparatus, a computer system for process control and some accessorial mechanisms, such as an inert gas protection system and a powder- bed preheating system, as shown in the schematic diagram in Figure 2.3.

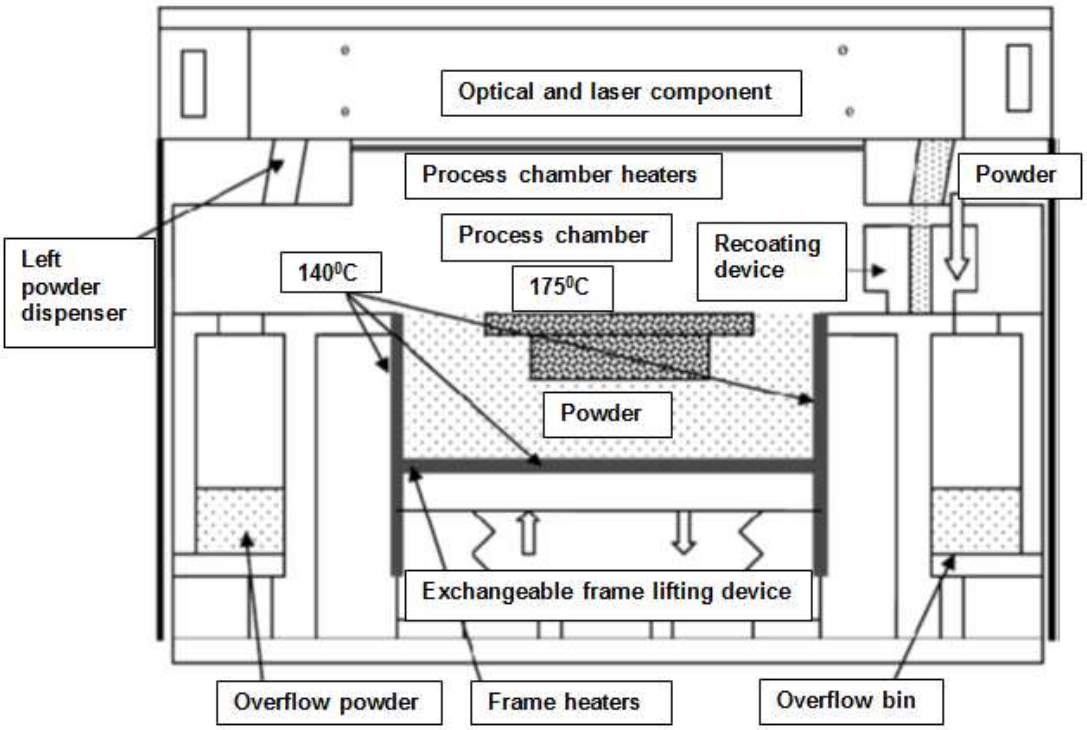


**Figure 2.3. Schematic diagram of the EOS P700 system** [30]

In the LS process, a bed of polymeric powder particles is preheated by the process chamber heaters to close to the melting transition and above the temperature necessary for recrystallization during cooling. The preheated powder limits the energy input necessary from the laser to cause sintering, which avoids large thermal differentials that would otherwise result in part distortion [31].

The general LS operational procedures are as follows;

- First, a new layer powder is spread to cover the platform. The process chamber heater is used to preheat the bed of polymeric particles to close to the melting transition and above the temperature necessary for recrystallization during the cooling cycle.
- The protective inert gas is fed into the sealed building chamber to reduce the interior oxygen content to below a required percentage to avoid the risk of explosion when handling large amounts of powder.
- A layer of the loose powder with the required thickness is deposited onto the previous layer by the recoating device.

- The laser beam scans the powder layer and sinters the powder together according to the CAD data of the components to be built. At the same time, the new layer is joined to the layer below it.
- When the sintering of the cross-section is complete, the platform moves down a distance equal to the layer thickness in preparation for the next powder deposition from the recoating device.
- The above procedures, including powder spreading and laser treatment, are repeated and the components are built in a layer-by-layer manner until completion [8], [30].

The whole process is carried out in a sealed building chamber, filled with nitrogen protective gas, which minimises the oxidation and degradation of the powder during processing, and the temperature is kept just below the melting point of the powder. Once the manufacturing is completed, the entire building chamber is cooled slowly to maximize material crystallization to provide added strength, reduce stress development and improve dimensional accuracy [12], [32]. After the parts are removed from the powder bed, the unsintered powder is cleaned off the parts and the required finishing operations are performed. This process creates fully functional parts as well as high quality patterns for many end uses. Parts with excellent surface quality are produced without support structures, thereby avoiding time-consuming tasks such as the generation, assembly and removal of supports. Several parts can be built in one job and one can add new parts during the building process [33].

### 2.2.2 Binder jetting

BJ was first developed at Massachusetts Institute of Technology (MIT), USA, during the early 1990s [34]. This technology can create parts of any geometry with materials such as ceramics, polymers and composites. In BJ, two materials are used, namely powder-based material and a binder. The binder acts as an adhesive between powder particles and layers. The binder is usually in liquid form and the build material in powder form [35]. The binder only connects the exposed particles together, through either a solvent welding or chemical reaction, with no thermal processing necessary and building efficiency is improved since no cooling cycle is involved [36]. The unbound

powder supports the printed part so that complicated freeform parts with undercuts can be manufactured without support structures, as shown in Figure 2.4 below. In order to allow effective binding between successive layers, each layer must be kept to the minimum thickness. The final parts have significant porosity, which may require infusion of a reactive resin or wax to provide suitable surface finish and strength [32]. The main advantage of this technique is the use of various materials and an ambient processing environment.

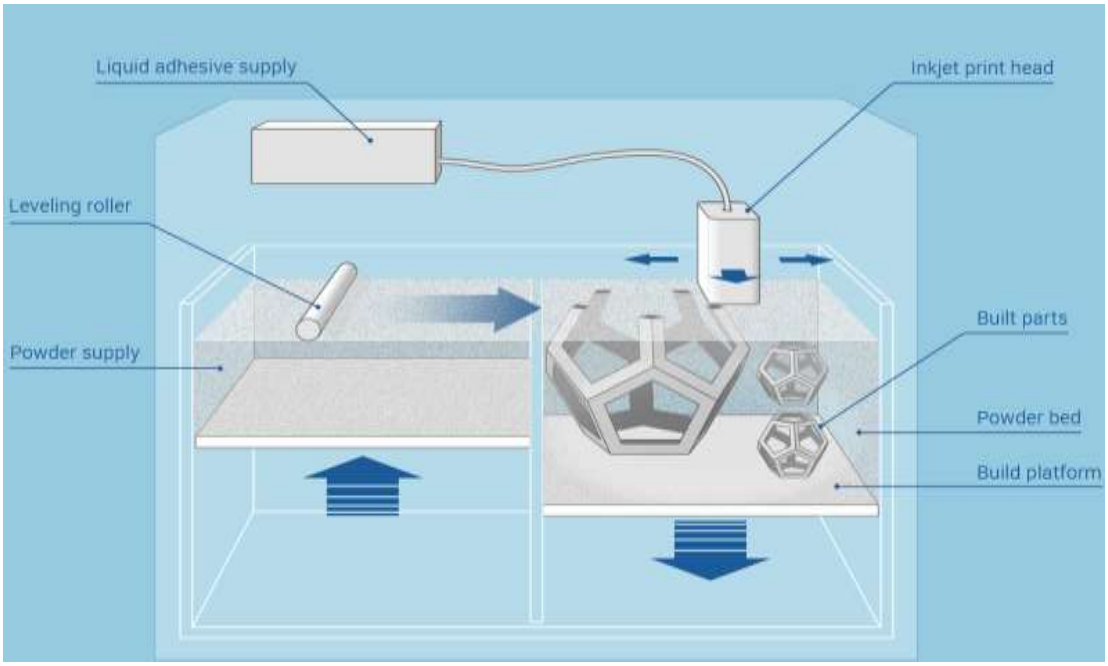


**Figure 2.4. Schematic diagram of a binder jetting machine** [37]

BJ – Step by step [24], [38]:

- Powder material is spread over the build platform using a levelling roller.
- A liquid bonding agent is applied through inkjet print heads selectively joining particles together where the object is to be formed.
- The build platform that supports the powder bed and object-in-progress is lowered by a distance corresponding to the layer thickness of the sliced CAD model.
- Another layer of powder is spread over the previous layer. The formation of the part occurs where the liquid binds the powder.

- Unbound powder remains in position surrounding the object and acts as support.
- The process is repeated until the entire part is built in the power bed.

The dimensional accuracy and quality of the final part depend on particle size of the powder, viscosity of the binder, interaction between binder and powder and the speed of the binder deposition [39]. Even for large 3D models, the accuracy is still maintained because there is no danger of heat distortion as the printing process takes place at room temperature. In plastic processes, the unprinted material is recyclable [37].

## 2.3 Investment casting

IC typically makes use of mobile slurry to form a hard shell with a highly smooth surface [40]. Unlike other casting processes, IC produces near-net shape parts with excellent surface finish and dimensional accuracy. IC converts an expendable pattern into a solid metal part following a multiple-steps process. The process uses expendable patterns and ceramic shells. In shell making, the first coat is important for surface quality and heat transfer properties in this process. Therefore, this coat should be of uniform thickness in all intricacies of the pattern. Intricate parts that are difficult, if not impossible to machine or forge, can be manufactured using the IC process [41]. However, it must be noted that when a die is used to make a pattern, it must be still be possible to remove the pattern from the die [8].

There are two main techniques used to manufacture IC parts, depending on the type of mould used. These are either block moulds or shell moulds [3].

- Block moulds – this technique involves pouring refractory ceramic slurry around a wax pattern assembly contained in a flask. One of the main disadvantages of this technique is that a very thick ceramic shell surrounds the cast metal. This is an insulator and causes slow cooling and therefore poor metallurgical structures. Another problem is that the solid ceramic block prevents contraction of the metal as it cools and this can lead to failure of the casting.

- Shell moulds – the shells are produced by covering a wax assembly with several ceramic layers. The first layer is normally a fine coating (the face coat) so that a good surface finish on the casting will be obtained. Successive layers are made up of ceramic slurry and refractory sand, with drying periods in between layers.

Factors affecting the casting process [42]:

- The sacrificial pattern used;
- Material used to make the mould;
- Solidification of the molten metal;
- Flow of the molten metal into the mould cavity;
- Heat transfer during solidification.

### 2.3.1 Conventional investment casting process

The conventional IC process is a complex, multi-step process; production of the IC ceramic shell mould is a crucial part of the whole process. Conventional IC has benefited many industries as an economical means for mass-producing quality near-net shape metal parts with high geometric complexity and acceptable tolerances. The economic benefits of traditional IC are limited to mass production. The high costs and long lead-time associated with the development of hard tooling for wax pattern moulding renders conventional IC uneconomical for low-volume production [43].

The basic steps in the production of conventional investment cast components using a ceramic shell mould are shown in Figure 2.5 [44]. First step in conventional IC is tooling and pattern making, including the die being manufactured using traditional manufacturing methods. The wax is then injected into the die to produce wax copies of the desired castings. These copies are known as sacrificial patterns [45]. Patterns are assembled by attaching a gating system. The gating is also made of wax and if the patterns are of small size they are clustered together to form a tree. The shell is then built by dipping the pattern assembly in liquid ceramic slurry followed by layers of sand stucco; this is referred to as “investing”. In this process, the face coat, also known as the primary coat of the mould, is developed by

dipping the pattern into fine ceramic slurry. The face coat is a dense uniform layer and the most crucial stage in the process, because it is directly exposed to molten metal during the casting process. It must be carefully applied to avoiding entrapment of air bubbles [46]. Inconsistency of the face coat and stucco can cause casting defects like rough surface, inclusions and dimensional discrepancies. Once the face coat is fully dried, the successive dipping, that includes intermediate and back-up coats, is repeated until the required shell thickness that is capable to withstand the stresses of the casting process is achieved. The assembly is left to dry in the open air between different dipping steps [47].

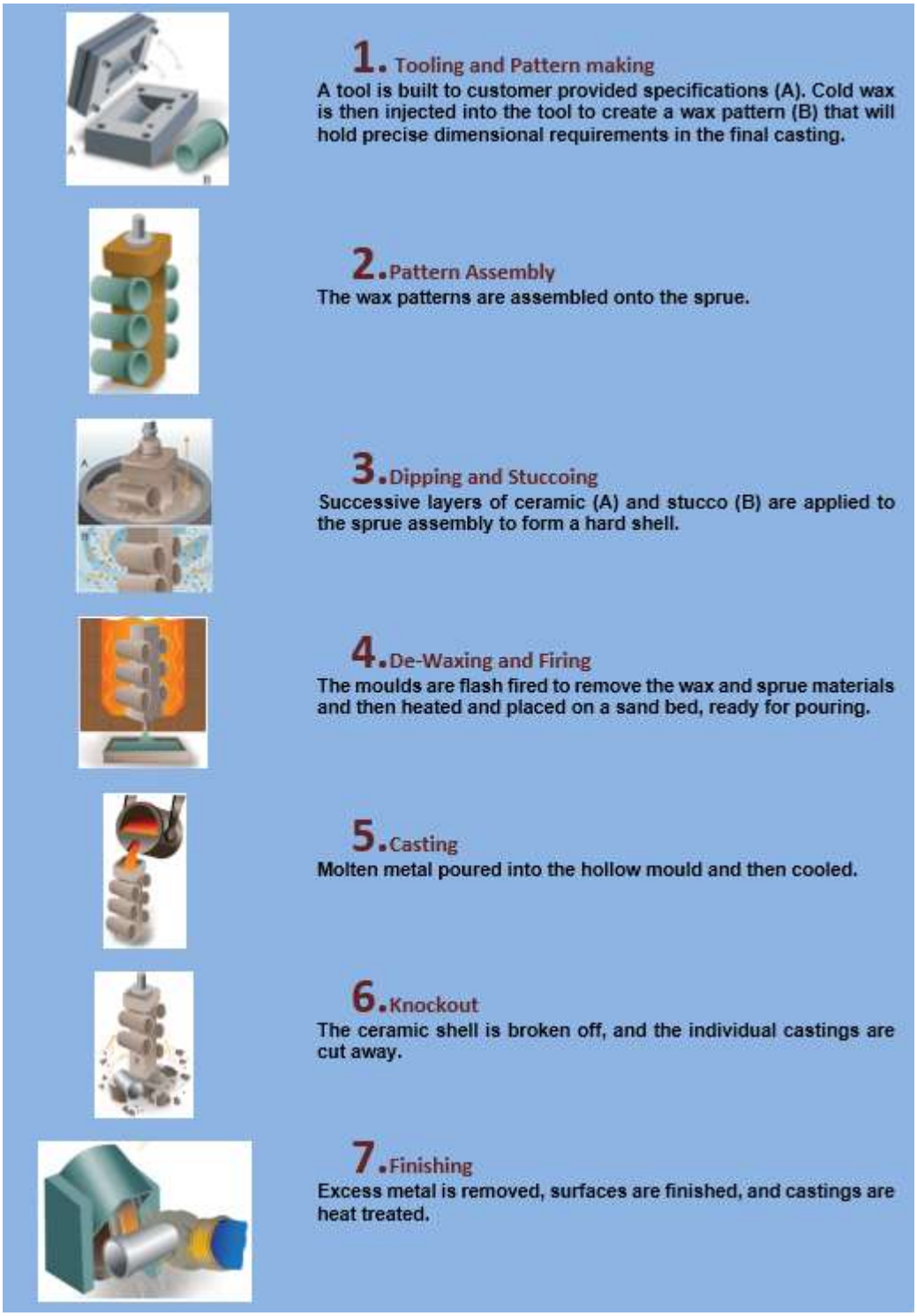


**Figure 2.5. Basic principles of the conventional IC process** [44]

Once the ceramic is dry, the wax is melted out (de-waxing) by placing the shell in a steam autoclave, creating a negative impression of the pattern within the shell. The wax can be reclaimed and used for moulding the runner systems [48]. After de-waxing, the mould is fired in a furnace to give full

strength and to bring it nearer to the melt temperature of the metal. The casting then takes place. Metal is melted in a crucible until it reaches its specified temperature and then it is poured into the mould and left to cool. Prior to pouring, the empty mould is preheated so that the pouring happens while the empty mould is still hot, allowing molten metal to flow easily through the empty mould and to allow the casting to shrink as it cools [49]. Once cool, the shell material is removed from the metal. Knocking off can be done by hammer, high-pressure water blast, vibratory table or chemical substances. After the shell material has been removed, the parts are cut off the sprue and the gates are ground off [50].

### 2.3.2 Rapid investment casting process

The (RIC) process uses AM technology to produce patterns for IC [51]. RIC was introduced in 1989 with the use of block moulds [52]. In the RIC process, the steps are still similar to the conventional IC but there are adjustments, alterations and substitutions to be made. In the first step, namely pattern making, the pattern is manufactured through AM technology, replacing the wax pattern and therefore eliminating the need for tooling, as shown in Figure 2.6. In the tree assembly step, vents are also added to the AM pattern to promote airflow. Furthermore, there must be an extra dipping to ensure an increase in shell thickness. Lastly, during the burnout process, the pattern will combust and release some gas, therefore, high temperature and a long duration furnace cycle is required followed by a shell wash [2], [53].

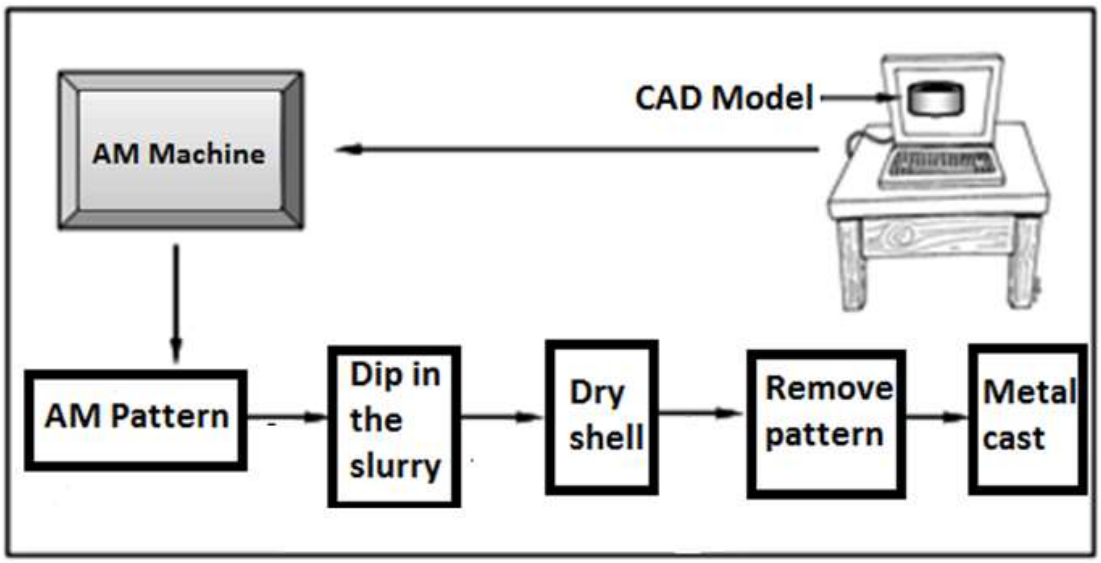


**Figure 2.6. Schematic diagram of IC by AM technology, adapted from** [54]

In RIC, the key consideration is pattern modification to prevent shell cracking and minimize residual ash. During the burnout process, the pattern applies stress to the shell due to the expansion of the pattern when heat is applied. Hence, shell cracking occurs when the stress induced by the pattern is greater than what the shell can resist. Ceramic shells have a very low coefficient of thermal expansion, so any expansion of the pattern during the burnout cycle may cause the shell to crack [55].

### 2.3.3 Comparison of conventional and rapid investment casting

The conventional IC process can be lengthy and cost intensive for the development of a complex product. The key advantage of RIC is that it eliminates the need for tooling for low-volume production typical in prototyping, pre-series, customized or specialized component production [56]. Injection moulds for wax patterns are expensive and the building of the tool can take 6 to 14 weeks. By using RIC patterns, the tooling cost is eliminated and the lead time for a cast part is reduced to just five weeks on average [8], however, this depends on the efficiency of the supplier. Shell cracking is still a main problem in RIC. Foundries are doing research while AM suppliers have developed techniques to overcome this problem [34]. The number of foundries that can convert AM patterns into metal using IC is still relatively

low, especially in developing countries. Moreover, AM parts have stair-casing steps on curved surfaces as a result of the layer-by-layer manufacturing process and require special finishing [9]. The successive handling process is the same irrespective of how the model has been produced, as shown in Figure 2.7, be it by using conventional wax pattern techniques or RIC technology [8].

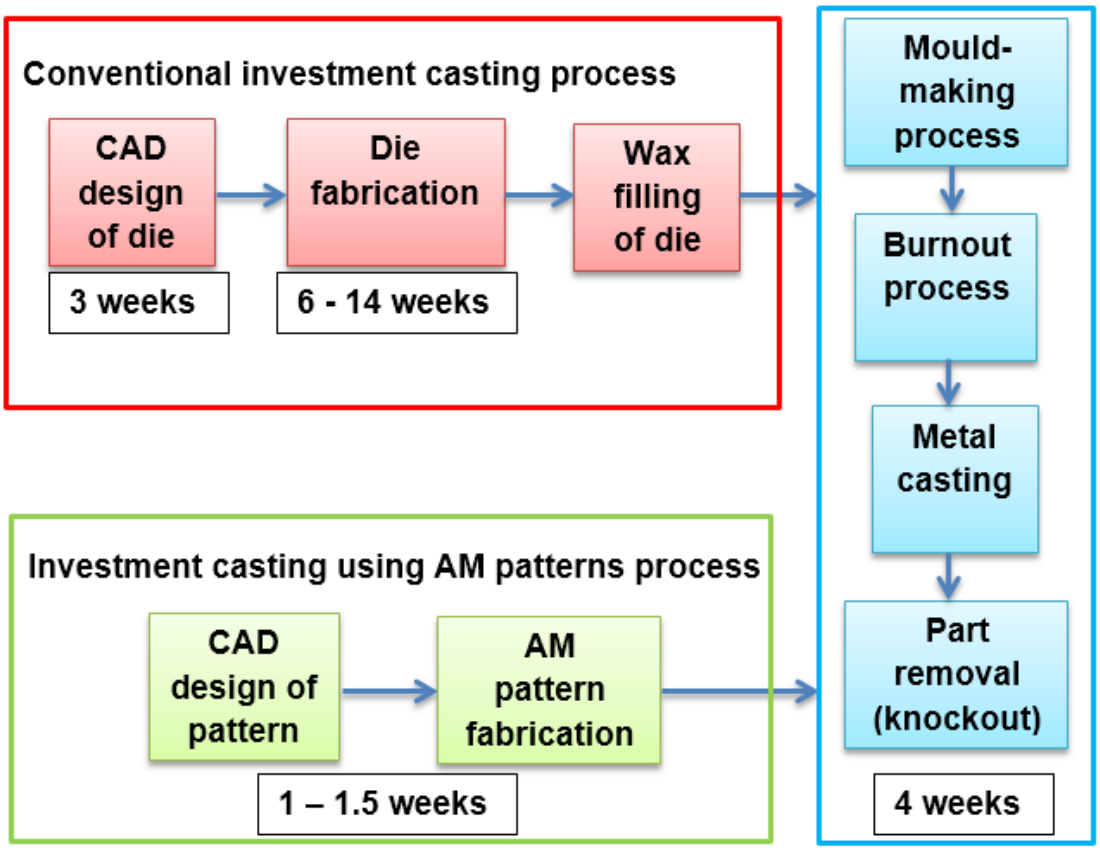


**Figure 2.7. Comparison of conventional investment casting and rapid investment casting processes (adapted from** [8]**)**

The main benefit to the foundry industry from using AM technology as compared to the conventional techniques is that as products are developed towards production, it is likely, if not certain, that there will be changes to the design, this changes can be done with less time and cost [57]. Conventionally, each iteration requires more effort (and more costs) to modify tooling, while by using AM patterns for the development process, there is no need to commit to tooling until the design has finally been frozen [58]. Moreover, in an

increasingly competitive world, foundries are striving to build strategic links with their key customers, and to be seen to be pro-active in their customers' businesses. By getting sample quantities of castings early, foundries are helping their customers to win business and show their commitment [59].

## 2.4 Polymer powders used for producing AM patterns

### 2.4.1 PrimeCast®

PrimeCast® 101 is a grey polystyrene powder. It is suitable for use in all EOS polymer systems, namely EOSINT P 350 with Upgrade `99 and exchangeable frame, P 360, P 380, P 380i, P 385, P 390 and P 700. The recommended layer thickness is 0.15 mm [60]. It can be used as patterns for IC because it possesses excellent dimensional accuracy, high surface quality and good strength. However, special measures against shell cracking are necessary [61]. Table 2.2, Table 2.3 and Table 2.4 show the mechanical, material and thermal properties of PrimeCast® 101.

**Table 2.2. Mechanical properties of PrimeCast® 101 adapted from** [60]

| | | |
|---|---|---|
| Tensile strength, X-/Y-direction | DIN EN ISO 527 | 5.5 ± 1.0 N/mm$^2$ |
| Tensile strength , Z-direction | DIN EN ISO 527 | 1.2 ± 0.3 N/mm$^2$ |
| Tensile modulus | DIN EN ISO 527 | 1600 ± 250 N/mm$^2$ |
| Elongation at break | DIN EN ISO 527 | 0.4 ± 0.1% |

**Table 2.3. Material properties of PrimeCast® 101** [60]

| | | |
|---|---|---|
| Average particle size | Coulter counter | 80 ± 5 µm |
| Bulk density | DIN 53466 | 0.61 ± 0.02 g/cm³ |
| Density of laser-sintered parts | EOS method | 0.70 - 0.85 g/cm³ |

**Table 2.4. Thermal properties of PrimeCast® 101** [60]

| | | |
|---|---|---|
| Glass transition temperature | DIN 53765 | 105 ± 1 °C |
| Material destruction | DIN 51006 | 250 - 550 °C |
| Remaining ash content | EOS method | 0.002% |

PrimeCast® must be kept in cool, dark, ventilated storage and closed containers with the temperature not exceeding 40 ºC. During the design, the part produced from this material must be scaled to compensate for the shrinkage occurring when the laser-sintered parts cool down [62].

### 2.4.2 PMMA

PMMA is a transparent thermoplastic with high mechanical strength, high Young's modulus and low elongation at fracture. It does not shatter on rupture [63], is one of the hardest thermoplastics and is relatively scratch resistant. Properties of PMMA are shown in Table 2.5.

**Table 2.5. Properties of PMMA, adapted from** [64]

| | |
|---|---|
| Particle thickness | 55 µm |
| Tensile strength | ≥ 200 MPa |
| Yield point | 1% |
| Binder-type | Polypor B |
| Burnout temperature | 700 °C |
| Residual ash content | < 0.01 weight % |
| Especially suited for | Investment casting, design model |
| Advantages | Sharp edges; for highest accuracy and true-to-details; useable particle material |

Castings made from PMMA patterns produced by AM are characterized by a significant surface porosity due to the BJ manufacturing process and that is why an impregnation process is required. PMMA is an acrylic material with excellent burnout properties when used as sacrificial pattern for IC [65]. During the burnout process, patterns manufactured from this material do not have a shell breakage problem. This is due to their negative thermal expansion coefficients [13].

## 2.5 Aluminium alloys used for IC

Aluminium casting alloys are the most versatile of all common foundry alloys [66]. For aluminium alloys to be used in casting, they must contain strengthening elements and sufficient amounts of eutectic-forming elements, usually silicon. The aluminium-silicon phase diagram in Figure 2.8 shows a simple eutectic-forming system, which facilitates the commercial viability of most high volume aluminium casting. When the silicon content ranges from 4% to the eutectic level of about 12%, this permits production of much more intricate shapes with greater variations in section thickness and yield castings with high surface and internal quality. This is due to the effect of silicon; increasing fluidity, reducing cracking and improving feeding to minimize shrinkage porosity [67].

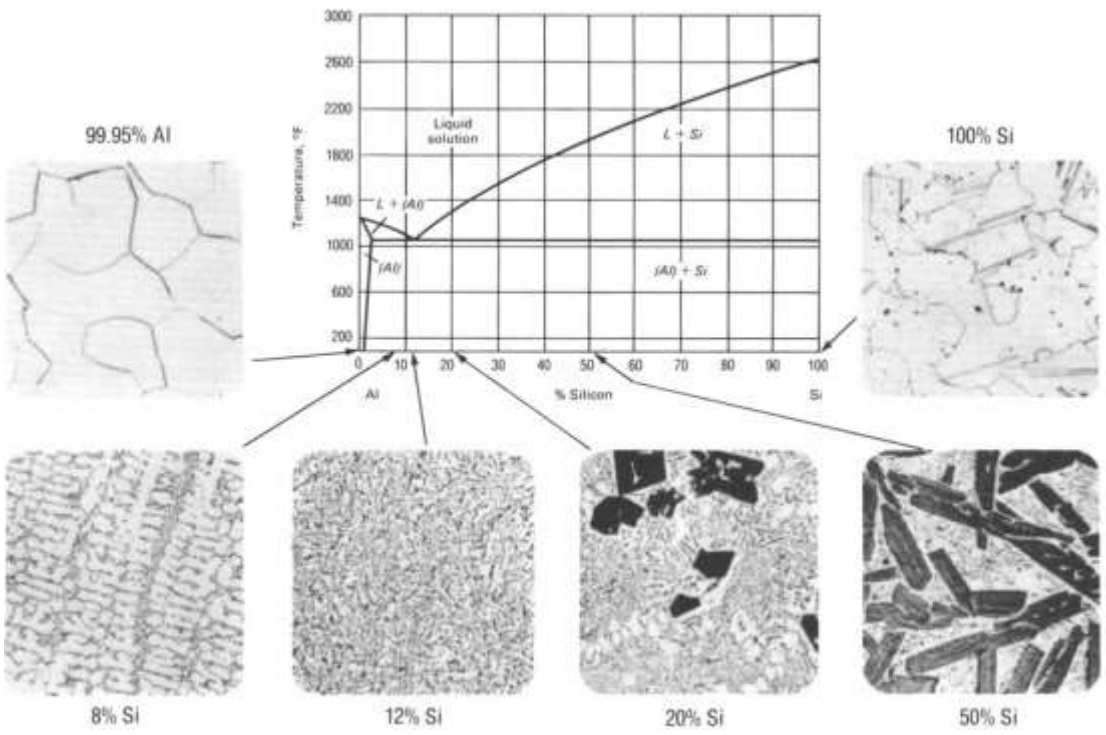


**Figure 2.8. Aluminium-silicon phase diagram and cast microstructures of pure components and of alloys of various compositions** [67]

These alloys are used in IC as they have the following characteristics [67], [68], [69]:

- Good fluidity for filling thin sections;
- Low melting point relative to those required for many other metals;
- Rapid heat transfer from the molten aluminium to the mould providing shorter casting cycles;
- As hydrogen is the only gas with appreciable solubility in aluminium and its alloys, hydrogen solubility in aluminium can be readily controlled by processing methods;
- Many aluminium alloys are relatively free from hot-short cracking and tearing tendencies;
- Chemical stability;
- Good as-cast surface finish with lustrous surfaces and little or no blemishes.

For this study, aluminium alloy A356 was used as it has high fatigue strength, resistance to corrosion, fluidity and has excellent castability properties. A356 is classified as an aluminium-silicon alloy and it is used when good castability and good corrosion resistance is needed [70]. Table 2.6 shows the chemical composition of this alloy.

**Table 2.6. Chemical composition of A365 alloy (wt%)** [71]

| *Si* | *Fe* | *Cu* | *Mn* | *Mg* | *Zn* | *Ti* | *Al* |
|---|---|---|---|---|---|---|---|
| 6.5–7.5 | 0.2 | 0.2 | 0.1 | 0.25–0.45 | 0.1 | 0.1 | Balance |

This alloy is one of the most popularly used in foundries and there is a demand for it in South Africa. It is normally used in automotive transmission cases, aircraft pump parts and water-cooled cylinder blocks. The liquidus and solidus temperatures of A356 are 615 $^{\circ}$C and 555 $^{\circ}$C, respectively [70].

## 2.6 Metrology techniques

To measure is to determine the dimension, quantity or capacity of objects. The technology that deals with measurements is referred to as metrology. Metrology covers all aspects relating to theory and practice and any kind of measurement, independent of the particular domain of science and technology [72]. AM technology poses a wide variety of challenges for metrology because it produces complex geometries that are often not comprised of simple geometric elements, such as circles, cylinders and planes.

### 2.6.1 Co-ordinate measuring machine

A co-ordinate measuring machine (CMM) is commonly used to measure the parts produced by AM technology. These machines are good at a wide variety of applications and are not expensive [73]. A CMM has a platform on which the workpiece to be measured can be placed and moved linearly or can be rotated. The probe on the head of lateral or vertical movement records all the measurements. Moreover, CMMs can record the measurements of complex profiles with high sensitivity of about 0.25 µm [74]. The CMM has a digital readout or it can be linked with computers for online inspection of parts [73]. Figure 2.9 shows the typical configuration of CMMs elaborating the X, Y, Z movement of the machine.

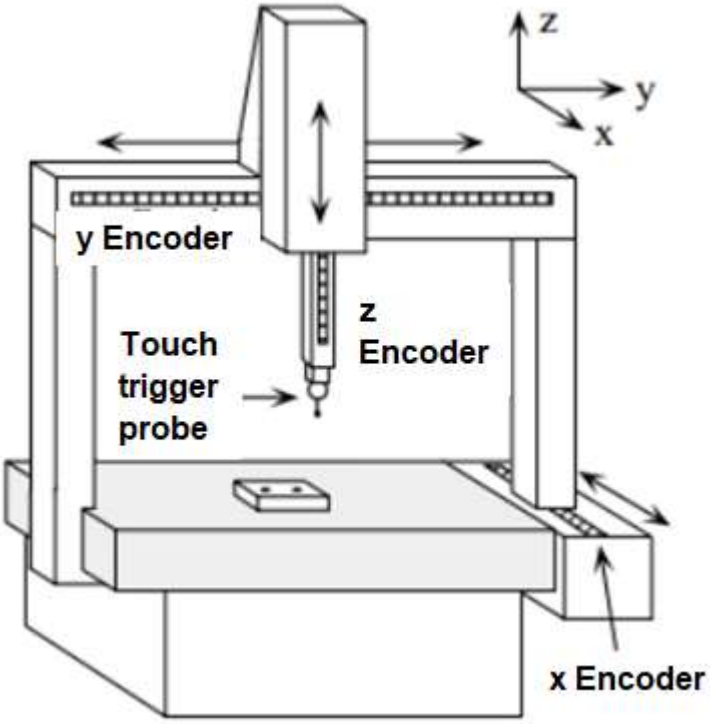


**Figure 2.9. Typical example of a CMM** [75]

### 2.6.2 Ace 3D measuring arm

The development of AM, going from a prototype and pilot production technology into a mature manufacturing technology, has resulted in a higher demand for methods and technologies for measuring. The Ace measuring arm from Kreon Technologies is a portable CMM system; it allows the user to work in the metrological lab and in the workshop. The flexibility of these 3D scanners saves time and ensures reliable 3D measurement. Figure 2.10 shows the scanning arm with Solano red laser scanner.

**Figure 2.10. Ace 3D measuring arm** [76]

The ace measuring arm is the ideal system for 3D measurements with and without contact. It can be equipped with a hard probe or a touch probe. It can efficiently scan and probe in the same measuring range, especially for the alignment operations. The scanning arm with a Solano red laser scanner has a maximum accuracy of 30 µm with a line resolution of 140 µm and a maximum laser scanning speed of 40 000 pts/sec [76].

### 2.6.3 Micro-CT scanner

Another technique that can be used to measure parts produced by AM technology is an industrial X-ray computed tomography (CT) system. This technique was introduced as dimensional metrology tool in 2005 and it is the latest technology in coordinate metrology, following CMMs and optical 3D scanners [77].

The industrial X-ray CT has several advantages compared to the CMM: non-destructive inspection of internal geometrical features, verification of parts in assembled state, simultaneous dimensional quality control, and reconstruction of complete and high-density point clouds in a relatively short time. In CT scanning, 3D external and internal structures of the sample are computed with X-ray radiographs of the sample that are taken over a full 360º rotation [78].

A typical industrial X-ray CT system consists of an X-ray source, a sample stage and detector, as shown in Figure 2.11 below [79]. This innovative dimensional measuring technique involves acquisition of multiple X-ray projections taken from different angular positions around the object and allows a full 3D reconstruction of the geometry of the measured object by using dedicated computer algorithms [80]. This machine is probably the best for this study but is expensive. It is ideal for measuring intricate parts and can measure both internal and external features. CT can compare the CAD geometry with the AM grown part and then compare the cast part with the grown part and the CAD design geometry [81].

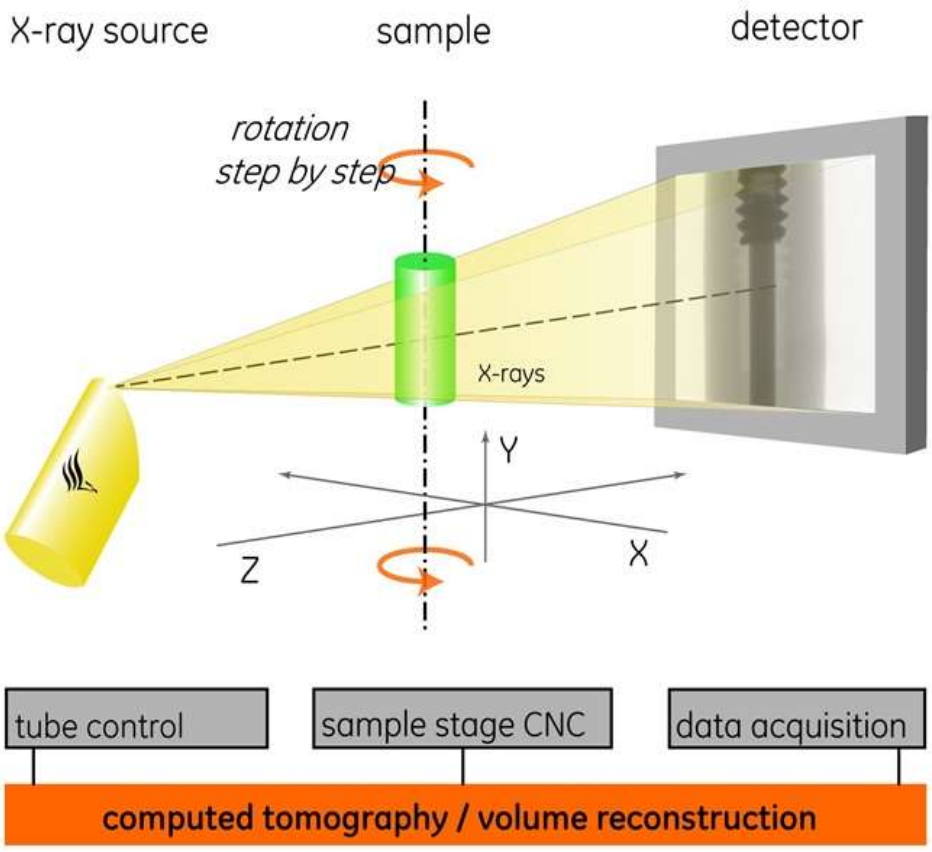


**Figure 2.11. Block diagram of a typical CT scanning system [79]**

Micro-CT scanning is an X-ray transmission imaging technique in 3D, similar to the method used in hospital CT scans, but on a smaller scale with greatly increased resolution [82]. Figure 2.12 shows the micro-CT scanner at Stellenbosch University (SU). It has two X-ray tubes, one with a reflection type

target and the other with a transmission target [83]. Table 2.7 shows the basic specifications of the micro-CT system at SU.


**Figure 2.12. General Electric Phoenix V|Tome|X L240 / NF180 Micro-CT scanner** [84]

**Table 2.7. Basic specification of the micro-CT scanner at SU** [82]

| ***Parameters*** | ***Reflection-type target*** | ***Transmission target*** |
|---|---|---|
| Voltage (kV) | 10–240 | 10–180 |
| Current (µA) | 5–3000 | 5–880 |
| Typical best voxel size (µm) | 5 | 2 |
| Beam angle ($^0$) | Approx. 30 | Approx. 180 |
| Sample limits (for single scan volume, multiple scans possible in X and Y with stitching) | | |
| Weight (kg) | 50 | 50 |
| Height (mm) | 320 | 320 |
| Width (mm) | 300 | 300 |
| Typical maximum wall thickness of sample per material type, for best quality (mm) | | |
| Steel | 10 | |
| Rock | 40 | |
| Plastic | 100 | |
| Wood | 200 | |

The reflection-type target has a maximum voltage of 240 kV, while that of the transmission-type target is 180 kV. This instrument is used for samples larger than 10 mm up to 300 mm in its longest axis. Objects containing metal or rock are preferably scanned using the micro-CT scanner because of its high-power tube, which allows up to 240 kV and high current in reflection mode [84]. Typical scan times for the micro-CT scanner are between 30 min and 1.5 hours, depending on the resolution and quality requirements.

## 2.7 Related studies

The focus of this study is in a field in which little research has been done. Initial work done by Dimitrov et al. [8] on rapid pattern making for IC of a light metal discussed various issues relating to the possibilities of improving the IC process through shortening lead times while still maintaining affordable costs and required quality. Four process chains for RIC, namely, direct pattern fabrication, direct die fabrication, indirect tool fabrication and direct shell fabrication were outlined. With direct pattern fabrication, a comparison was done between patterns produced from three AM technologies namely, a 3D-Printer (Z-Corp), laser sintering and a Thermojet, using a Mitutoyo Bright 710 CMM machine with a calibrated accuracy of 5 µm and volumetric accuracy of 6.1 µm. The part used for benchmarking was designed within tooling projects from the FP6 Framework and this is the same benchmark part used in this study.

From the results found with aluminium casting, after evaluating descriptive statistics, features measured and the dimensional accuracy indexed, a conclusion was drawn that there was a significant difference between the accuracy of the patterns produced by the different AM technologies. The LS pattern produced the best casting in terms of dimensional accuracy followed by Thermojet and then 3D-Printer (Z-Corp). The surface finish results indicated that the Thermojet pattern had the best surface quality with a $R_a$ value of 4.13 µm, followed by the 3D-Printer (Z-Corp) pattern and then the LS pattern. The LS polystyrene pattern had a $R_a$ value of 21.2 µm. It was also concluded that most patterns produced from AM technologies had a certain shelf life, depending on the material used and the environment they were kept

in. If the pattern is kept beyond its shelf life, such pattern can sag and change life and ultimately the dimension.

A recent article by Tom Mueller [85] compared the patterns and castings from four AM technologies, namely stereolithography (QuickCast™), laser sintering (QuickForm™), Projet printing (Projet Wax™), and Voxeljet binder jetting (PMMA). In the first part of the article he compared the performance of the printers, the second part compared the operating costs and in the last part the four leading methods of creating printed patterns for IC were compared. In the last part of the article, he mentioned that shell cracking in the autoclave during the burnout process was by far the most common cause of failure in AM patterns. He clearly indicated that from his experience there had not been a single case of shell cracking in the autoclave when Voxeljet patterns were used.

When using AM patterns, foundries were encouraged to add extra dips to the shells to overcome the tendency of some AM patterns to crack the shells in the autoclave. Pattern durability was an important aspect in casting because patterns are subjected to force in both assembly and in dipping. Most fragile patterns must be handled with care to avoid breaking during assembly and initial dips. The other variation from the conventional IC process is the assembly; vents are applied on most patterns produced by AM technologies. AM patterns will not melt completely in an autoclave de-waxing step, therefore, they must be burned out in the furnace. Even though the residual ash levels of these materials is typically low, there can be enough ash remaining in the shell to cause unacceptable ash-related surface defects in the casting. To avoid such defects, many foundries cool the shell to room temperature after burnout. The ash is then removed by either blowing out the shell with compressed air or rinsing it with water.

The analysis was based on the author's experience and it was concluded that there was no single 'best' pattern-printing technology. For each of the four technologies, applications existed for which it was the best alternative.

Clearly, requirements for IC vary considerably depending on the application of the casting.

## 2.8 Summary

In this chapter, the general process chain of AM was presented together with the benefits and limitations using AM processes. Two AM technologies, namely LS and BJ were presented as well as the advantages and disadvantages of each technology. The main disadvantage of an AM process is the staircase steps that are created between the layers as parts are manufactured layer by layer.

In section 2.3, the two types of IC methods, block- and shell mould, were discussed and factors affecting the casting process were listed. Both conventional IC and the RIC process were discussed stating the benefits and drawbacks of each process compared to the other. The comparison between the two IC processes was presented with emphasis on time saving.
Polymers used for this research were also discussed, as well as the aluminium alloy used in the casting process. Discussions on the metrology techniques suitable for AM parts were presented, providing detail on the micro-CT scanner at SU.

Furthermore, a summary of related studies was presented. From this literature study it was found that no direct comparison had been done on patterns for IC-built by PrimeCast® and PMMA materials.

# Chapter 3: Methodology

## 3.1 Introduction

This chapter describes the methodology that was followed to compare PrimeCast® and PMMA processed through AM as means of producing patterns for the IC process. The steps followed in the methodology are shown in Figure 3.1.

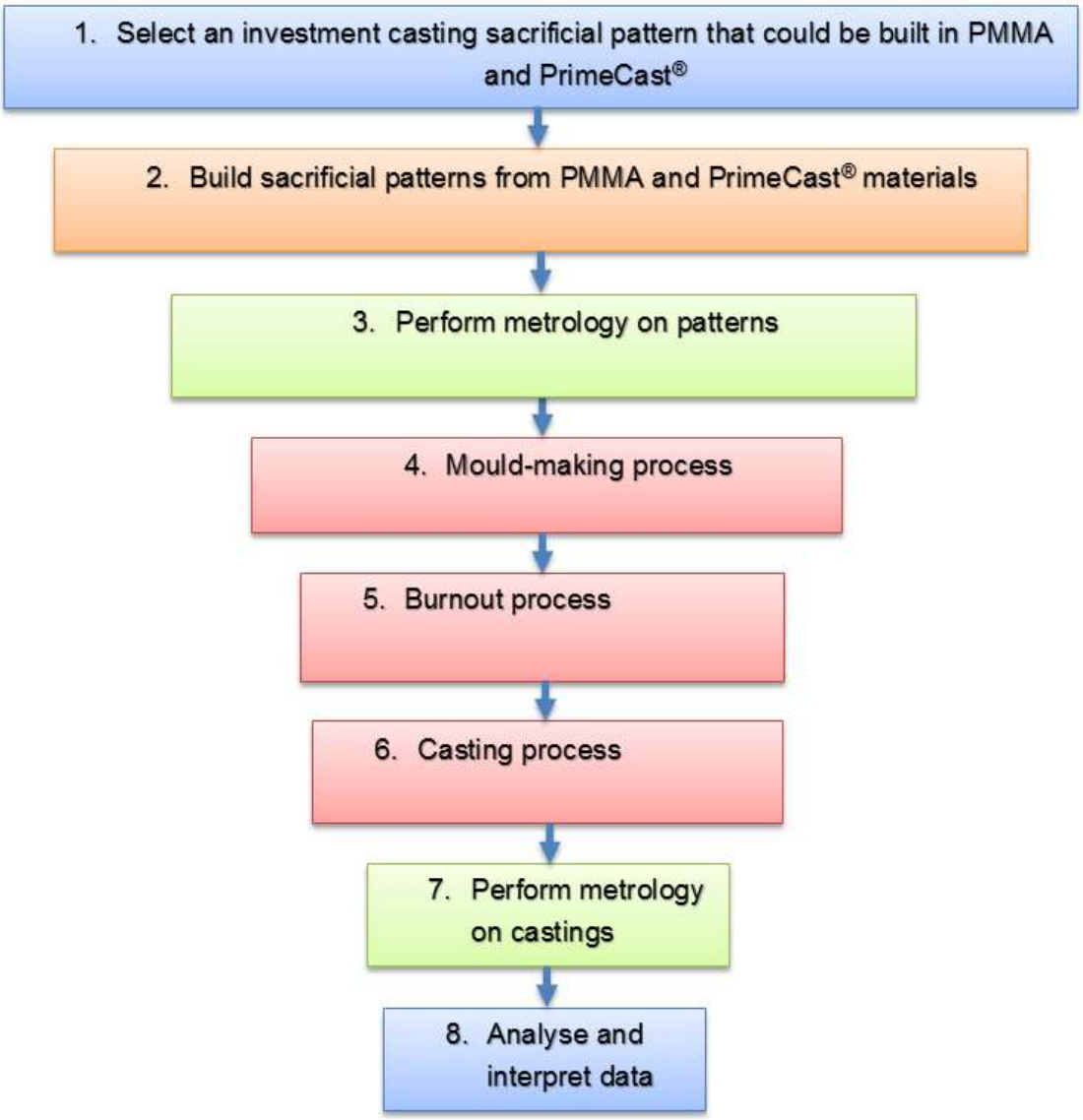


**Figure 3.1. Methodology diagram**

## 3.2 Standard test part

As a first step, the geometry of the sacrificial pattern to be built in both PMMA and PrimeCast® material was decided on, as illustrated in Figure 3.1. A standard test part that was designed within the tooling projects of the FP6 Framework of the European Commission (EC) was selected [8]. Figure 3.2 shows the test part and Table 3.1 displays every feature on this standard part with its specific purpose, quantity and nominal size.

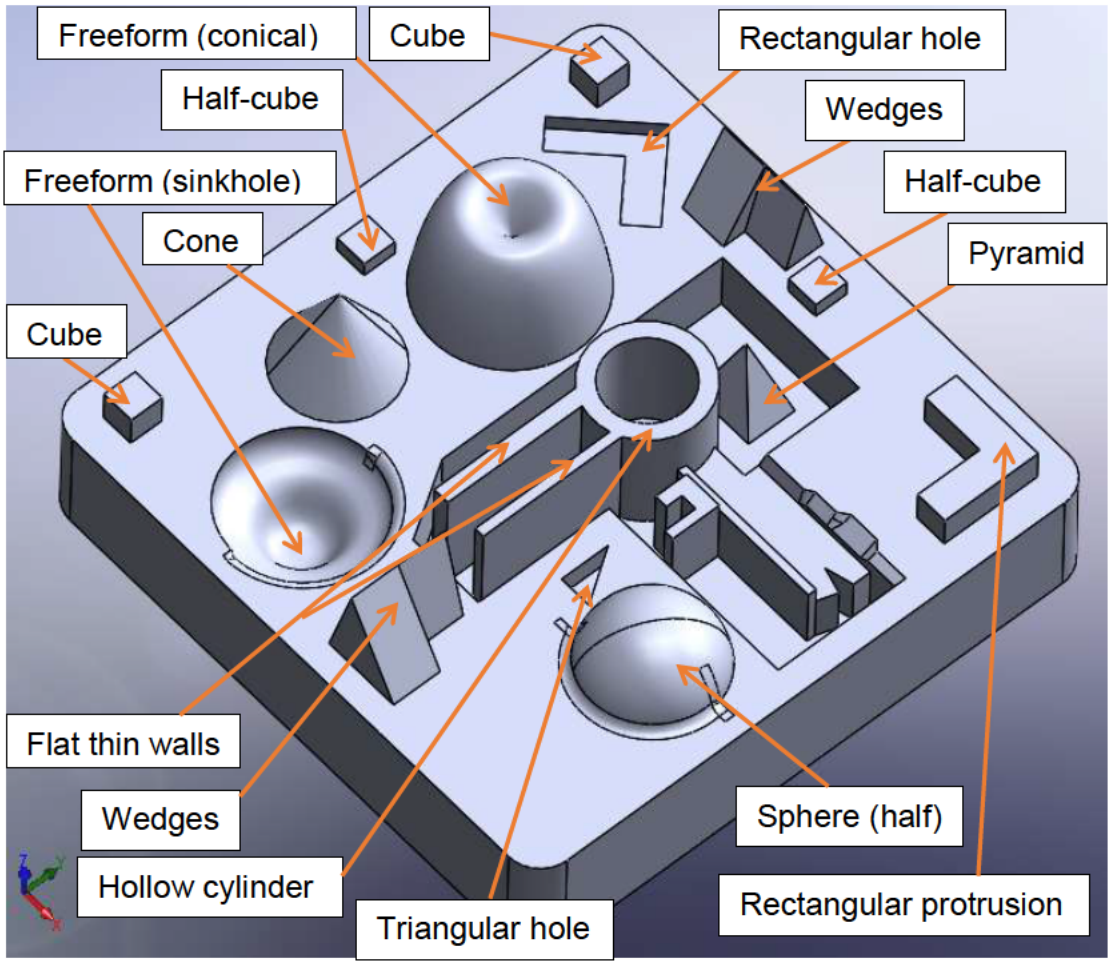


**Figure 3.2. standard test part** [8]

**Table 3.1. Features of the standard part and their specific purposes** [8]

| ***Feature*** | ***Purpose*** | ***Quantity and Nominal size*** |
|---|---|---|
| Cubes | Straightness, repeatability, linear accuracy | 2 (8 × 8 × 8 $mm^3$)<br>2 (8 × 8 × 4 $mm^3$) (Half-Cube) |
| Rectangular protrusion | Perpendicularity, linear accuracy | 1 (25 × 8 × 8 $mm^3$) |
| Pyramid | Angularity, accuracy | 1 (12 × 17 × 20 $mm^3$) |
| Sphere (half) | Symmetry, repeatability of a constantly changing sloping profile, axial runout, radial runout | 1 (ø35 mm) |
| Cone | Constant sloping profile, taper, axial runout, radial runout, symmetry | 1 (ø30 × 26 $mm^2$) |
| Freeform (conical) | Non-constant sloping profile axial runout, radial runout, symmetry | 1 (ø40 × 30 $mm^2$) |
| Freeform (sinkhole) | Non-constant sloping profile axial runout, radial runout, symmetry | 1 (ø30 × 20 $mm^2$) |
| Wedges | Angularity | (X direction 20 × 20 $mm^2$)<br>(Y direction 20 × 25 $mm^2$) |
| Rectangular hole | Perpendicularity | 1 (25 × 8 × 5 $mm^3$) |
| Cylindrical hole/ Hollow cylinder | Concentricity, circularity, accuracy | 1 (ø30 × ø20 × 27 $mm^3$) |
| Triangular hole | Angularity, perpendicularity | 1 (10 × 8 × 4 $mm^3$) |
| Flat thin walls | Parallelism, thickness | 1 (35 × 27 × 5 $mm^3$)<br>1 (35 × 27 × 3 $mm^3$) |
| Square base | Flatness, straightness, parallelism | 1 (150 × 150 $mm^2$) |
| Mechanical features | Competence of machine to build particular features (visual inspection) | Freeform, chamfer, fillet |
| Yes/No features | Machine's ability to build certain features (visual inspection) | Small triangular hole, small cross-shaped hole, thin walls |

## 3.3 Building of sacrificial patterns

Once the geometry of the pattern was decided on, the patterns were then built through the two AM technologies. Both patterns were infiltrated with wax to increase the strength and to fill the space between grains of material so that the slurry did not penetrate the pattern during the mould-making process.

### 3.3.1 PMMA patterns

Four PMMA patterns were manufactured using a Voxeljet VX1000 3D printer at VUT. Table 3.2 illustrates the technical data for this machine. Complex components, up to a length of 1000 mm, can be produced quickly and easily.

**Table 3.2. Technical data of Voxeljet VX1000**

| | |
|---|---|
| AM technology | Binder jetting |
| Maximum build size | 1000 mm × 600 mm × 500 mm (L × W × H) |
| Maximum build volume | 300 L |
| Minimum layer thickness | 0.15 mm |
| Accuracy | ±0.4% (min. ±0.3 mm) |
| Resolution x, y | Up to 600 dots per inch (23.6 Dots per mm) |

The pattern after wax infiltration is shown in Figure 3.3(a).

### 3.3.2 PrimeCast® patterns

The machine used to manufacture four PrimeCast® patterns was an EOSINT P380 at CUT. The technical data of this machine is given in Table 3.3.

**Table 3.3. Technical data of EOSINT P 380**

| | |
|---|---|
| Effective building volume | 340 mm × 340 mm × 620 mm (B × D × H) |
| Building speed (material dependent) | 10–25 mm height/h |
| Layer thickness (material dependent) | Typically 0.15 mm |
| Support structure | Not necessary |
| Laser type | $CO_2$, 50W |
| Precision optics | F-theta lens |
| Scan speed | 5 m/s |
| Power supply | 32 A |
| Power consumption (nominal) | 4 kW |
| Nitrogen generator | Integrated (optional) |
| Compressed air supply | Minimum 5 000 kPa: 6 $m^3$/h |

The large build volume of the EOSINT P 380 allows the efficient production of a broad range of parts. To prepare 3D CAD data, EOS offers EOSPACE software. This software positions parts automatically in such a way that the build envelope is optimally used and the required building height is therefore reduced to a minimum.

The pattern after wax infiltration is shown in Figure 3.3(b).

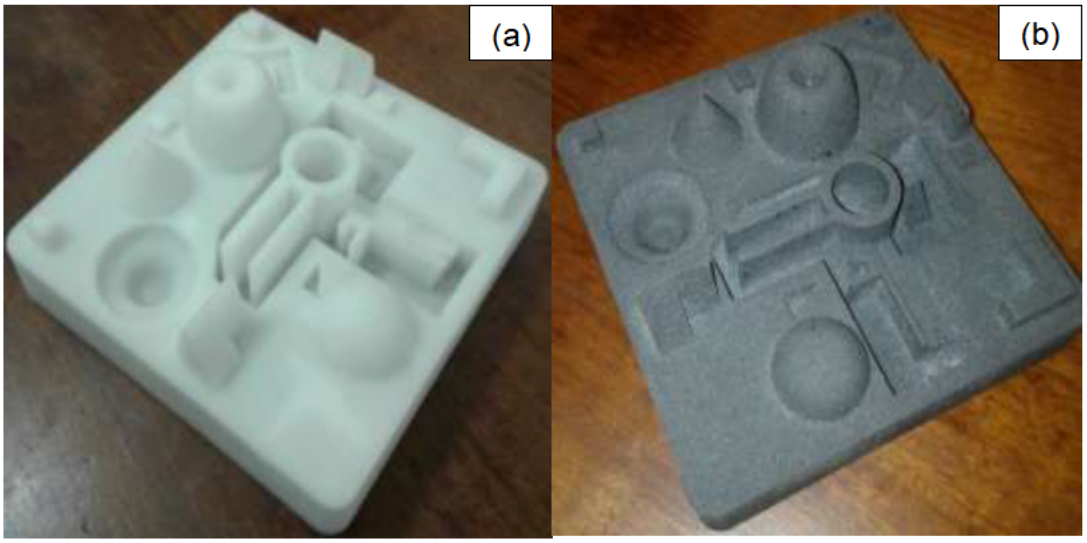


**Figure 3.3. (a) PMMA test part pattern and (b) PrimeCast® pattern**

## 3.4 Metrology on patterns

Two patterns, one each in PrimeCast® and PMMA, were scanned using a General Electric Phoenix V|Tome|X L240/NF180 micro-CT scanner at SU. The metrology was done a week after their manufacturing. The X-ray settings used were 200 kV and 100 µA. The machine acquires 3000 images in a full rotation with an image acquisition time of 600 ms per image, with no averaging and no skipping of images. Detector shift was activated to minimize ring artefacts. The sample was positioned on the scanner's rotating stand at an angle so that no feature was parallel to the X-ray beam as it rotated, also ensuring that the object would not move during scanning. During rotation, the detector cannot detect any feature that is parallel to the X-ray beam. Background calibration was performed and the scan time was approximately 30 minutes per scan. Reconstruction of the sample was done with system-

supplied Datos reconstruction software. Analysis was performed with Volume Graphics VGStudio Max 3 voxel data analysis and visualization.

## 3.5 Mould making

During the research for this study, mould making and casting was done at CSIR. The mould making process of the patterns was done in just two weeks after the manufacturing of the patterns. During these two weeks, the patterns were kept in a mould making room that was maintained cool and dry, away from humidity. Additionally, and to prevent water absorption, the patterns were kept in a sealed plastic bag with a desiccant. The patterns were prepared by attaching gates and vents to the AM patterns. Ten vents were attached to the PrimeCast® pattern while no vents were used with the PMMA pattern, as shown in Figure 3.4. The gating and vents were produced by wax injection using suitable dies. The gates were positioned in such a way that during casting the molten metal would start filling the bigger-sized features. Subsequently, the assemblies were cleaned using wax pattern cleaner and de-ionized water to remove any debris and carbon from the wax. The assemblies were then left to dry in the open air.

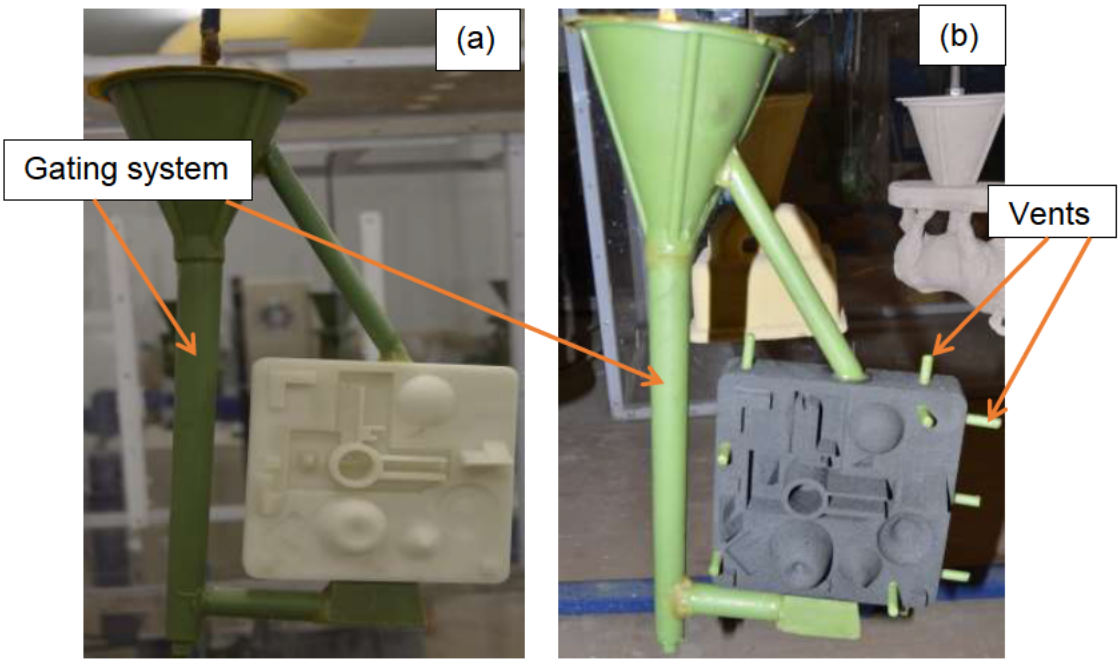


**Figure 3.4. (a) Sacrificial patterns with gating and vents, (b) PMMA and PrimeCast®**

Once the assemblies were dry, they were dipped in a container with rotating primary coat. The primary slurry consisted of inoculated cobalt aluminate. The assemblies were dipped into the slurry very slowly and carefully to make sure that no air was entrapped while dipping. When the assemblies were taken out of the slurry, it was ensured that no bubbles were trapped on the assemblies and, if present, they were removed. This could affect the casting, because this coat allows for the reproduction of fine-detailed features on the surface of the part. The dipping was followed by stuccoing with fine alumina sand and the assemblies were left to dry. The dipping and stuccoing was repeated four times, with subsequent drying for four hours. Lastly, they were dipped in the backup coat (fibre-reinforced fused silica) and stuccoed with fine fused silica sand after the first dipping and then coarser silica sand after the last dipping. The assemblies were left to dry for 24 hours at 22 °C. The flow diagram in Figure 3.5 illustrates the process.

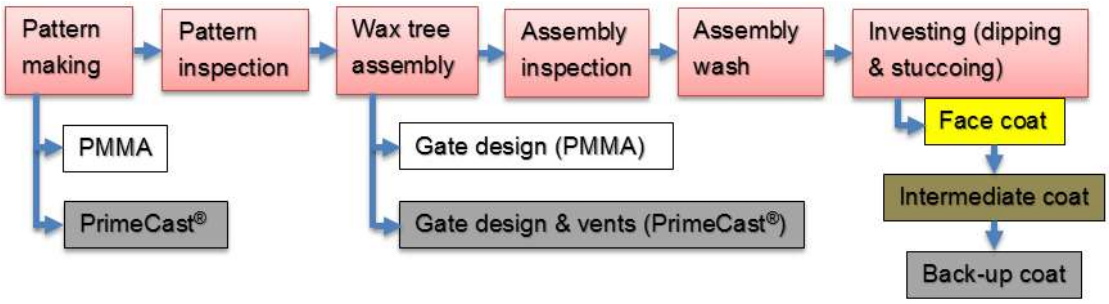


**Figure 3.5. Flow diagram of the mould-making process**

## 3.6 Burnout processes

### 3.6.1 Burnout procedure for PMMA patterns

PMMA patterns were burned out in an autoclave; the mould was faced down and heated to a temperature of around 90 °C. At this temperature the wax used for gates melted out first leaving an opening for the patterns to flow through. The patterns softened at 73 °C, the temperature was then raised to 250 °C to allow the patterns to flow out. The remainder of the pattern that did not flow out was burned out in a furnace at a temperature of around 750 °C for 4 hours without any problems.

### 3.6.2 Burnout procedure for PrimeCast® patterns

In a first attempt to burn out the PrimeCast® pattern, it was melted out in the autoclave using the same setting as for the PMMA patterns. However, shell cracking occurred to all the shells with PrimeCast® pattern during the autoclaving of the pattern, and the shells were irreparable. It was then decided to redesign the PrimeCast® pattern to adhere to the IC process. During the redesigning process, EOS, the supplier of the PrimeCast®, was consulted on how to go about the redesign and what burnout procedure should be followed for PrimeCast® patterns to be suitable for IC.

The redesign included manufacturing the pattern with a low-laser power setting and a special burnout process. Eight PrimeCast® patterns were built at CUT with skin thickness of 1 mm but at different laser power settings. The laser power settings were 75%, 80%, 85% and 90% of the available 50 W. Two patterns per laser power setting were produced. The revised pattern removal process included two stages: autoclaving and a burnout process. The vents had to be opened before autoclaving to allow for the quick flow of the pattern out of the shell during autoclaving. The wax that was used for gates and vents was melted out completely at around 150 °C using a boiler clave at the CSIR. The surface of the PrimeCast® pattern started to melt but could not flow out at this temperature. The pressure was then increased to 5 Bar and the temperature to around 200 °C for 2 hours. Most of the pattern material started to flow out, leaving grey residue on the shell walls, as shown in Figure 3.6(a).

During autoclaving the pattern could flow out of the shell as quickly as possible through the vents. The shells were then taken to a furnace for burnout and the temperature was gradually increased until it reached 650 °C, as shown by the temperature profile in Figure 3.7. At this temperature, the shells were white, which was an indication that all the PrimeCast® material had burned out completely, as shown in Figure 3.6(b).

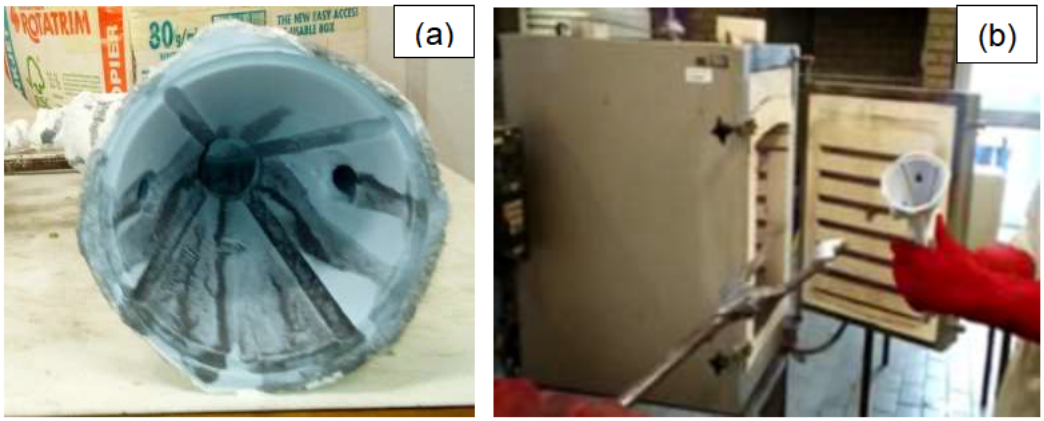


**Figure 3.6. (a) Shell with grey pattern residue and (a) white clean shell after removal from the furnace**

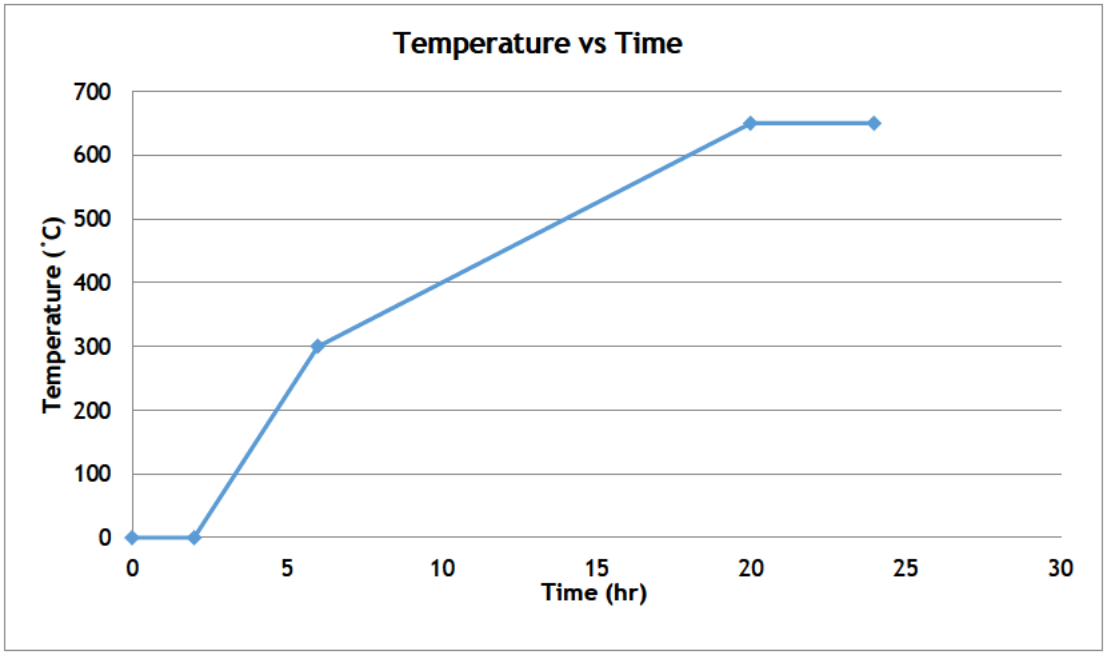


**Figure 3.7. Temperature profile used for the burn-out furnace**

## 3.7 Casting process

When the entire pattern residue had been removed from the shells, the shells were cooled. The burnout process was successfully performed in all three PMMA patterns and all eight PrimeCast® patterns that the mould making was done. The vent holes in the shells made by using the PrimeCast® patterns were patched using high temperature glue. The shells were then preheated to 600 ˚C just before pouring molten metal into them. The clay graphite crucible used with the furnace was pre-heated while empty in order to minimize the

temperature gradient across its walls. The crucible was preheated slowly to 200 °C for 2 hours to eliminate any moisture. The temperature was gradually raised to 1100 °C on full power to achieve a uniform bright red condition over the whole crucible. The temperature was then dropped to 700 °C over 8 hours before the crucible was fed with aluminium ingots. It was important that the crucible body temperature was equivalent to or slightly above that of the molten metal in order to minimise thermal stress.

The aluminium ingots were cleaned before they were placed into the crucible to avoid contamination of the molten metal or flame due to impurities. They were loaded into the crucible very loosely at the time until the required quantity had been melted to avoid the ingots expanding and cracking the crucible. The temperature of the molten metal was recorded just before it was poured into the shell cavity, as show in Figure 3.8 below.


**Figure 3.8. The furnace showing the recorded temperature during melting of aluminium alloy**

The liquidus temperature of aluminium A356 is 615 °C, therefore, the temperature of 670 °C was recorded as the pouring temperature for the molten metal. The oxide layer was removed prior to pouring. During the pouring, the hot shells were removed one by one from the furnace and then filled with molten metal as shown in Figure 3.9. The filling was done carefully so that no air was trapped during filling. After the shells were filled with molten

metal, they were left to cool in the air. The final step was to clean-up the castings by removing the shells and grinding off the gates and vents. The casting process was a success in all shells.


**Figure 3.9. (a) Pouring of the molten metal into the shell and (b) the shell with molten metal left to cool in the air**

## 3.8 Metrology on castings

Four best castings, two produced from PrimeCast® patterns and two from PMMA patterns, were scanned using the General Electric Phoenix V|Tome|X L240/ NF180 micro-CT scanner at SU. The castings produced from PrimeCast® patterns were labelled PC1 and PC2, while those from PMMA patterns were labelled PMMA1 and PMMA2. The scanning procedure was the same as outlined in Section 3.4. The samples were imaged using a tube acceleration voltage of 200 kV and 200 µA current. The measurements consisted of 3000 X-ray transmission images, taken around a full 360° rotation and each image exposure time was 600 ms. The micro-CT scanner settings were the same for all the samples scanned and are illustrated in Table 3.4 below. The samples were also fixed to the table to ensure that they would not move during scanning, as shown in Figure 3.10.

**Table 3.4. Micro-CT scanner settings**

| ***Geometry*** | | ***Detector*** | | ***X-ray*** | |
|---|---|---|---|---|---|
| Voxel size | 125 µm | Average | 1 | Voltage | 200 kV |
| Magnification | 1.6 | Skip | 0 | Current | 200 µA |

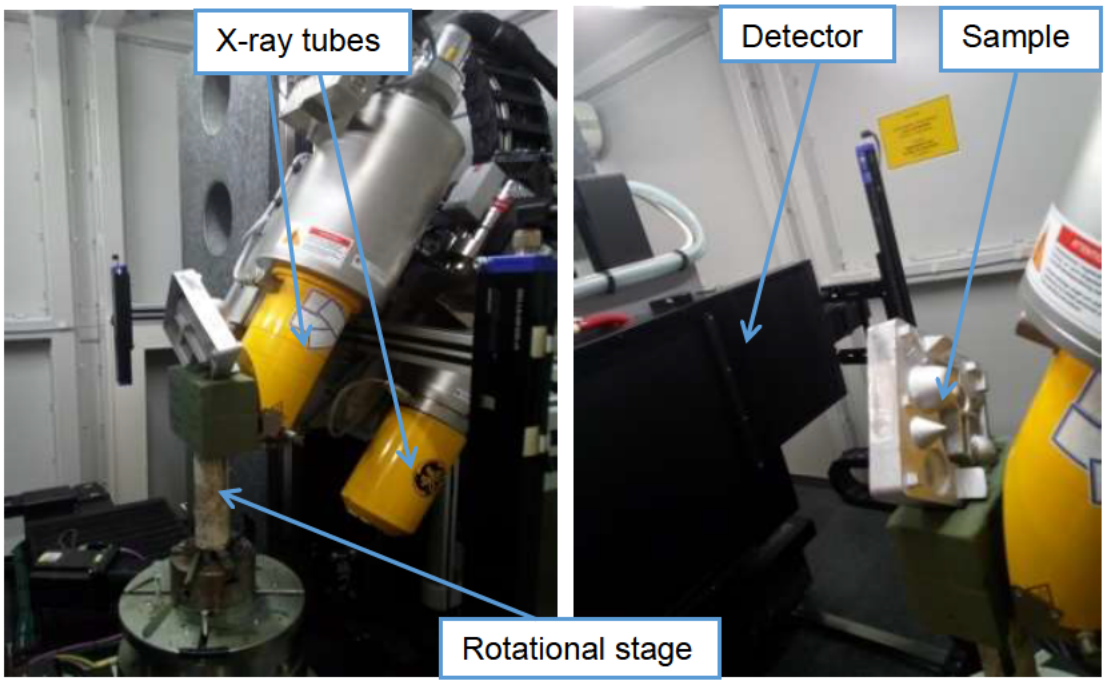


**Figure 3.10. Sample positioned on the scanner's rotational stage**

Once the acquisition of the CT scan was completed, CT calibration and reconstruction algorithms were used to reconstruct the 3D CT volume. In order to determine the accuracy of the castings produced from the PMMA and PrimeCast® patterns, scanned images of the castings were compared to the original CAD models. The actual-to-model comparison was performed by analyzing the deviation of the measured complex features of the standard part to the CAD representation. This comparison was sensitive to the sequence of file, that is, which data was set as model and which was set as actual. Depending on the geometry of the part, the difference between a reversed analysis was not just a reversed sign but could have significant differences in the magnitude of deviations.

The scanned images were acquired by a reconstruction process consisting of complex algorithms that transform the stack of 2D X-ray images to a 3D volume model. The data included both internal and external features from the acquired projections. Surface determination was then performed to identify the surface of the reconstructed 3D CT model, as shown in Figure 3.11 (a), and after this step the dimensional analyses on the 3D CT model was done

using a nominal/actual comparison of Volume Graphics VGStudio Max 3 voxel data analysis and visualization.

In order to make the comparison, the SolidWorks CAD model (Figure 3.11 (b)) and the 3D CT surface-reconstruction model needed to be aligned. The alignment tool used was an automatic best fit. Once the two models were aligned, a simple 3D comparison option automatically created a coloured view showing all the dimensional differences between the two models according to the colour scale on the left, in mm as shown in Figure 3.11(c).

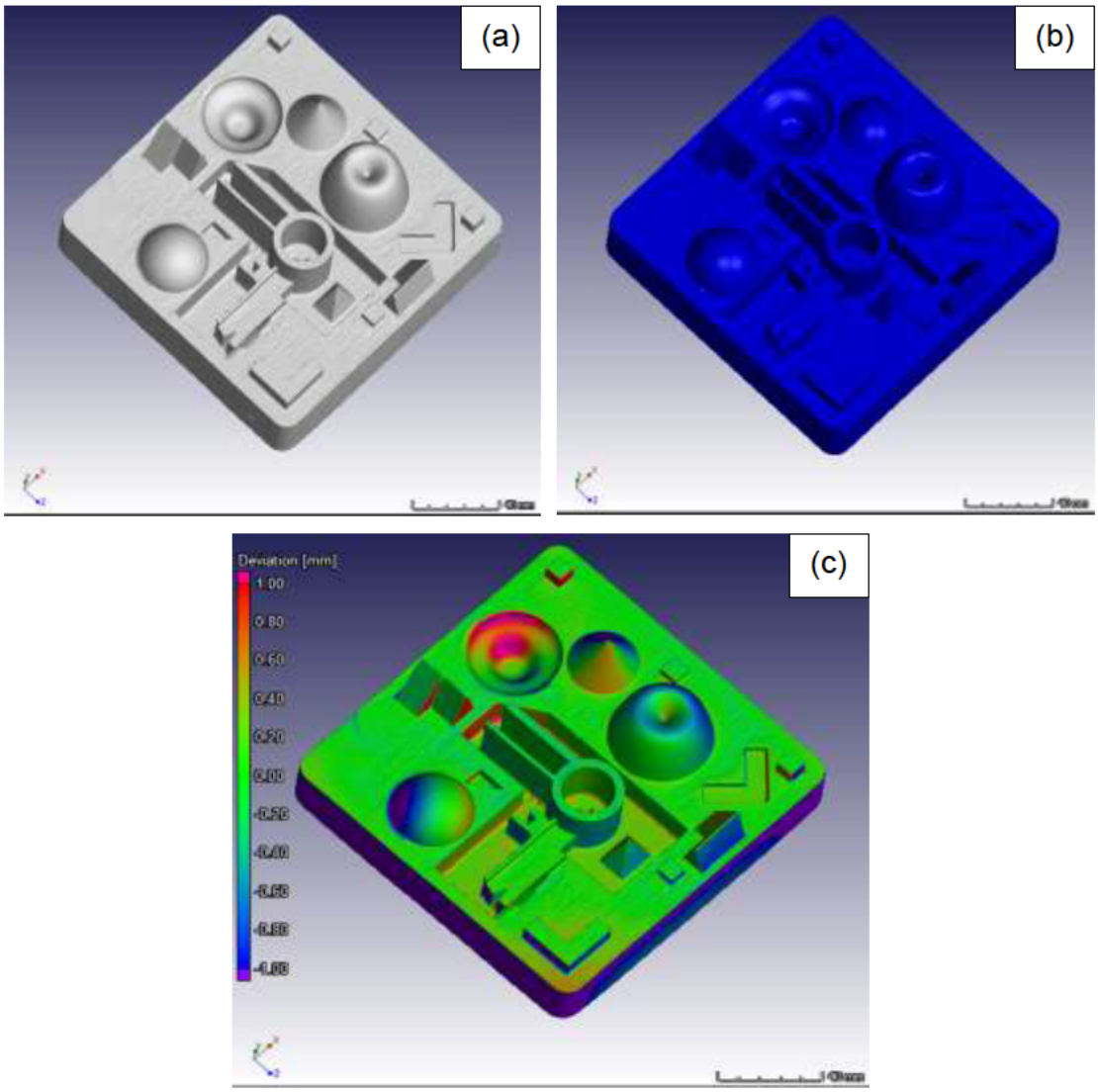


**Figure 3.11. (a) Reconstructed 3D CT model, (b) original CAD model and (c) comparison of 3D CT image to CAD model**

## 3.9 Summary

The research methodology that was followed for this study was discussed in this chapter, including the building of PMMA and PrimeCast® patterns, metrology on patterns, shell mould making and casting, as well as metrology on the castings. The metrology on the castings was performed on samples that were visually inspected to be the best out of all produced castings. Table 3.5 below summarises the number of patterns and castings per process as illustrated in this chapter.

**Table 3.5. Summary of the number of patterns and castings per process**

| ***Process*** | ***Number of patterns and castings*** | | |
|---|---|---|---|
| | ***PMMA*** | ***PrimeCast®*** | |
| | | ***First attempt*** | ***Redesign plan*** |
| Pattern making | 4 | 4 | 8 |
| Metrology on patterns | 1 | 1 | - |
| Mould making | 3 | 3 | 8 |
| Burnout process | 3 | 3 | 8 |
| Casting process | 3 | - | 8 |
| Metrology on castings | 2 | - | 2 |

# Chapter 4: Results and Discussions

## 4.1 Approach on the presentation of the results

The micro-CT scanning results from the methodology conducted, as described in Chapter 3, will be presented and discussed in this chapter, as outlined in Figure 4.1. Comparisons between the scanned images of the patterns versus the CAD model will be presented for both the PMMA and PrimeCast® patterns. The dimensional accuracy of each pattern as a whole will be analyzed in detail and the dimensional accuracy of some features will be discussed in relation to their locations on the standard part. Furthermore, the results of the two types of patterns will be compared and their differences and commonalities will be discussed. The analysis of the results is based on a tolerance varying from -0.3 mm to 0.3 mm.

For the castings from the two types of sacrificial patterns, the scanned images were also compared to the CAD models, as was done with the scanned images of the patterns. The results of the castings will be discussed in almost the same way as the results of the patterns. Finally, the dimensions of the castings relative to their corresponding patterns will be discussed.

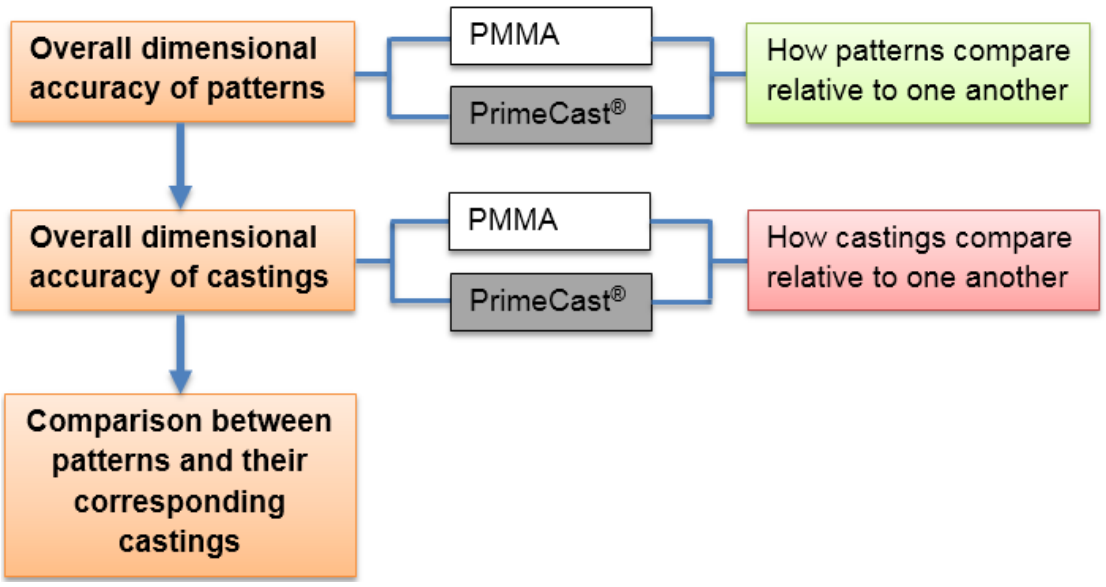


**Figure 4.1. Layout of Chapter 4**

## 4.2 Redesigned PrimeCast® pattern

The redesigned patterns had 10 vents, all with a diameter of 10 mm. The mass of the pattern material flowed out through the vents during the autoclaving. Thereafter there was little pattern material left and this was thermally decomposed during the burnout procedure.

The shells that had patterns produced at laser power settings of 75% and 80% had no cracks. There were cracks in the shells that had patterns produced at laser power settings of 85% and 90% only. The cracks can be seen on the edges of the surrounding walls of the castings in Figure 4.2. However, these were just minor cracks and the moulds were recovered by applying high temperature glue. The high temperature glue was also used to seal the vents that were opened during dewaxing. The casting process was carried out on all eight shells, but the metrology was only performed on two castings that were visually inspected as the best casting, that is, the one made from a pattern produced at a laser power of 75%.

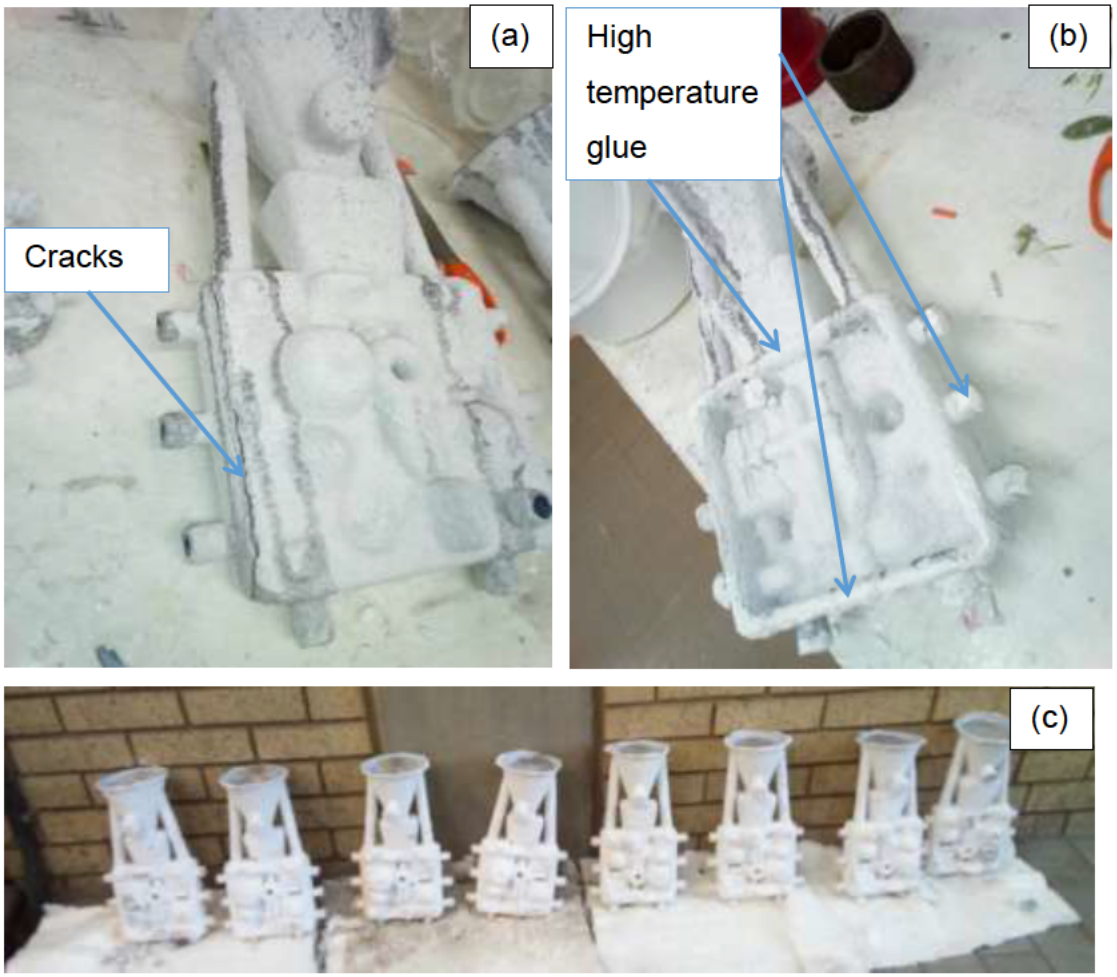


**Figure 4.2. (a) Cracked shell, (b) high temperature glue applied to the cracked shell and (c) all the metal alloy shells during solidification**

## 4.3 Overall accuracy of the patterns

It was possible to perform high-dimensional accuracy measurements of the whole part non-destructively with the micro-CT scanner at SU. The tolerances were then set to -0.3 mm to 0.3 mm for all the comparison and colours represent all the dimensional differences between the CAD model and the CT surfaces. The best-fit range is represented in green while warm colours (yellow and red) denote the area where the CT scan measurements are larger than the original CAD model and the cold colour (blue) indicate smaller measurements. The pink and purple indicate where the part is outside the parameters set for the analysis.

### 4.3.1 CT scan to CAD comparison of PMMA pattern

Figure 4.3 shows the comparison of the CT-scanned PMMA with the CAD model. The periphery of the PMMA pattern is mostly blue with hints of red. The pattern indicates blue on the flat surfaces diagonally from the corner with the cube to the corner next to the half-sphere. This indicates that the pattern is slightly smaller on the flat surfaces compared to the CAD. Along the other diagonal, from the corner with the rectangular protrusion to the corner nearer to the cube, there is predominantly green with traces of red. There are traces of red especially on the sharp corners and edges. The repeatability with the many cubes on the part shows poor accuracy, because one cube is predominantly green while the other is red.

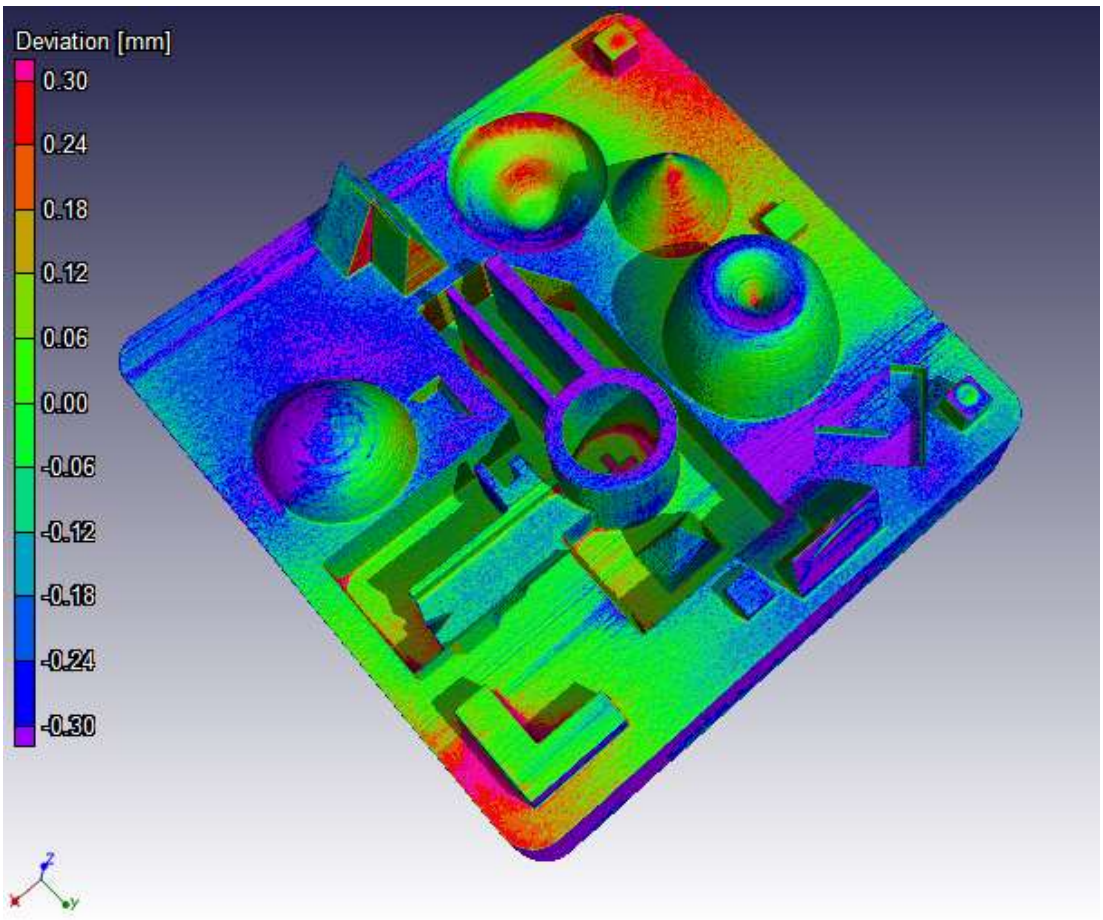


**Figure 4.3. Comparison of the CT PMMA pattern with the CAD model**

The two cubes indicate different dimensional accuracy; one cube is predominantly red with traces of green while the other is predominantly blue with traces of green. Both cubes are situated at the periphary of the pattern.

The half-cubes also present different dimensional accuracy depending on their location on the pattern. The top of the rectangular protrusion is green. This indicates good dimensional accuracy on the top flat surface. The vertical inner sides, towards the middle of the part, are predominantly red while the vertical outer sides, towards the periphery, are blue.

The non-constant sloping profile of the freeform (sinkhole) on the test geometry is covered with red, green and blue. Although green is more dominant than the other colours, blue and red are still significant. The top surface of the freeform (conical) feature is blue, and the constant sloping profile is green with just dots of reds. The cone was used to check for constant sloping profile, taper and symmetry. Green, blue and red can be seen on the surface of the cone, although green appears to be the dominant colour. The flat surfaces at the centre of the pattern are green and the pyramid is also green with traces of blue. The hollow cylinder at the centre of the part is predominantly green on the curve surface with drops of blue but its top flat surface is blue. In addition, this is also seen on the flat walls, with the vertical walls green with hints of blue, but the top flat surfaces are blue.

The deviation distributions represent the surface area in $mm^2$ against the deviation in mm. The deviation distribution of all points measured on the PMMA pattern shows a normal shape that has it peak on the left and tails to the right, as shown in Figure 4.4.

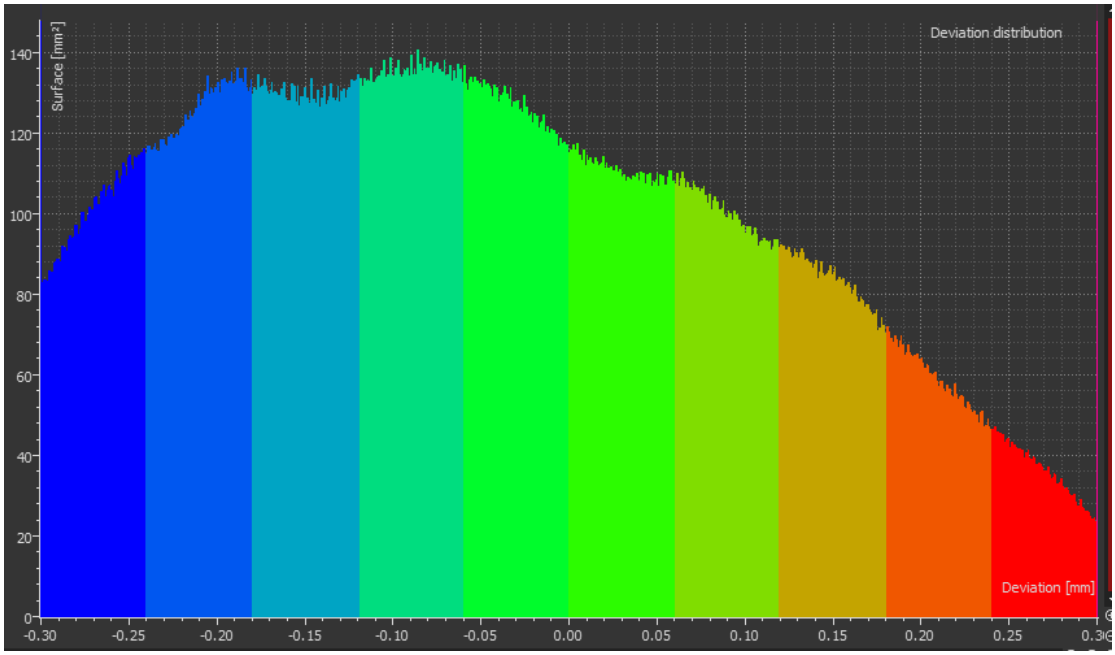


**Figure 4.4. Deviation histogram of the CT-scanned PMMA pattern from the CAD model**

The peak is at -0.10 mm and most of the surface area of the full volume is in the negative indicating that the produced pattern is generally smaller compared to the CAD model. From the deviation distribution, green is spread from -0.12 mm to 0.12 mm showing the highest fraction of about 41% of the total surface area.

### 4.3.2 CT scan to CAD comparison of PrimeCast® pattern

Figure 4.5 shows the comparison of the CT-scanned PMMA with the CAD model.

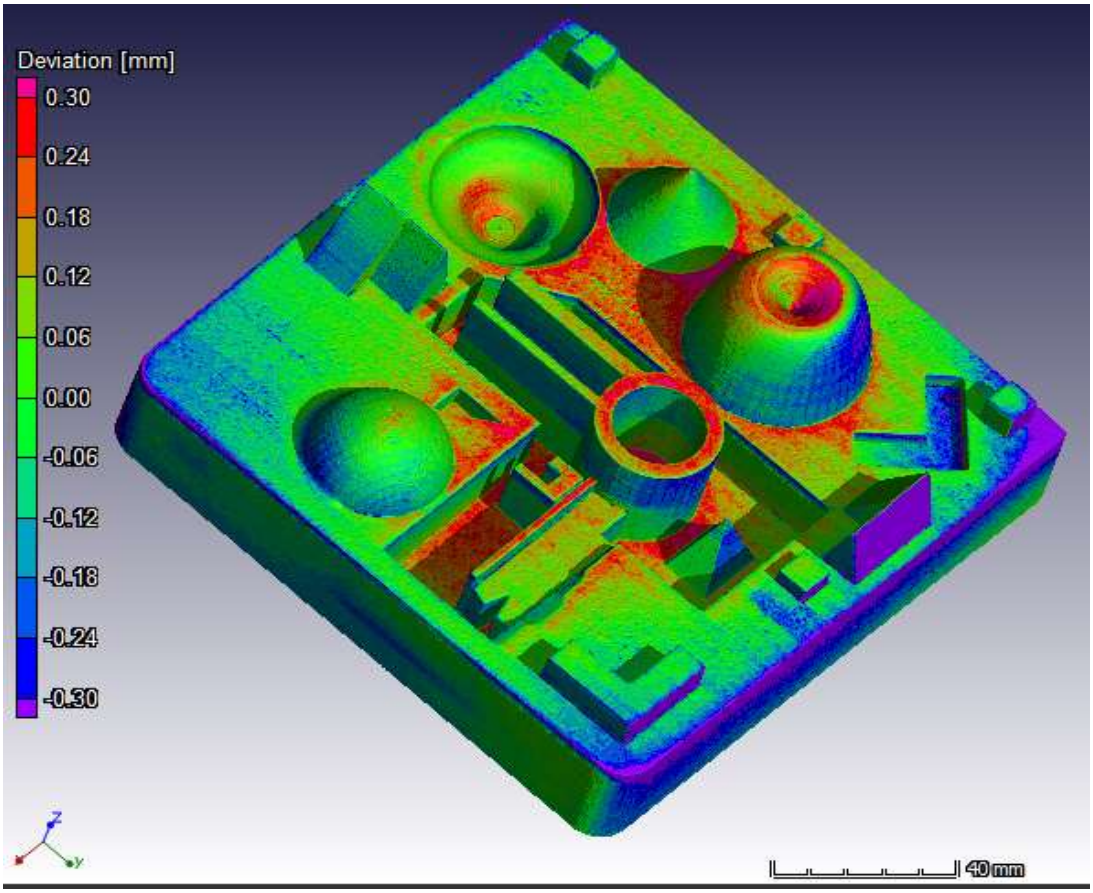


**Figure 4.5. Comparison of the CT PrimeCast® pattern with the CAD model**

The PrimeCast® pattern is predominantly green and red is seen mostly towards the centre. The surfaces towards the edges of the full volume on the top view are blue. Cubes of the pattern indicate good accuracy and repeatability; the colours on all cubes are almost the same. The walls are predominantly green with hints of blue. The cubes have only two colours; green and blue. The cubes show best-fit and smaller measurements. All corners and edges of the cubes are blue while the flat top surfaces are predominantly green. The corners and edges of the cubes are also sharp as are those of the rectangular protrusion. The top of the rectangular protrusion is predominantly green with touches of blue. The vertical inner sides are green and the vertical outer sides are fairly green and blue. The corners are blue showing smaller dimensions. From the literature it was suggested that a small radius should be applied to the corners and edges as AM technologies experience challenges in producing sharp corners and edges [7].

The non-constant sloping profile of the freeform (sinkhole) feature shows excellent dimensional accuracy; it is predominantly green with a small fraction of blue followed by red. Red is observed on the top surface of the freeform (conical) feature and the curved surface is dominated by green with a smaller portion of blue. The cone revealed good dimensional accuracy with green on the constant sloping profile. Constant sloping profiles, taper, axial runout, radial runout and symmetry of the cone are well-replicated from the CAD model. The sharp point of the cone is blue showing that the AM technology was not able to replicate the sharp point from the CAD model.

The shape of the deviation distribution of all points measured in the PrimeCast® pattern complies with a normal distribution with one peak almost at the centre of the deviation distribution, as shown in Figure 4.6. Green covers the largest area indicating good dimensional accuracy. Green is spread from -0.12 mm to 0.12 mm and it represents the highest fraction of the surface area. Red covers from 0.12 mm to 0.3 mm while blue covers -0.12 mm to -0.3 mm.

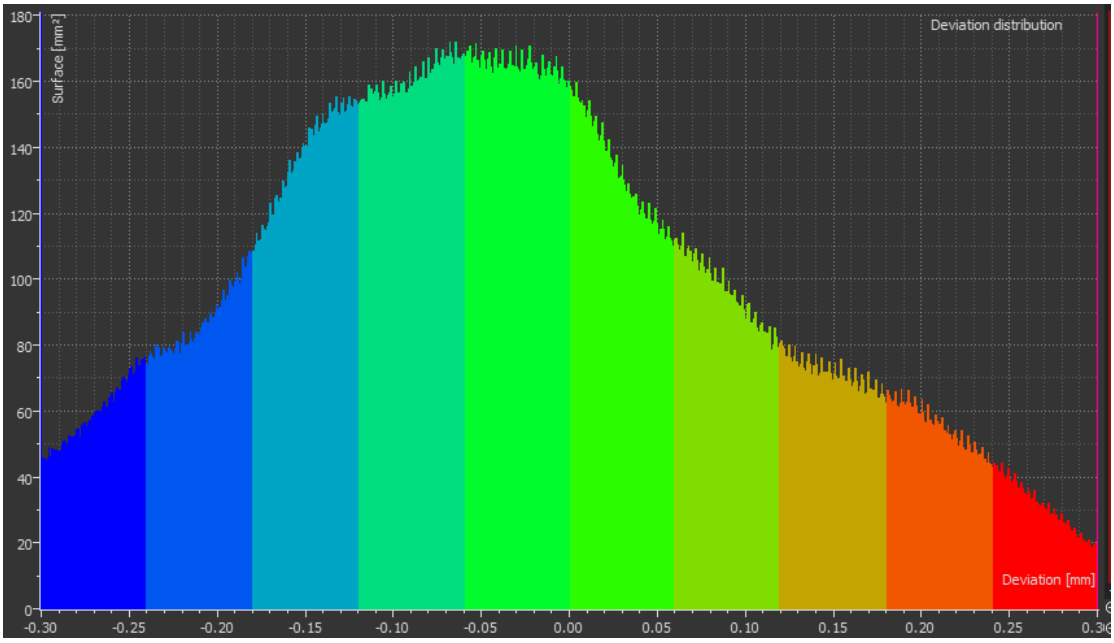


**Figure 4.6. Deviation histogram of the CT scanned PrimeCast® pattern from the CAD model**

### 4.3.3 Comparison of the sacrificial patterns

The cone and the half-sphere from the PrimeCast® pattern are fully covered in green while that of the PMMA pattern are covered in green with traces of red and blue. Therefore, the PrimeCast® pattern showed better dimensional accuracy than the PMMA for these features. The cube situated at the top corner on to the part orientation is predominantly red on the PMMA pattern (Figure 4.7a) and predominantly green on the PrimeCast® pattern (Figure 4.7b). The freeform (sinkhole) for both patterns is represented almost the same, that is predominantly green with traces of red. The inner flat surfaces of the central features of the PMMA pattern is covered in green while those of the PrimeCast® pattern are predominantly red with traces of green. The top surface of the PrimeCast® pattern is hinted with hot colours, that is yellow and red, while that of the PMMA pattern is hinted with cold colours, that is blue and purple. In both patterns, the surrounding walls of the patterns are noticeably covered in purple and blue, as shown in Figure 4.7.

Blue that is mostly seen on the PMMA pattern is well represented in the deviation distribution in Figure 4.7c. The deviation distribution of PrimeCast® pattern (Figure 4.7d) is narrower and its peak is closer to the zero, this clearly shows better dimensional accuracies than the deviation of the PMMA pattern.

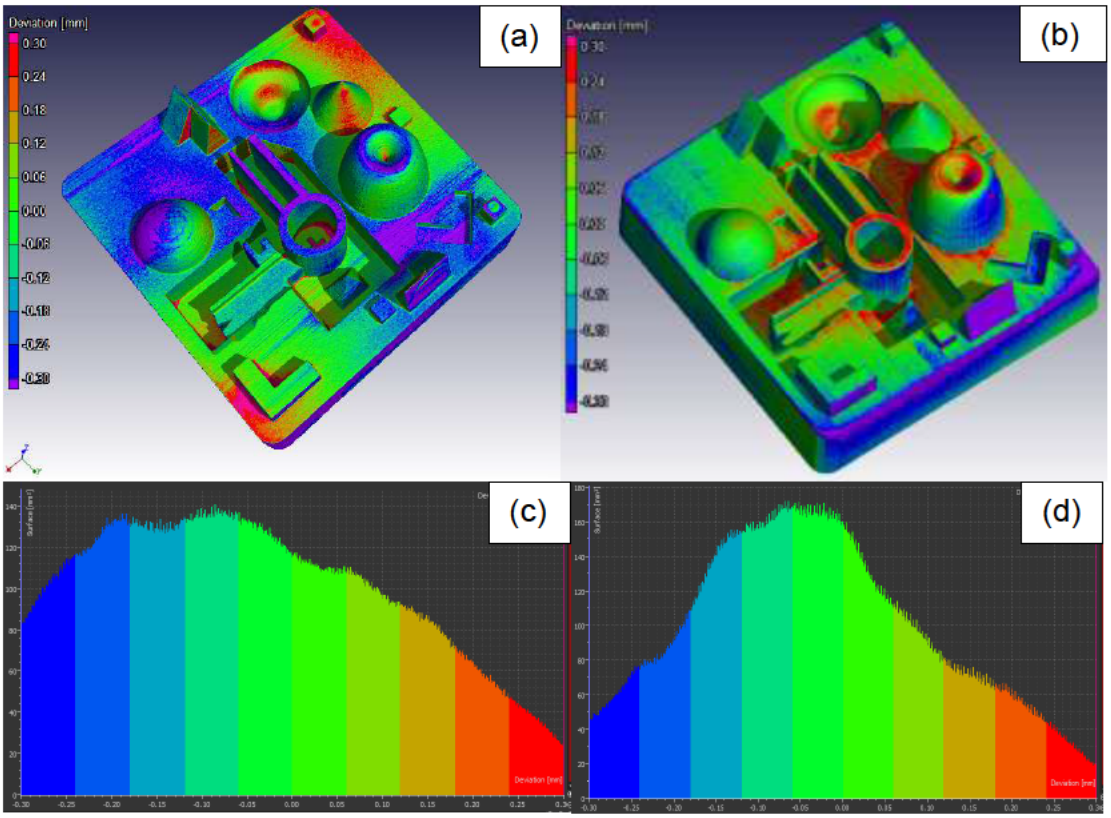


**Figure 4.7. Comparison between (a) PMMA and (b) PrimeCast® sacrificial patterns, (c) deviation histogram of PMMA pattern and (d) deviation histogram of PrimeCast® pattern**

The chart in Figure 4.8 represents the overall comparison between the sacrificial patterns used in this study. The comparison is based on the relative surface areas of the patterns under the deviation curves.

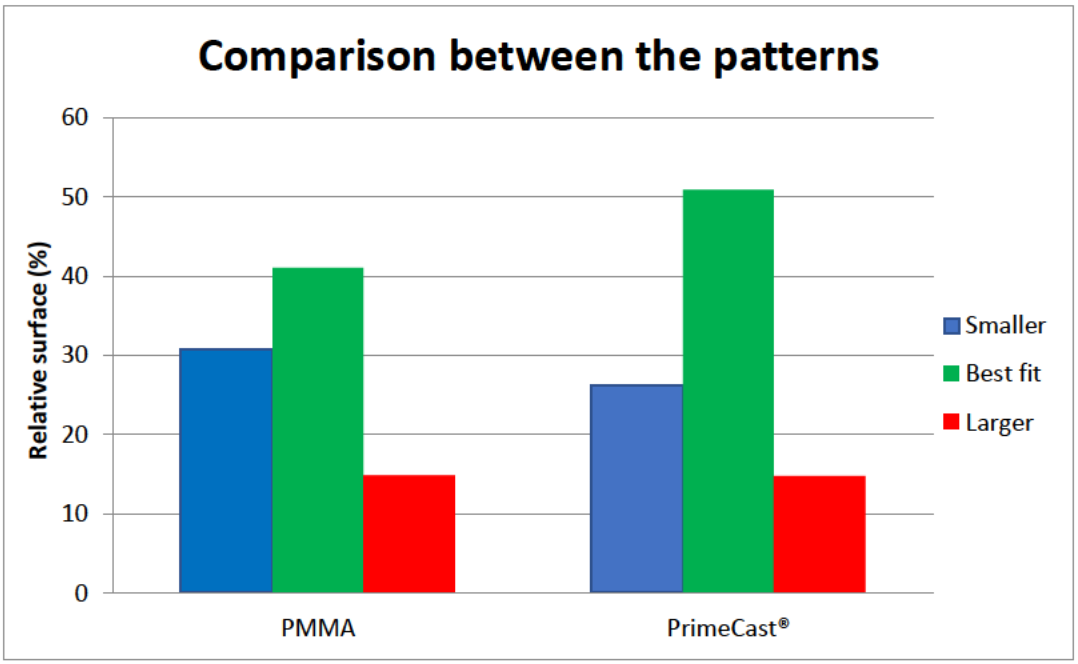


**Figure 4.8. Chart of the overall CT results of the PMMA and PrimeCast® patterns**

The overall relative surface area of the PMMA pattern between the tolerances -0.3 mm to 0.3 mm is 88% and that of PrimeCast® is 92%. The best fit for the PrimeCast® is 10% better than that of the PMMA, while there is 5% more blue on the PMMA pattern than that of the PrimeCast®. The red for both patterns is almost the same. The overall dimensional accuracy of both patterns is represented by green, blue, red and purple. There is no pink in either of the patterns signifying that there are no measured deviations from the CAD above 0.3 mm. This clearly indicates that PrimeCast® pattern is better than the PMMA pattern.

## 4.4 Overall accuracy of the castings

The micro-CT scanning results of the castings produced from the PrimeCast® and PMMA patterns were analysed similarly to the technique used with the patterns. Although two castings were scanned from both the PrimeCast® and PMMA patterns, only one casting from each pattern is discussed in this section. In this section, all the analysis was based on the tolerance range of -1.5 mm to 1.5 mm because above 95% of the total surface area of both castings was covered with this range. The results from the castings showed

pink and purple, indicating where the deviations of the parts from the CAD model were outside the parameters set for the analysis.

The scanning results for the second set of castings are presented in Appendix G.

### 4.4.1 CT scan to CAD comparison of casting from the PMMA pattern

Figure 4.9 shows the comparison of the CT-scanned casting from the PMMA pattern with the CAD model.

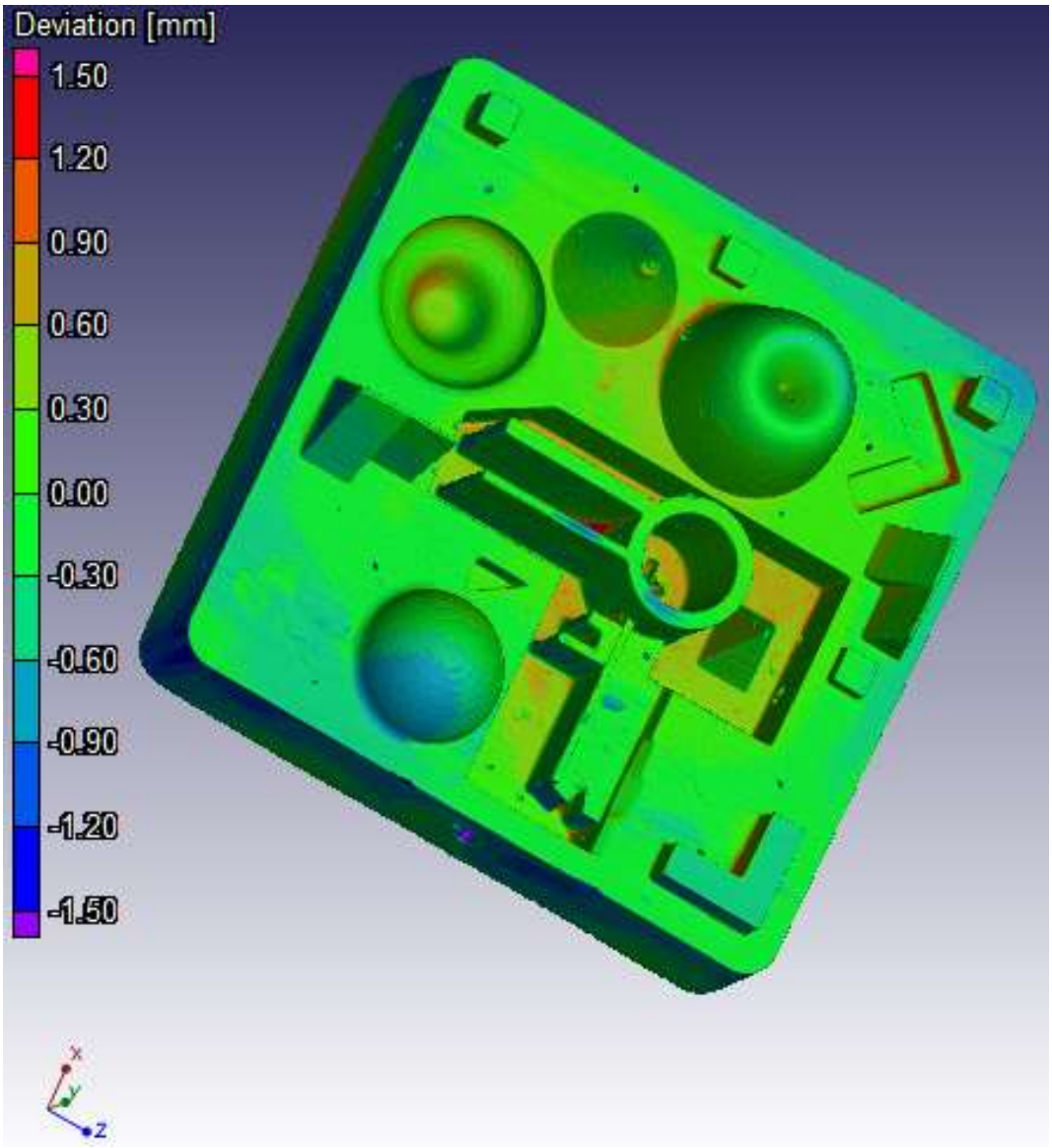


**Figure 4.9. Comparison of the CT-scanned casting from the PMMA pattern with the CAD model**

The comparison of the central area of the casting with the CAD indicated significant areas of green with smaller areas of blue and red. Purple and blue are mostly seen on the periphery of the casting, Green is seen on the top flat surfaces of the thin walls and flat surface of the rectangular hole and triangular hole. The cubes, located on the periphery of the casting, are green with tracess of both red and blue, while the half-cubes are green with hints of red and they are also situated on the peripheries of the casting. The wedges are mostly green with hints of red and blue, with the blue seen on the walls that are facing towards the peripheries of the casting. The sides of the half-sphere and freeform (conical) that are facing towards the periphery are predominantly blue.

The features that are at the centre of the casting are predominantly green with hints of red, while the inner surface of the hollow cyclinder is predominantly green. The pyramid is significantly green with drops red. The flat surface at the centre of the casting is predominantly green with traces of red, which is an indication of deviation around 1.5 mm. The vertical walls of the depression surrounding the pyramid and the hollow cylinder are predominantly green. The sides of the freeforms (conical and sinkhole) and cone that are facing the centre of the casting are predominantly green with hints of red.

Figure 4.10 shows the deviation distribution of the casting from the PMMA pattern, the X-axis range from -1.5 mm to 1.5 mm. Almost 98% of the total surface area of the casting was covered in this range. The shape of the deviation distribution of all points measured in the casting from PMMA pattern complies with a normal distribution with one peak. Green covers the largest area indicating good dimensional accuracy. Green is spread from -0.6 mm to 0.6 mm and it represents the highest fraction of the surface area. Blue is spread from -0.6 mm to 1.5 mm and covers 12% of the total surface area. Red covers 4% and its spread from 0.6 mm to 1.5 mm.

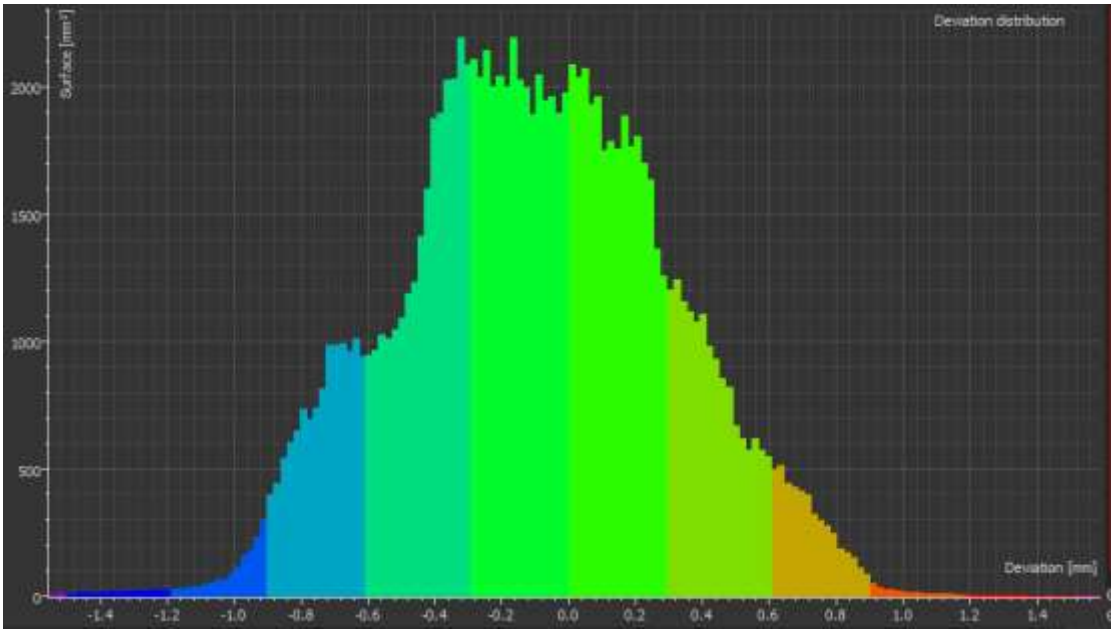


**Figure 4.10. Deviation histogram of the CT-scanned casting from the PMMA pattern as compared to the CAD model**

### 4.4.2 CT scan to CAD comparison of casting from the PrimeCast® pattern

Figure 4.11 shows the comparison of the CT-scanned casting from the PrimeCast® pattern with the CAD model. The casting from the PrimeCast® pattern indicates purple and blue on the surrounding walls of the part, while mostly green and red on the top flat surfaces. The constant sloping surfaces of the wedges are green, while the vertical surfaces facing towards the periphery of the casting are blue. The top flat surface of the rectangular protrusion is green and the vertical walls are blue. The two cubes have different dimensional accuracy, as seen from the colours on each cube. The one cube is green on the top flat surface and predominantly blue on the vertical surfaces, while the other is green on the top flat surface and predominantly red on the vertical surfaces. A similar tendency is seen with the half-cubes.

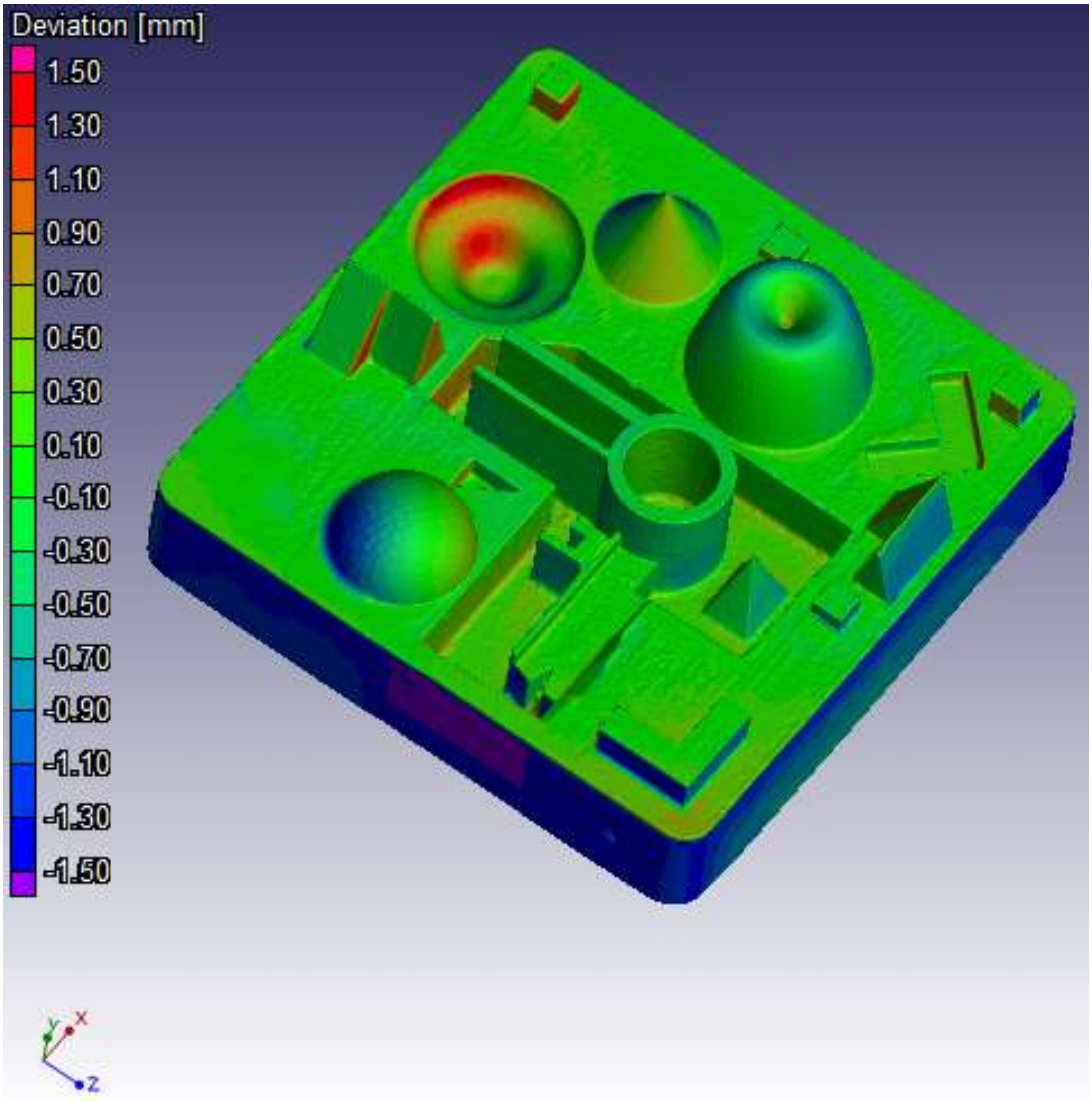


**Figure 4.11. Comparison of the CT-scanned casting from the PrimeCast® pattern with the CAD model**

The central features are predominantly green, with the flat surface of the centre depression being green with drops of red and the pyramid being green with traces of blue. The thin walls are green and the inner surface of the hollow cylinder is also green with traces of red, while the outer surface is green with areas of blue. The non-constant sloping profile of the freeform (conical) is predominantly red on the surface facing the periphery and green on the surface facing the centre of the part.

Figure 4.12 shows the deviation distribution of the casting from the PrimeCast® pattern. The X-axis range from -1.5 mm to 1.5 mm because 98% of the total surface area was covered in this range. The shape of the deviation distribution of all points measured in the casting from PrimeCast® pattern seem to have two peaks, the other at the centre and the other at far left. Green covers the 64% of the total surface area and it is spread from -0.6 mm to 0.6 mm representing the highest fraction of the surface area. Blue is spread from -0.6 mm to 1.5 mm and covers a significant total surface area of 22%. Red covers the remaining 12% and its spread from 0.6 mm to 1.5 mm.

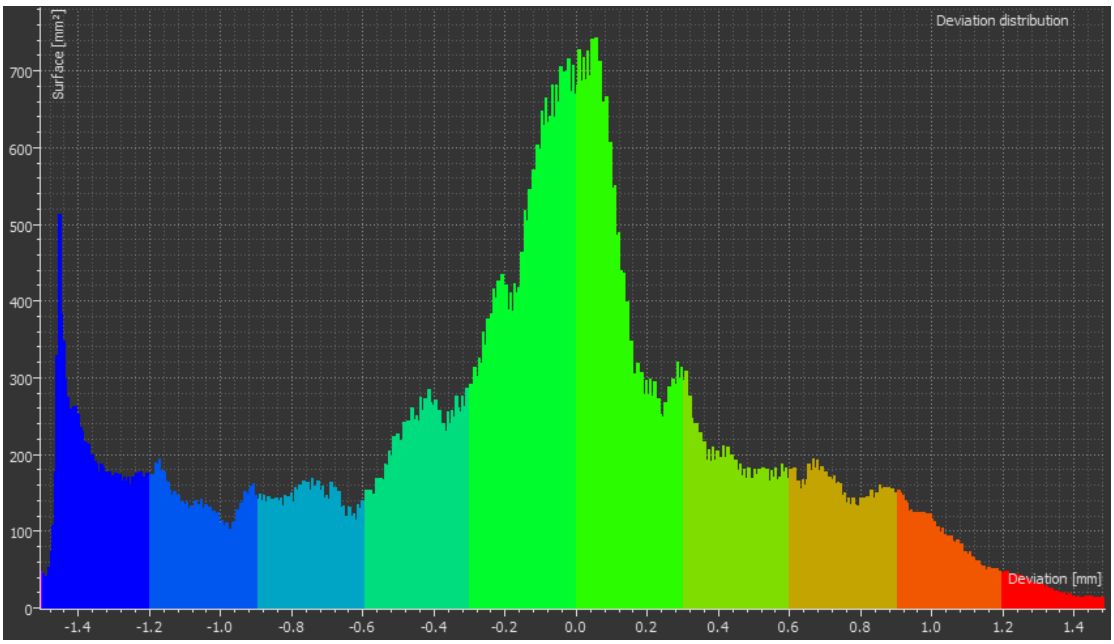


**Figure 4.12. Deviation histogram of the CT-scanned casting from the PrimeCast® pattern as compared to the CAD model**

### 4.4.3 Comparison of the castings from the two types of pattern

The outer walls of both castings are predominantly purple, that is, they are significantly smaller than -1.5 mm. Towards the part periphery the flat surface of the casting from the PMMA pattern is covered in red, green and blue, while that from the PrimeCast® pattern is covered predominantly blue with hints of purple. The rectangular protrusion on the casting from the PMMA pattern is fully covered in green, while that from the PrimeCast® pattern is mostly green on the top flat surface with blue on the vertical surfaces. The inner flat surface of the central depression of the casting from the PMMA pattern is covered in

green with hints of red while that of casting from the PrimeCast® pattern mainly green as show in Figure 4.13.

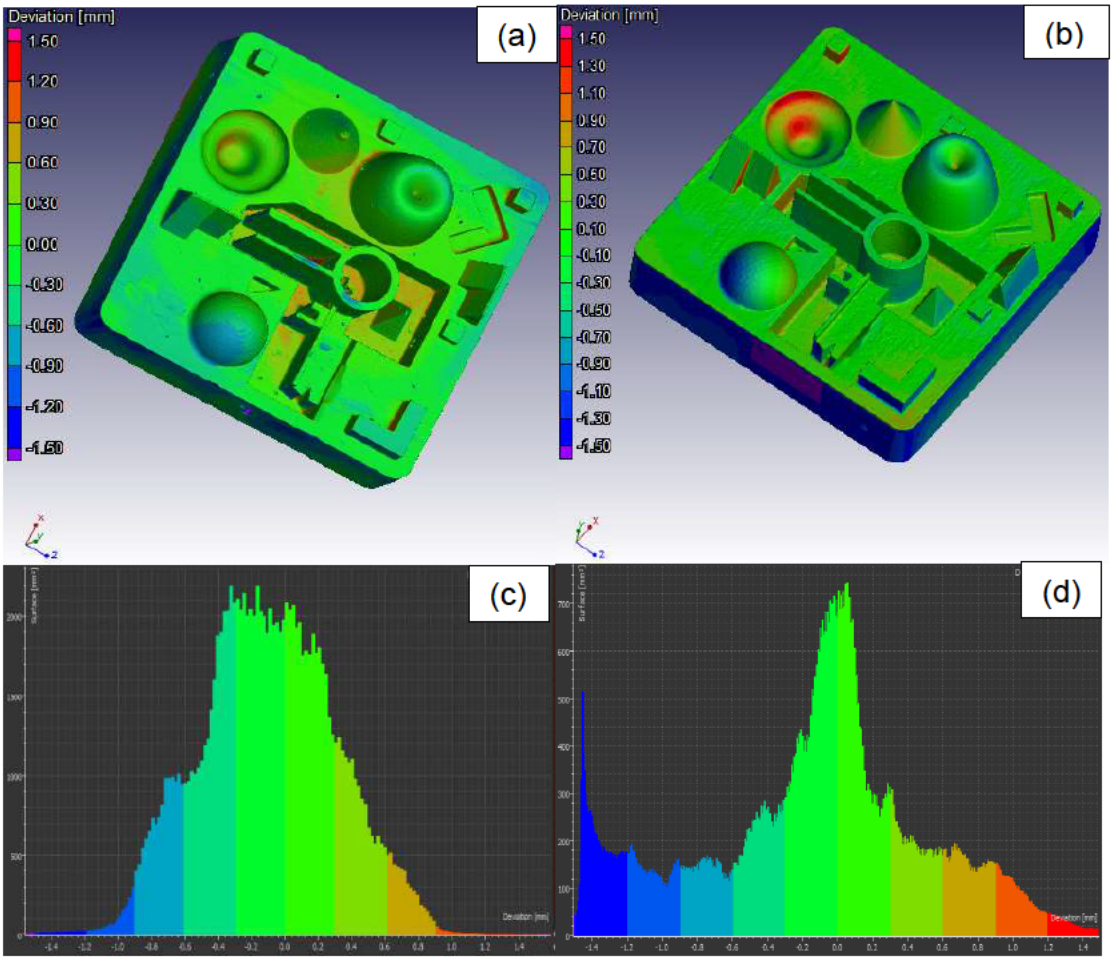


**Figure 4.13. Comparison between the castings from (a) the PMMA and (b) the PrimeCast® sacrificial pattern, and (c) deviation histogram of PMMA pattern and (d) deviation histogram of casting from PrimeCast® pattern**

The surrounding walls of the central depression of the both castings are predominantly green. The flat top surfaces of the hollow cylinder and the thin walls are mostly green for castings from PrimeCast® pattern while that from PMMA pattern are green with traces of blue. The cones on the casting from PrimeCast® pattern is hinted in blue on the surface facing the periphery and hinted red on the one facing the centre of the casting. While the cone from casting from PMMA pattern is predominantly green. The half-spheres on both castings are relatively green. The half-sphere for both castings are

predominantly green with traces of blue on the surfaces facing the periphery of the casting.

The deviation distribution of the casting from PMMA and PrimeCast® pattern are compared in Figure 4.13 (c) and (d) respectively. The peaks of both histograms are almost at the centre of the distribution, although the casting from PrimeCast® pattern has another peak at left. The deviation distribution of the casting from PMMA pattern has significantly higher green surface area than that from the PrimeCast® pattern. The blue in the castings from PrimeCast® pattern is significantly higher than that from PMMA pattern.

The results from the deviation distribution from both castings are represented in a bar chart Figure 4.14.

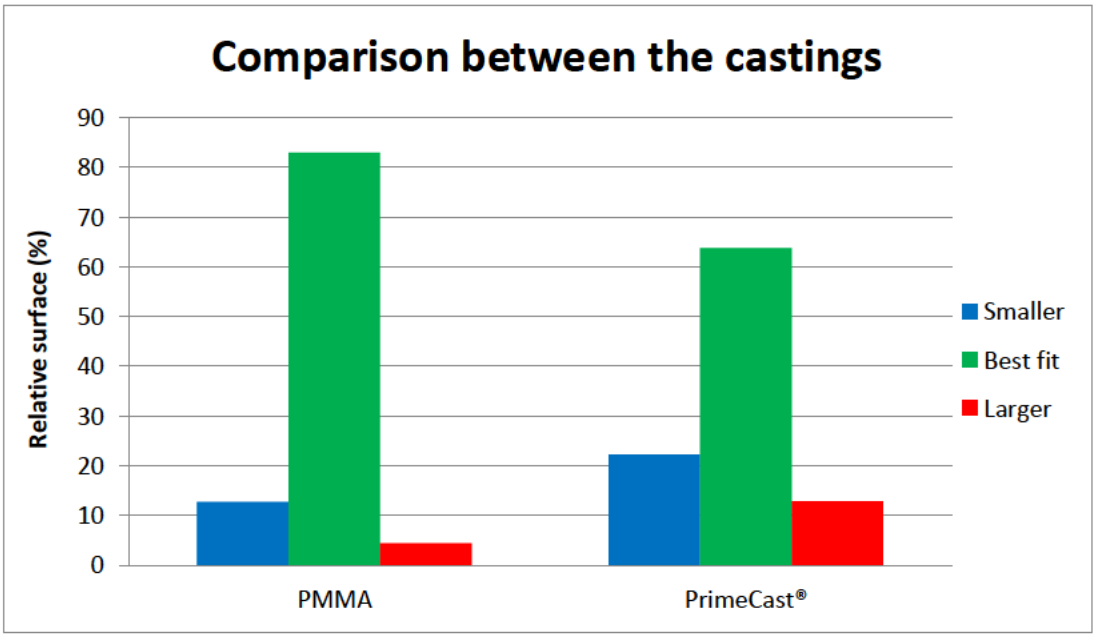


**Figure 4.14. Chart of the comparison between the castings from the two sacrificial patterns**

The overall relative surface area of both castings is 98% in the measurement range (-1.5 mm to 1.5 mm). The significant difference is seen on the area covered in green, where casting from the PMMA pattern covers about 82% of the total surface area and casting from the PrimeCast® pattern covers 64%. In both castings, the area covered in green is followed with the one that is

covered in blue. Casting from the PMMA pattern covers 12% and that from PrimeCast® pattern covers 22% of the total surface area. The area covered in red is significantly smaller for both castings, this is to say there was no extra metal on the castings.

## 4.5 Comparison between patterns and castings

A summary of the statistical comparison between the patterns and their corresponding castings, as related to the dimensions of the CAD model, is tabulated in Table 4.1. The statistical comparison was done with the tolerance range of -0.3 mm to 0.3 mm for both patterns and castings.

**Table 4.1. Comparison between the patterns and their corresponding castings, both related to the CAD model**

| ***Statistics*** | ***Patterns*** | | ***Castings*** | |
|---|---|---|---|---|
| | ***PMMA*** | ***PrimeCast®*** | ***PMMA*** | ***PrimeCast®*** |
| **Mean deviation from the CAD (mm)** | -0.04 | -0.03 | -0.02 | -0.01 |
| **Standard deviation (mm)** | 0.15 | 0.14 | 0.17 | 0.15 |
| **Percentage within measurement range (%)** | 87.65 | 92.47 | 51.82 | 44.67 |

The relative surface areas of the castings complying with the CAD are generally less as compared to their corresponding patterns for the tolerance range from -0.3 mm to 0.3 mm. The casting from the PMMA pattern is 35.83% less accurate than the relative surface area of its corresponding pattern, while the casting from the PrimeCast® pattern is 47.67% less accurate than the relative surface area of the corresponding pattern. In both cases, the mean deviations of the castings from the CAD are smaller than those of their corresponding patterns.

For direct comparison, the results of the PMMA pattern and its corresponding casting are represented side by side in Figure 4.15. The range of deviation distribution of the casting was changed to -0.3 mm to 0.3 mm so that the

range (on the X-axis) can be the same for both pattern and casting for ease of analysis. Therefore, this resulted in a different casting results than the ones in section 4.4.1 and 4.4.2 above.

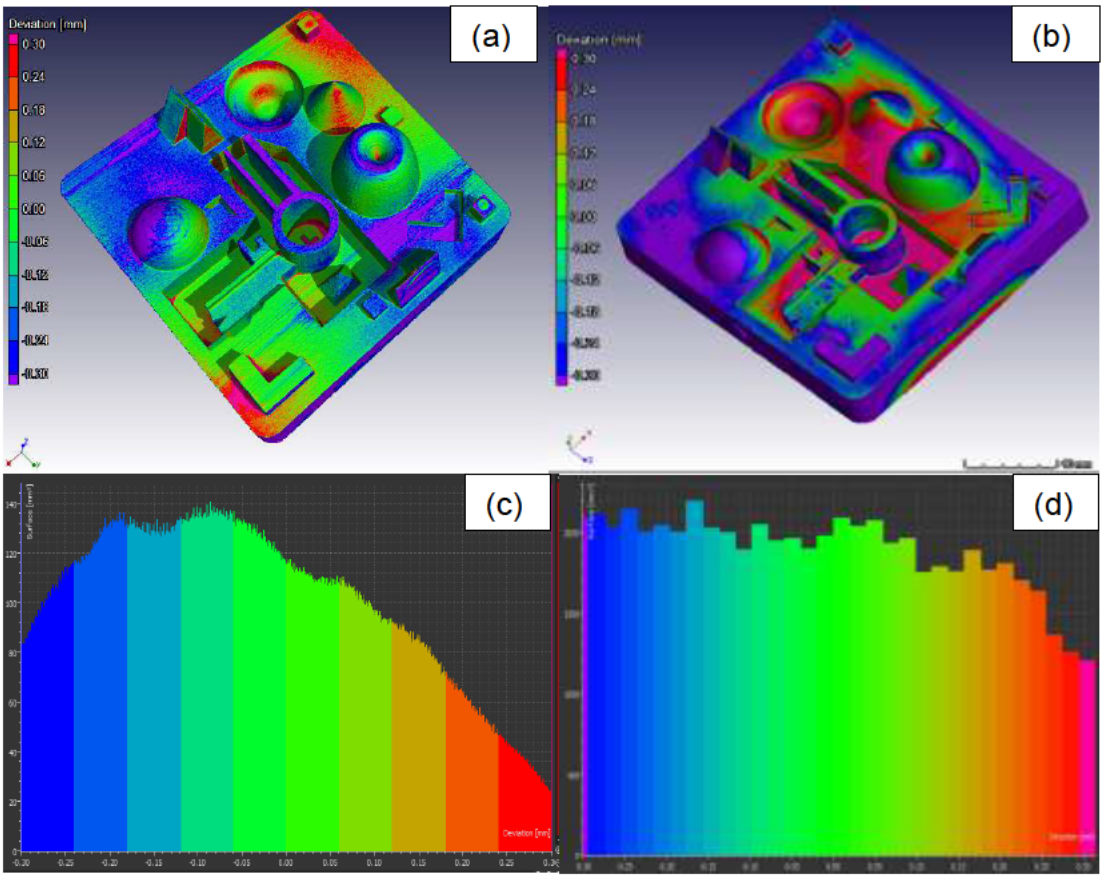


**Figure 4.15. (a) PMMA pattern, (b) casting from the PMMA pattern, (c) deviation histogram of PMMA pattern and (d) deviation histogram of casting from PMMA pattern**

The peripheries of the PMMA casting are mainly covered in purple, while that of pattern is covered in different colours. The cube on the right and the rectangular protrusion of the PMMA casting are fully covered in purple, while that of the pattern are both covered in green and blue. The freeform (sinkhole) had hints of red on its surface on the pattern, but for the PMMA casting, most of the surface is red and pink with smaller green areas. The rectangular protrusion of the casting is fully covered in purple while that of pattern is green on the top flat surface with hint of purple on the vertical surfaces. The inner flat surface at the centre of the casting is covered in pink, while that of the

pattern is predominantly green with hints of red. The top flat surfaces of the thin flat walls of the casting are largely green with hints of purple while that of the pattern are fully covered in purple. The pyramid from both pattern and casting has almost the same dimensions because the colours covering it are almost the same.

The shape of the deviation distribution from this range of points on the casting from the PMMA pattern is almost flat, as shown in Figure 4.15d. Green is spread from -0.12 mm to 0.12 mm showing the highest fraction of the total area of the casting.

Figure 4.16 shows the results of the PrimeCast® pattern and its corresponding casting.

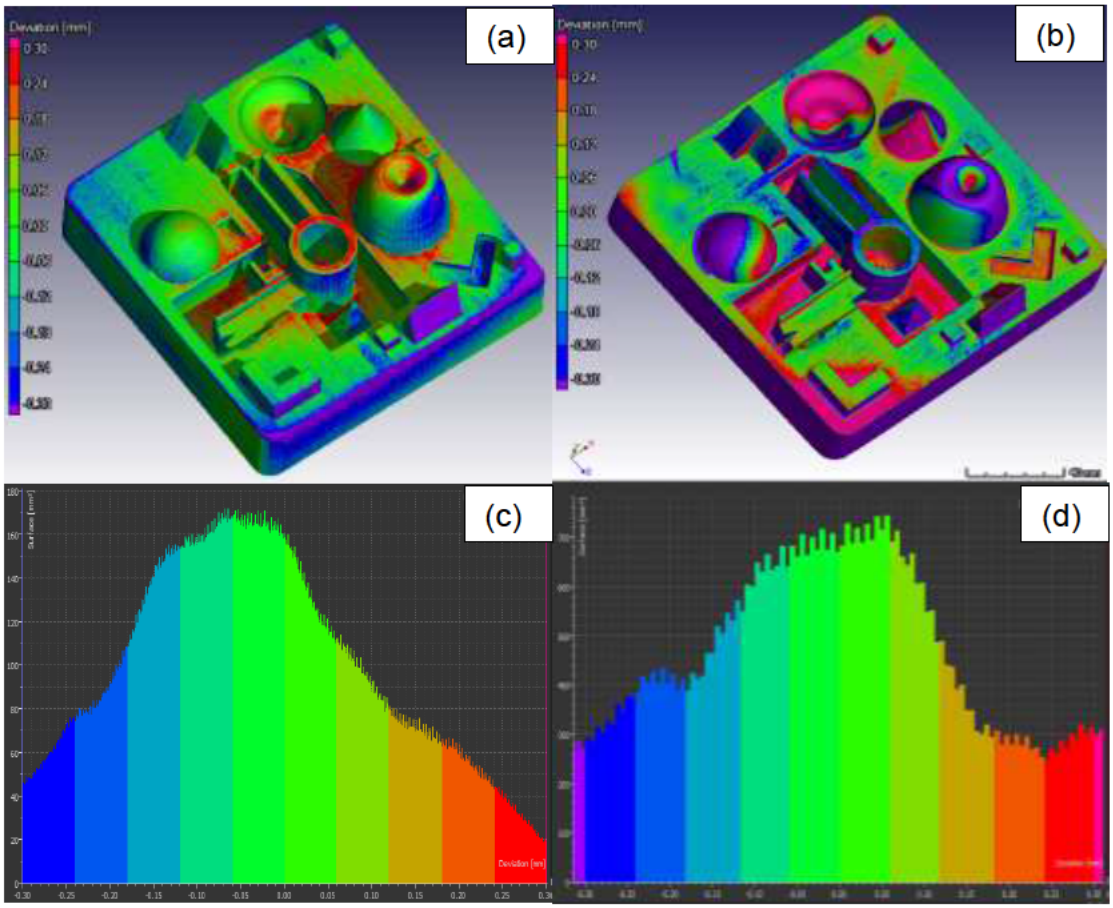


**Figure 4.16. (a) PrimeCast® pattern, (b) casting from PrimeCast® pattern, (c) deviation histogram of PrimeCast® pattern and (d) deviation histogram of casting from PrimeCast® pattern**

The cone on the PrimeCast® pattern is covered fully in green while that of the casting is covered in pink and purple and so is the half-sphere. The surrounding walls of pattern are covered in blue with hint of green while that of the casting is fully covered in purple. The flat surface of the hollow cylinder was covered in red with a hint of green on the pattern but on the casting, it was predominantly green. The top flat surface of the rectangular protrusion of both pattern and casting is covered in green. The pyramid and half-cube next to the wedges of both the pattern and casting have almost the same dimension as the colours covering them are almost the same on all surfaces. The inner flat surface at the centre of the casting is covered in pink while that of pattern is primarily red with a hint of green.

Purple is mostly seen on the features of the casting which had a hint of blue on the pattern, and pink is seen on the features of the casting that were hinted in red on the pattern. The shape of the deviation distribution from this range of points on the casting from the PrimeCast® pattern complies with a normal distribution, with the peak at the centre of the deviation range, as shown in Figure 4.16.

## 4.6 Casting defects

Another factor that influenced the dimensional accuracy of the casting results was the presence of casting defects, as shown in Figure 4.17. The geometrical results showed casting defects that could be associated with bubbles, which might have been entrapped in the pattern wall by the primary slurry during mould making. As shown in Figure 4.17a, they appear as small, smooth spherical- or oval-shaped excess metal on the casting. There are noticeable irregularly shaped masses on the casting represented in pink on the 3D view.

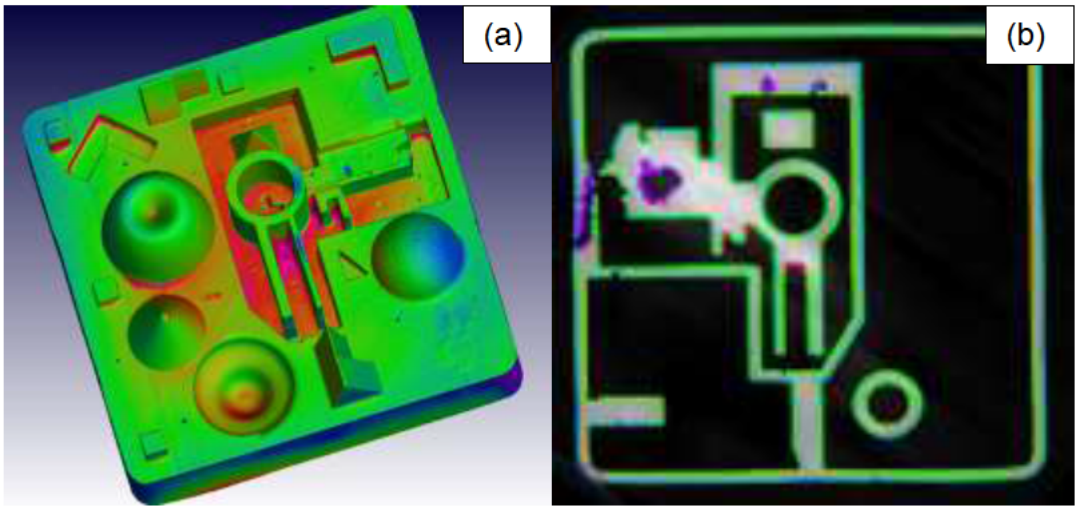


**Figure 4.17. Casting defects on a casting: (a) 3D view (a) and (b) sectional view**

On the surface of the cast part, there were round smooth-walled cavities of varying diameter that exhibited slightly oxidized surfaces. These were the result of gas entrapment: during casting, turbulent flow mixes the air that is exiting the mould with the metal that is entering. These bubbles float to the surface of the metal but are trapped by the solidifying metal [86].

There was shrinkage in the gate, which appears as an opening from the outside to the inside at the place where the gating was attached to the pattern and is presented in purple, as seen on the sectional view in Figure 4.17b. This is due to the molten alloy shrinking as it solidifies and inadequate feeding of the metal from the gating system to prevent a cavity from forming.

Visual inspection revealed there was excess metal on the slot towards the centre of the cast part. This appeared as an irregularly shaped mass attached to the casting. It might have been due to failing of thin or weak areas of the shell during dewaxing or casting, allowing metal to leak into the void in the shell.

# Chapter 5: Conclusions and Future work

## 5.1 Conclusions

In this study, comparisons were done between the CAD design and the patterns built from two different AM technologies, namely laser sintering of PrimeCast® material and binder jetting of PMMA. From the pattern results it can be concluded that both technologies were able to produce the selected test part within acceptable tolerances, but it was also clear that they did not achieve the same accuracy. Based on the pattern results, the PrimeCast® pattern performed slightly better than the PMMA pattern in terms of accuracy compared to the CAD model. For both patterns, the outer walls of the patterns had slightly smaller dimensions than the CAD model. Patterns produced from both AM technologies offers an effective tool-less solution for IC patterns as opposed to wax patterns.

As other authors discovered, in this study it was also found that in IC using AM patterns, a special method is still required to remove a pattern from the mould cavity. Shell cracking was experienced with the initial PrimeCast® patterns and a redesign method had to be established to avoid this. With the modified designs there was no shell cracking during the burnout process with the laser power settings of the laser sintering machine at 75% and 80% of full power. The PrimeCast® patterns that were built with laser power of 85% to 90% caused shell cracking during the burnout process. There was no shell cracking experienced with the PMMA pattern.

In this study, the use of the PrimeCast® and PMMA materials as sacrificial patterns for the IC process has been validated: Aluminium A356 was successfully cast from the two types of sacrificial patterns. PrimeCast® patterns need more care during mould making and the burnout process compared to PMMA patterns. The need for removal of vents from castings produced from PrimeCast® patterns through grinding may impact negatively on the accuracy of these castings.

Castings from PMMA patterns show less differences in dimensional deviation compared to castings from PrimeCast® patterns. Like patterns, the castings still indicate small dimensions on the surrounding walls. As seen from the results there were no feature with sharp corners and edges that was replicated well on the final casting. AM patterns are built in layer upon layer, which means the build layer edges may be reproduced in the casting surface (staircase effect) and should not be misinterpreted as casting defects during inspection process.

It is clear from the results obtained that for castings produced from PrimeCast® and PMMA patterns, typical deviations of ±1.5 mm on average can be expected. The standard part used for this study had sharp edges and corners. From visual inspection of the built AM patterns it was evident that the sharp edges and corners were not well-replicated, which confirmed that this remains a challenge for these AM technologies. Small triangular holes and cross-shaped holes were also not copied well from the CAD model to the AM part.

From the results of this study, a general statement on which type of pattern produced the best casting is not possible. For simpler shapes, both technologies provide rather good results as evidenced by cubes, rectangular protrusions and pyramid. However, for complex shapes such as thin walls, freeforms (sinkhole and conical) and cones both technologies did not perform quite well, somewhat PrimeCast® better than PMMA. Each pattern type had its advantages and limitations, which will influence selection of a specific technology depending on the end user's application.

## 5.2 Recommendations for future work

Future studies should aim at improving the dimensional accuracy of the two patterns by optimising the process parameters with regard to the following:

- Orientation of the part in the AM machine (0º, 45º, 90º);
- Compensation for shrinkage of the part during building;
- The temperature and build speed during the building process;
- Layer thickness;
- Wax infiltration.

# References


1. J. E. Fritz, “The Investment Casting Process,” https://www.investmentcasting.org/uploads/8/1/9/8/81988734/the_investment_casting_process_-_website.pdf [Accessed: 10-Jan-2018].
2. S. Pattnaik, D. B. Karunakar, and P. K. Jha, “Developments in investment casting process – A review,” *Journal of Materials Processing Technology*, vol. 212, no. 11, pp. 2332–2348, 2012.
3. K. Dotchev and S. Soe, “Rapid manufacturing of patterns for investment casting: Improvement of quality and success rate,” *Rapid Prototyping Journal*, vol. 12, no. 3, pp. 156–164, 2006.
4. “South Africa aiming to become a leader in additive manufacturing.” http://www.engineeringnews.co.za/article/south-africa-aiming-to-become-a-leader-in-additive-manufacturing-2015-12-04. [Accessed: 01-Feb-2016].
5. J. Gardan, “Additive manufacturing technologies : state of the art and trends,” *International Journal of Production Research*, vol. 7543, pp. 1–15, 2016.
6. J. P. Kruth, M. C. Leu, and T. Nakagawa, “Progress in Additive Manufacturing and Rapid Prototyping,” *CIRP Annals - Manufacturing Technology*, vol. 47, no. 2, pp. 525–540, 1998.
7. N. Guo and M. C. Leu, “Additive manufacturing : technology, applications and research needs,” *Front. Mech. Eng.*, vol. 8, no. 3, pp. 215–243, 2013.
8. D. Dimitrov, P. A. Hugo, and B. Deez, “Suitability of Layer Manufacturing Technologies for Rapid Pattern Making in Investment Casting of Light Metals,” *Proceedings of the 9th Annual RAPDASA International Conference*, Central University of Technology, Free State, 13–15 November 2008, pp. 1–14, 2008.
9. S. Wang, C. Shih, and X. He, “A Study on Investment Casting Directly with Plastic Rapid Prototype Patterns,” *Journal of Materials Science and Engineering*, vol. 4, no. 11, pp. 21–25, 2010.
10. R. Bott, “Dimensional accuracy of PMMA casting patterns produced by 3D printing after impregnation,” *Igarss 2014*, no. 1, pp. 1–5, 2014.

11. B. Ian, G. Deakin, and D. Rosen, "'Additive Manufacturing Technologies : 3D Printing, Rapid Prototyping, and Direct Digital Manufacturing ', 2nd Edition," no. 3, pp. 193–198, 2015.
12. T. J. Horn and O. L. Harrysson, "Overview of current additive manufacturing technologies and selected applications," *Science progress*, vol. 95, pp. 255–282, 2012.
13. T. Mueller, "A Comparison of 3D Printing Technologies Used to Make Investment Casting Patterns –," https://www.slideshare.net/TomMueller1/a-comparison-of-3d-printing-technologies-used-to-make-investment-casting-patterns-part-3 [Accessed 05-Jun-2018].
14. S. P. Soe and D. R. Eyers, "Property modelling FEA support structure generation for the additive manufacture of CastForm polystyrene patterns," *Polymer Testing*, vol. 33, pp. 187–197, 2014.
15. "Incorporation of new technologies in the European precision foundry industry," http://citeseerx.ist.psu.edu/viewdoc/download?doi=10.1.1.136.3432&rep=rep1&type=pdf [Accessed 18-April-2016].
16. ASTM International, "F2792-12a – Standard Terminology for Additive Manufacturing Technologies," 2012.
17. K. V. Wong and A. Hernandez, "A Review of Additive Manufacturing," *ISRN Mechanical Engineering*, vol. 2012 (2012), Article ID 208760, pp 1–10, 2012.
18. "Additive Manufacturing Technology Assessment," https://www.energy.gov/sites/prod/files/2015/02/f19/QTR%20Ch8%20-%20Additive%20Manufacturing%20TA%20Feb-13-2015_0.pdf [Accessed 10-Jan-2016].
19. "Implementing the South Africa additive manufacturing technology roadmap," *South African Journal of Industrial Engineering*, vol. 26, no.2, pp. 85–92, 2015.
20. "Investment Casting vs. Additive Manufacturing in Airbus Study." http://foundrymag.com/simulationit/investment-casting-vs-additive-manufacturing-airbus-study [Accessed: 02-Feb-2016].

21. A. Amendola, E. Hernández-Nava, R. Goodall, I. Todd, R. E. Skelton, and F. Fraternali, “On the additive manufacturing, post-tensioning and testing of bi-material tensegrity structures,” *Composite Structures*, vol. 131, pp. 66–71, 2015.
22. M. M. Ghazy, “Development of an Additive Manufacturing Decision Support System (AMDSS*)” A thesis submitted to the Faculty of Science, Agriculture and Engineering for the Degree of Doctor of Philosophy by October 2012* School of Mechanical and Systems Engineering,” October, 2012.
23. B. Conner, “Making sense of 3-D printing : Creating a map of additive manufacturing products and services,” *Additive Manufacturing*, vol. 1–4, pp. 64–76, 2014.
24. M. Kathryn *et al.*, “CIRP Annals – Manufacturing Technology Design for Additive Manufacturing : Trends, opportunities, considerations, and constraints,” *CIRP Annals – Manufacturing Technology.*, vol. 65, no. 2, pp. 737–760, 2016.
25. D. Dimitrov, K. Schreve, N. De Beer, P. Christiane, S. Africa, and S. Africa, “Three Dimensional Printing in the South African Industrial Environment of 3D Printers Year,” *South African Journal of Industrial Engineering*, vol. 19, no 1., pp. 195–213, 2008.
26. D. Drummer, D. Rietzel, and F. Kühnlein, “Development of a characterization approach for the sintering behavior of new thermoplastics for selective laser sintering,” *Physics Procedia 5*, vol. 5, no. 2, pp. 533–542, 2010.
27. “EOS Industrial 3D printing – Process, method and benefits.” [Online]. Available: http://www.eos.info/additive_manufacturing/for_technology_interested [Accessed: 01-Feb-2016].
28. D. D. Gu, W. Meiners, K. Wissenbach, and R. Poprawe, “Laser additive manufacturing of metallic components: materials, processes and mechanisms,” *Int. Mater. Rev.*, vol. 57, no. 3, pp. 133–164, 2012.
29. S. Junk and M. Tränkle, “Design for additive manufacturing technologies: New applications of 3d-printing for rapid prototyping and rapid tooling,” in

*ICED 11 – 18th International Conference on Engineering Design – Impacting Society Through Engineering Design*, vol. 5, pp. 12–18, 2011.

30. R. D. Goodridge, C. J. Tuck, and R. J. M. Hague, “Laser sintering of polyamides and other polymers,” *Prog. Mater. Sci.*, vol. 57, no. 2, pp. 229–267, 2012.
31. E. Bassoli, A. Gatto, L. Iuliano, and M. Grazia Violante, “3D printing technique applied to rapid casting,” *Rapid Prototyp. J.*, vol. 13, no. 3, pp. 148–155, 2007.
32. J. W. Stansbury and M. J. Idacavage, “3D printing with polymers : Challenges among expanding options and opportunities,” *Dent. Mater.*, vol. 32, no. 1, pp. 1–11, 2015.
33. P. Central, “Selective laser sintering : Applications and technological capabilities,” *Journal of Engineering Manufacture*, vol. 213, no. 5, pp. 435–449, 1999.
34. S. S. Gill and M. Kaplas, “Efficacy of powder-based three-dimensional printing (3DP) technologies for rapid casting of light alloys,” *The International Journal of Advanced Manufacturing Technology*, vol. 143521, pp. 53–64, 2011.
35. J. A. Slotwinski, “Additive Manufacturing : Overview and NDE Challenges 1,” https://ws680.nist.gov/publication/get_pdf.cfm?pub_id=914545 [Accessed 01-Jun-2017].
36. J. Stampfl and M. Hatzenbichler, “Additive Manufacturing Technologies”, *CIRP Encyclopedia of Production Engineering,* 2014.
37. “Binder Jetting –Additively – your access to 3D printing.” https://www.additively.com/en/learn-about/binder-jetting [Accessed: 01-Feb-2016].
38. J. Glasschroeder, E. Prager, and M. F. Zaeh, “Powder-bed-based 3D-printing of function integrated parts,” *Rapid Prototyping Journal*, vol. 21, no. 2, pp. 207–215, 2015.
39. C. Polzin, S. Spath, and H. Seitz, “Characterization and evaluation of a PMMA-based 3D printing process printing process,” *Rapid Prototyping Journal*, vol. 19, no. 1, pp. 37–43, 2013.
40. W. Everhart, S. Lekakh, V. Richards, J. Chen, H. Li, and K.

Chandrashekhara, “Corner Strength of Investment Casting Shells,” *International Journal of Metal casting,* vol. 7, no. 1, pp. 21–27, 2013.

41. J. S. Tu, D. M. Olinger, and A. M. Hines, “Computer-Aided Development of an Investment Casting Process,” *The Journal of the Mineral, Metal and Material Society,* vol. 45, no. 10, pp. 29–32, 1993.
42. W. Abdul-karem, N. Green, and K. F. Al-raheem, “Vibration-assisted filling capability in thin wall investment casting,” *The International Journal of Advanced Manufacturing Technology,* vol. 61, no. 9–12, pp. 873–887, 2012.
43. C. M. Cheah, C. K. Chua, C. W. Lee, C. Feng, and K. Totong, “Rapid prototyping and tooling techniques: a review of applications for rapid investment casting,” *The International Journal of Advanced Manufacturing Technology*, vol. 25, no. 3–4, pp. 308–320, 2005.
44. S. Jones and C. Yuan, “Advances in shell moulding for investment casting,” *Journal of Materials Processing Technology*, vol. 135, no. 2–3, pp. 258–265, 2003.
45. R. Prasad, “Progress in Investment Castings,” https://www.intechopen.com/books/science-and-technology-of-casting-processes/progress-in-investment-castings [Accessed 20-Feb 2016].
46. S. U. Adikary, “Design and development of ceramic mould for high precision investment casting,” https://pdfs.semanticscholar.org/e2a3/e66b1ba9745a20fa8db3eb0c252b01ba1c9a.pdf [Accessed 20-Jan-2017]
47. S. Mishra and R. Ranjana, “Reverse Solidification Path Methodology for Dewaxing Ceramic Shells in Investment Casting Process Reverse Solidification Path Methodology for Dewaxing,” *Materials and Manufacturing Processes,* vol. 25, no. 12, pp. 1385–1388, 2010.
48. “Investment Castings, Investment Casting Process – Paramount Industries.” http://www.paramountind.com/investment-casting.html [Accessed: 13-Feb-2016].
49. X. Chen, D. Li, H. Wu, and Y. Tang, “Analysis of ceramic shell cracking in stereolithography-based rapid casting of turbine blade,” *The International Journal of Advanced Manufacturing Technology,* vol. 55, no. 5–8, pp. 447–

455, 2011.

50. "Recommended Burnout Process," https://manufat.com/download/Formlabs_Castable_TDS.pdf [Accessed 10-Jan-2018].
51. M. F. M. Omar, S. Sharif, M. Ibrahim, H. Hehsan, M. N. M. Busari, and M. N. Hafsa, "Evaluation of Direct Rapid Prototyping Pattern for Investment Casting," *Advanced Materials Research,* vol. 463–464, pp. 226–233, 2012.
52. S. Wang, A. G. Miranda, and C. Shih, "A Study of Investment Casting with Plastic Patterns," *Materials and Manufacturing Processess*, vol. 25, no. 12, pp. 1482–1488, 2010.
53. Eagle Engineered Solutions, INC., "Rapid Additive Manufactured Investment Casting Ceramic Cores Technology and Application Update," *Investment Casting Institute Fall Conference and Technical meeting paper,* pp. 1–6, 2013.
54. S. Pattnaik, D. B. Karunakar, and P. K. Jha, "Developments in investment casting process – A review," *Journal of Materials Processing Technology*, vol. 212, no. 11, pp. 2332–2348, 2012.
55. O. M. F. Marwah, M. S. Shukri, E. J. Mohamad, M. A. Johar, and R. H. A. Haq, "Direct Investment Casting For Pattern Developed By Desktop 3D Printer Pattern," *8th International Conference on Mechanical and Manufacturing Engineering 2017,* vol. 135, pp. 1–8, 2017.
56. M. Seals, S. R. McKinney, P. J Stockhausen, S. R. Bottoms and A. P. Druschitz, "Evaluation Of 3D Printed Polymers For Investment Casting Expendable Patterns," *Transactions of the American Foundry Society*, vol. 122, pp.145–160, 2014.
57. M. Truscott, D. De Beer, L. Barnard, and G. Booysen, "Rapid prototyping techniques in medical sector," *Journal for New Generation Sciences – Rapid prototyping techniques in medical sector,* vol. 3, no. 1, pp. 148–159, 2005.
58. S. S. Ohol, "Improvisations in Investment Casting process using Economical Automation," https://www.researchgate.net/publication/299410941_Improvisations_in_Investment_Casting_process_using_Economical_Automation [Accessed 10-

Mar-2017].

59. "Additive Manufacturing Reduces Costs for Investment Casting." http://www.rapidreadytech.com/2014/03/additive-manufacturing-reduces-costs-for-investment-casting/ [Accessed: 01-Feb-2016].
60. "Material data sheet PrimeCast® 101 for EOSINT P Application," http://additivemanufacturingllc.com/wp-content/uploads/2015/04/Prime-Cast.pdf [Accessed 20-Feb-2016].
61. "Application notes PrimeCast 101 Reference documents Application notes," vol. 49, no. 0, pp. 1–8.
62. "Application notes Wax infiltration of parts made of PrimeCast® 101," vol. 49, no. 0, pp. 1–6.
63. M. Vasquez, "Analysis and Development of New Materials for Polymer Laser Sintering," A Doctoral Thesis. Submitted in partial fulfilment of the requirements for the award of Doctor of Philosophy of Loughborough University, pp. 1–21, 2012.
64. "Material data sheet for plastic parts," https://arti90.com/wp-content/uploads/2018/01/plastik.pdf [Accessed 20-Feb-2016].
65. M. Träxler, J. Ackermann, M. Juda, and D. Hirsch, "Polymethyl methacrylate (PMMA)," *Kunststoffe International journal*, vol. 101, no. 10, pp. 42–44, 2011.
66. R. Singh and M. Verma, "Investigations for reducing wall thickness of aluminium shell casting using three dimensional printing," *Journal* of *Achievements* in *Materials and Manufacturing Engineering,* vol. 31, no. 2, pp. 565–569, 2008.
67. "A356.0 Aluminium Casting Alloy (7Si-0.3Mg)," https://ahead4-hadleigh-castings.s3.eu-west-2.amazonaws.com/content/9be6417437c62c701d950454bd4d7756.pdf [Accessed 10-Jan-2016].
68. "Expanded Polystyrene (EPS) Pattern Application in Investment Casting and Chemical Removing," *Ceramic Materials,* vol. 63, no. 1, pp. 138–142, 2011.
69. M. Aliakbari, "Additive Manufacturing : State-of-the-Art, Capabilities, and Sample Applications with Cost Analysis," *Master of Science Thesis,*

*Production Engineering and Management, Department of Industrial Production, KTH Royal Institute of Technology*, 2012.

70. A. Bencomo, R. Bisbal and R. Morales, “Simulation of the aluminum alloy A356 solidification cast in cylindrical,” *Matéria (Rio Janeiro)*, vol. 13, no. 2, pp. 294–303, 2008.
71. M. Hajkowski, Ł. Ber, and J. Hajkowski, “Mechanical Properties of Al-Si-Mg Alloy Castings as a Function of Structure Refinement and Porosity Fraction,” *Archives of Foundry Engineering*, vol. 12, no. 4, 2012.
72. G. Stephan, J. Els, G. Booysen, and D. C. Blaine, “Case study: Application of microCT to the non-destructive testing of an additive manufactured titanium component,” *Nondestructive Testing and Evaluation*, vol. 4, pp. 1–7, 2015.
73. J. A. Slotwinski and E. J. Garboczi, “Metrology Needs for Additive Manufacturing powders,” *The Journal of the Minerals, Metals & Materials Society,* vol. 67, no. 3, pp. 538–543, 2015.
74. “Unit 8 Coordinate Measuring Machines (Cmm),” https://docplayer.net/35384596-Unit-8-coordinate-measuring-machines-cmm.html [Accessed 20-Feb-2016].
75. H. Qiu, Y. Yue, C. Lin, and K. Cheng, “An Improved Measuring Device for Autonomous Form Measurement of Free Form Surfaces on Machining Centers,” *Journal of Mechanical Engineering and Automation*, vol. 2, no. 4, pp. 65–73, 2012.
76. “KREON Solano Blue.pdf.” https://kreon3d.com/3d-scanners/solano-blue/ [Accessed 02-Jun-2016].
77. J. Angel and L. De Chiffre, “CIRP Annals – Manufacturing Technology Comparison on Computed Tomography using industrial items,” *CIRP Annals – Manufacturing Technology*, vol. 63, no. 1, pp. 473–476, 2014.
78. A. Karme, A. Kallonen, V. Matilainen, H. Piili, and A. Salminen, “Possibilities of CT scanning as analysis method in laser additive manufacturing,” *Physics Procedia*, vol. 78, pp. 347–356, 2015.
79. W. A. Kalender and Y. Kyriakou, “Flat-detector computed tomography (FD-CT),” *European Journal of Radiology*, vol. 17, no. 11, pp. 2767–2779, 2007.

80. V. Cnudde, B. Masschaele, M. Dierick, J. Vlassenbroeck, L. Van Hoorebeke, and P. Jacobs, “Recent progress in X-ray CT as a geosciences tool,” *Applied Geochemistry*, vol. 21, no. 5, pp. 826–832, 2006.
81. “Metrology for additive manufacturing production assurance,” https://msu.euramet.org/industry_2014/SRTs/SRT-i05.pdf [Accessed 02-Jun-2016].
82. S. Gerhard and A. Guelpa, “The CT Scanner Facility at Stellenbosch University : An open access X-ray computed tomography laboratory,” *Nuclear Instrument Methods in Physics Research B*, vol. 384, pp. 42–49, 2016.
83. S. Gerhard and A. Guelpa, “Comparison of medical and industrial X-ray computed tomography for non-destructive testing,” *Case Study Nondestructive Testing and Evaluation*, vol. 6, pp. 17–25, 2016.
84. “Introduction » CT Scanner Facility at Stellenbosch University.” http://blogs.sun.ac.za/ctscanner/introduction/ [Accessed: 18-Feb-2016].
85. T. Mueller, “A Comparison of 3D Printing Technologies,” https://www.slideshare.net/TomMueller1/a-comparison-of-3d-printing-technologies-used-to-make-investment-casting-patterns-part-1 [Accessed 05-Jun-2018].
86. “Atlas of Casting Defects,” https://www.abebooks.com/book-search/title/atlas-defects-castings/ [Accessed 20-Jun-2018].

# Appendix A: Europart_3mm_wall

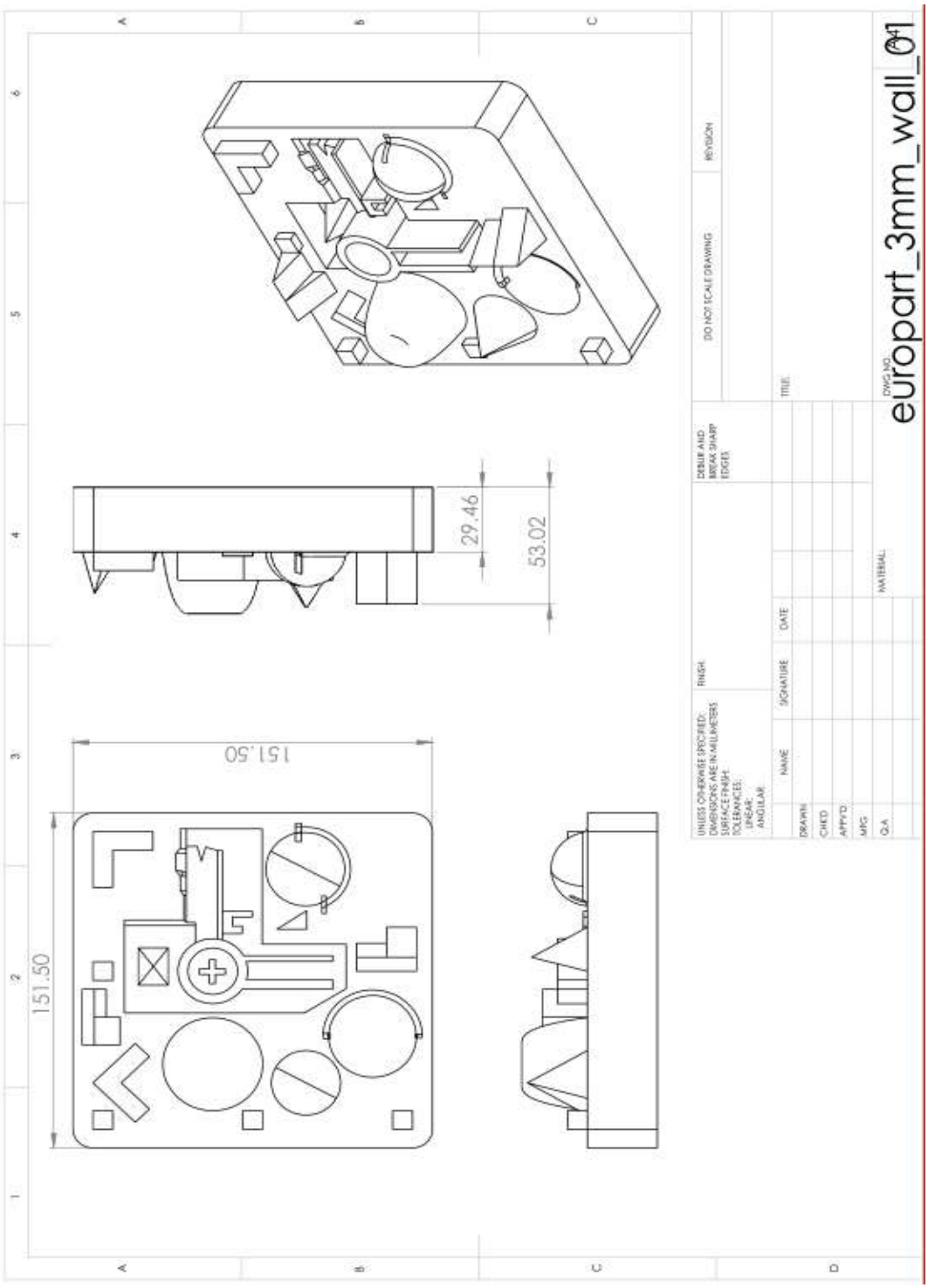

# Appendix B: Pattern results

## PMMA results

### *Full volume*

The full volume analysis of the PMMA pattern indicates blue on the flat surfaces, both in the top and bottom view, as shown in Figure B. 1.

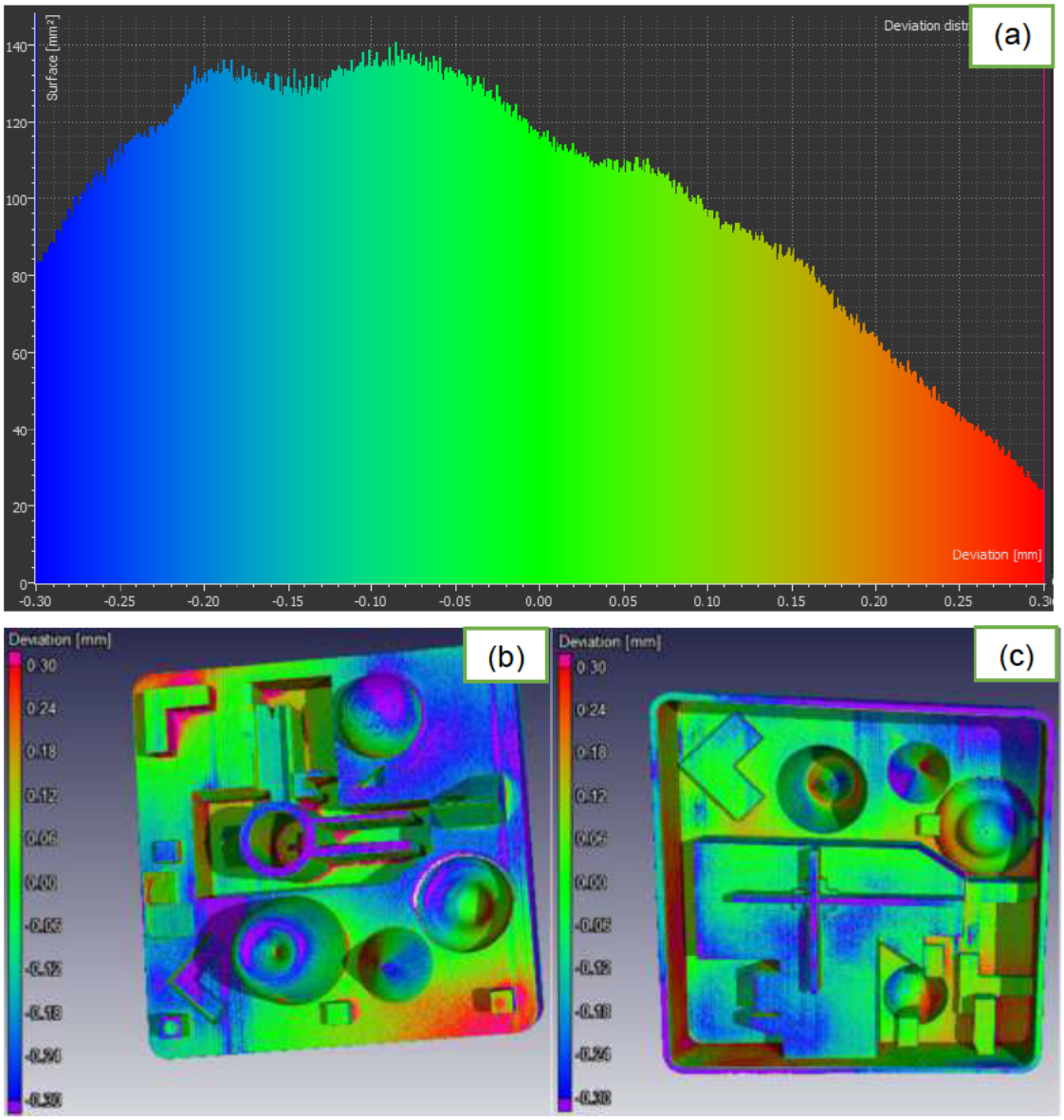


**Figure B. 1. Full volume: (a) Deviation distribution, (b) front view and (c) bottom view**

This indicates that the pattern is slightly smaller on the flat surfaces of the full volume compared to the CAD. There are traces of red, especially on the

sharp corners and edges. The repeatability with the many cubes on the part shows bad accuracy because one cube is predominantly green while the other is red. The outside of the full volume is mostly blue with hints of red. The deviation distribution of all points measured in the full volume shows a normal shape that has it peak on the left and tails to the right. The peak is at -0.10 mm and most surfaces area of the full volume is in the negative, indicating that the produced pattern is generally smaller compared to the CAD.

***Freeform (sinkhole)***

The non-constant sloping profile of the freeform (sinkhole) on the test geometry is covered with red, green and blue; these colours are seen in both top and bottom views in Figure B. 2. Although green is more dominant than other colours, blue is still significant. From the deviation distribution, green is distributed from -0.15 mm to 0.1 mm. The deviation distribution shape has two peaks towards left and right, but the centre still has significant surface area.

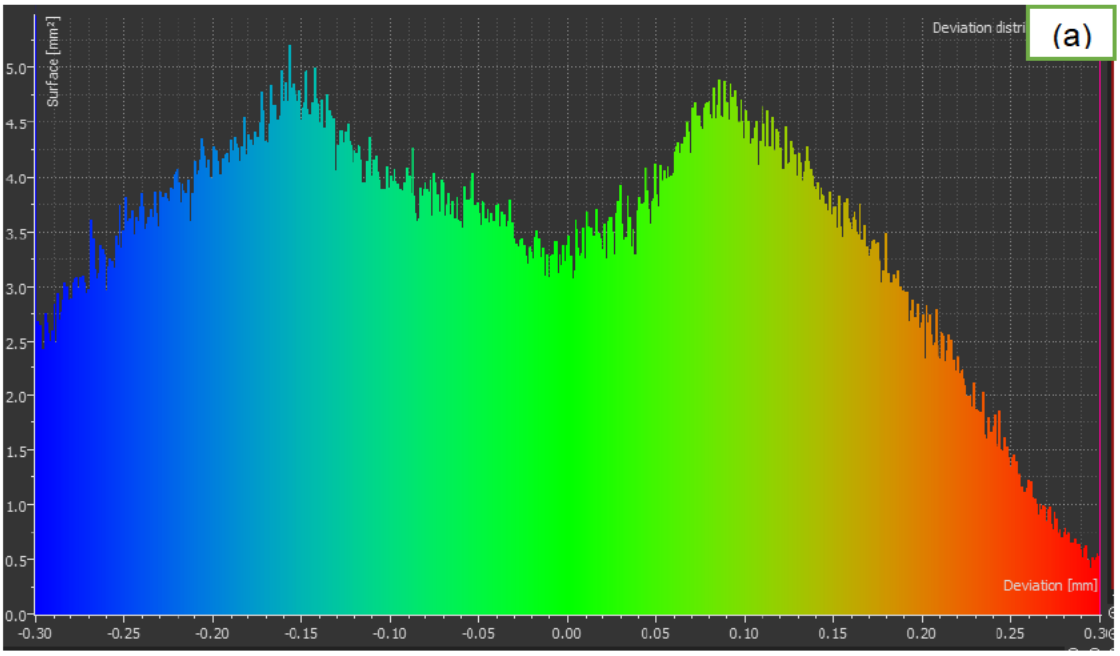

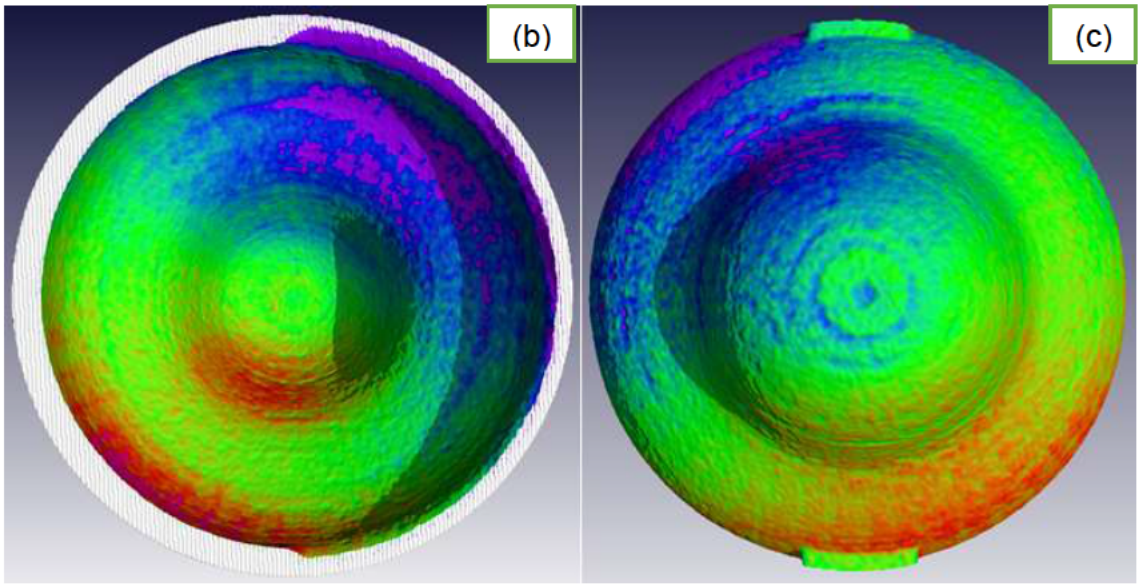


**Figure B. 2. Freeform (sinkhole): (a) Deviation distribution, (b) front view and (c) bottom view**

***Rectangular protrusion***

In Figure B. 3, the top of the rectangular protrusion is green; this indicates good dimensional accuracy on the flat surface. Vertical inner sides are prominently red while the vertical outer sides are blue. The deviation distribution has the highest peak at the centre of the distribution, with other peaks on the left and right of the distribution are evident. Green is in the range -0.15 mm to 1.0 mm in the distribution and this has the highest fraction of the total surface area, indicating a general good fit.

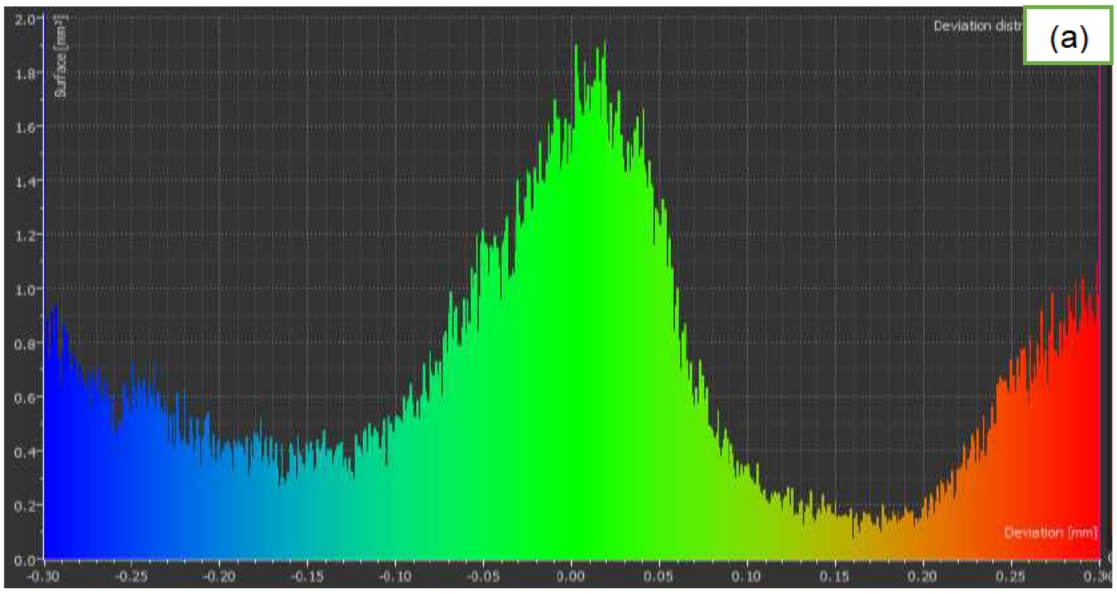

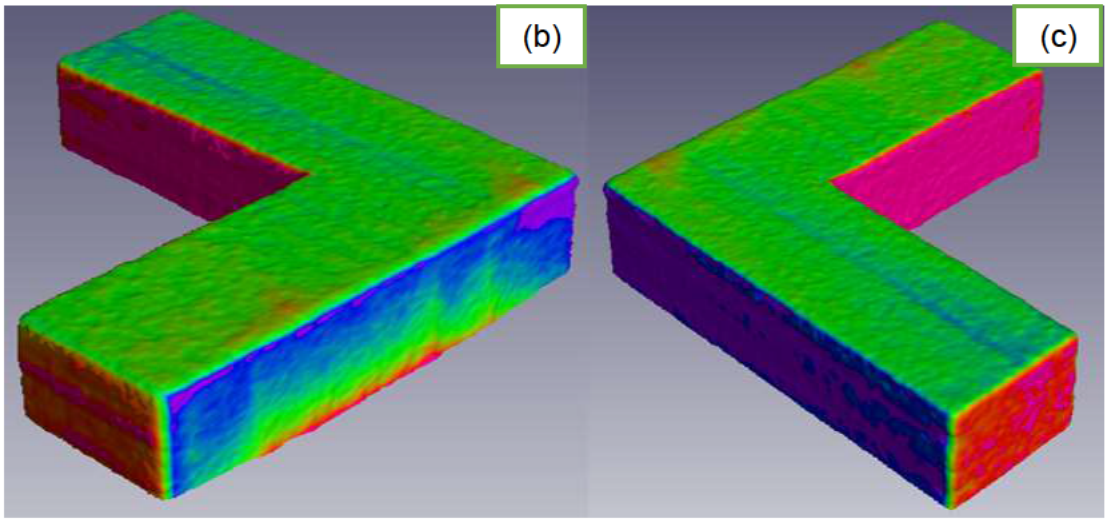


**Figure B. 3. Rectangular protrusion: (a) Deviation distribution, (b) top right view and (c) top left view**

***Freeform (Conical)***

The top surface of the freeform (conical) feature is blue, and the constant sloping profile is green with just dots of reds, as shown in Figure B. 4. The deviation distribution is skewed to the right and the peak is slightly off centre towards the left (-0.1 mm) while the tail stretches to the right. From the deviation distribution, green is spread from -0.15 mm to 0.15 mm showing the highest fraction of the total surface area.

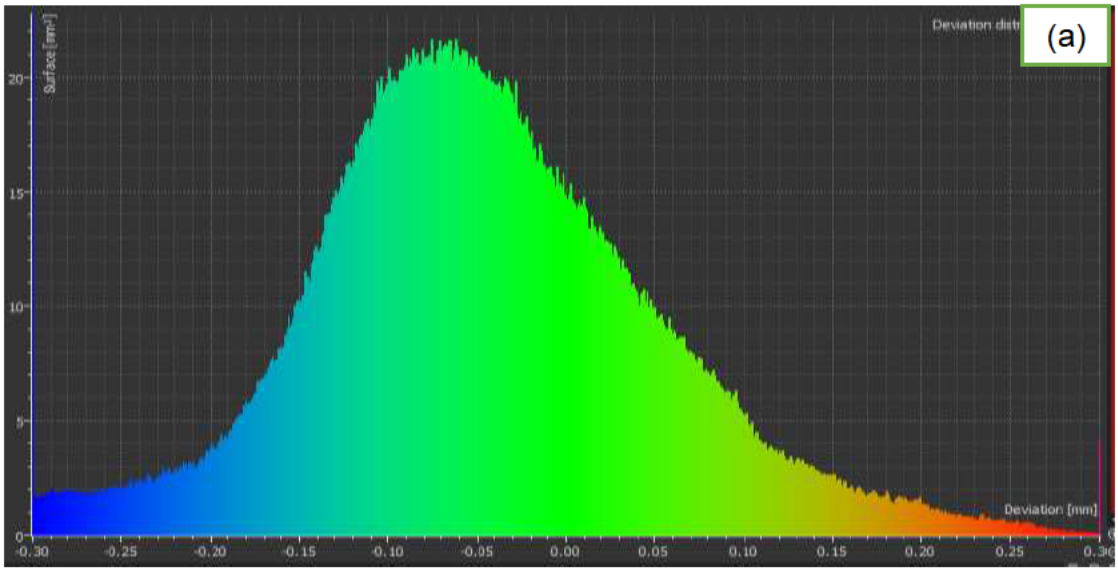

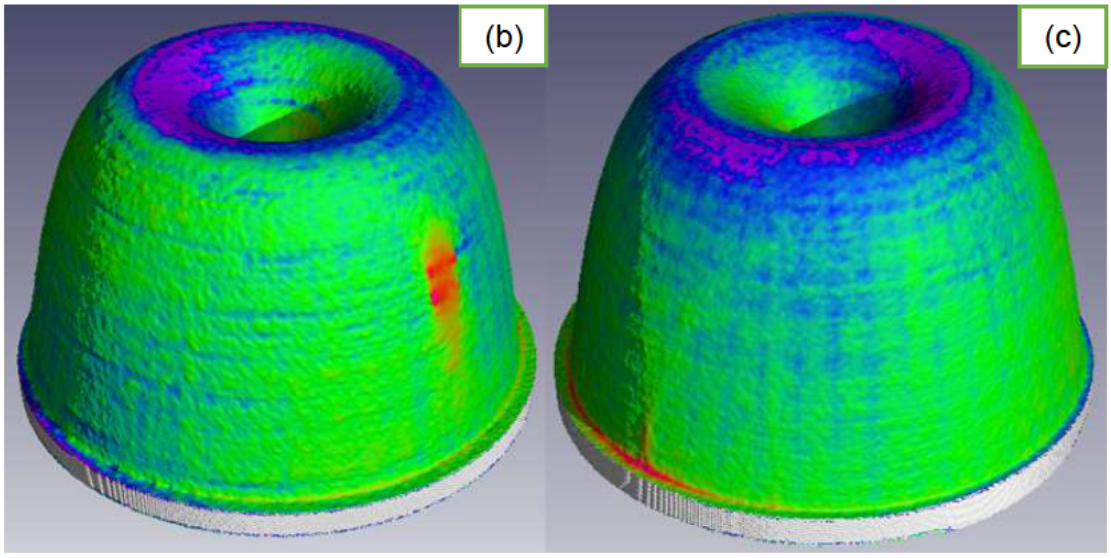


**Figure B. 4. Freeform (Conical): (a) Deviation distribution, (b) top right view and (c) top left view**

***Cone***

The cone was used to check for constant sloping profile, taper and symmetry. Green, blue and red can be seen on the surface of the cone, although green appears to be the dominant colour. From the deviation distribution in Figure B. 5, the shape has two peaks, with a significant surface area at the centre of the distribution.

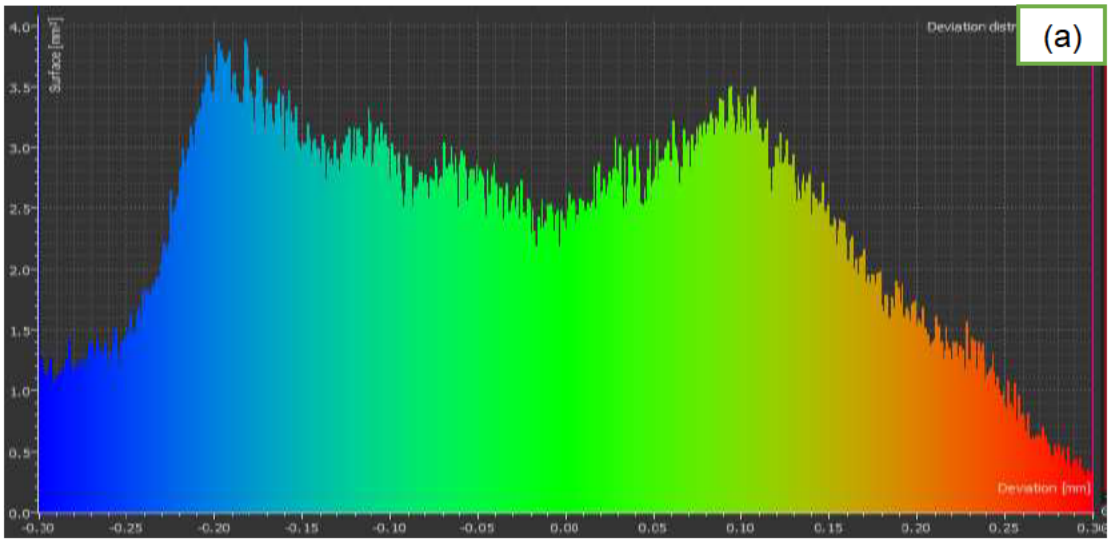

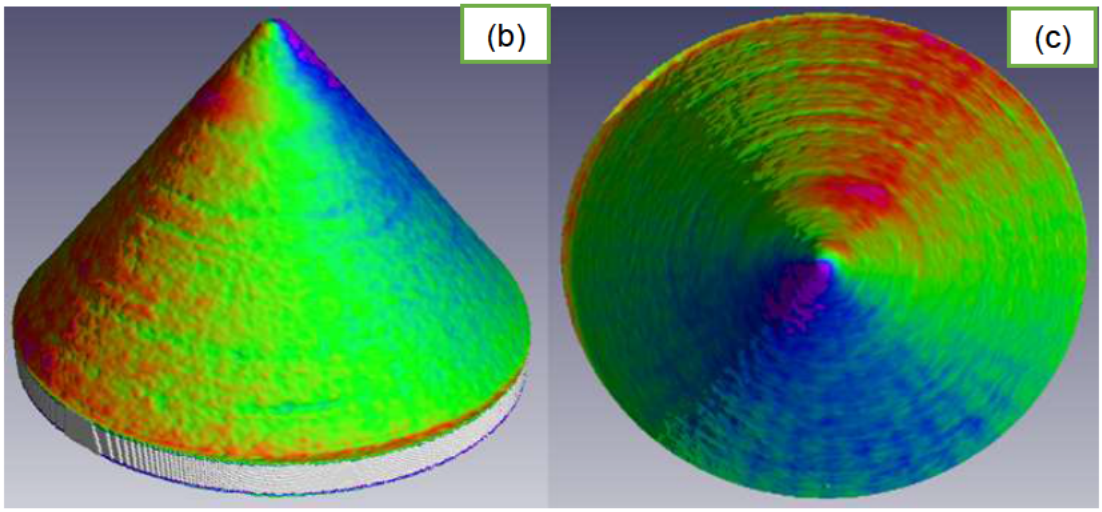


**Figure B. 5. Cone: (a) Deviation distribution, (b) top right view and (c) top view**

***Cube***

Figure B. 6 shows the deviation colour from a cube; both views are almost covered with blue and red. There is green on the top surface but it is insignificant. This is well-demonstrated in the deviation distribution that indicates two peaks on the right and left. From the deviation distribution, green is spread from -0.1 mm to 0.1 mm, showing the smallest fraction of the total surface area.

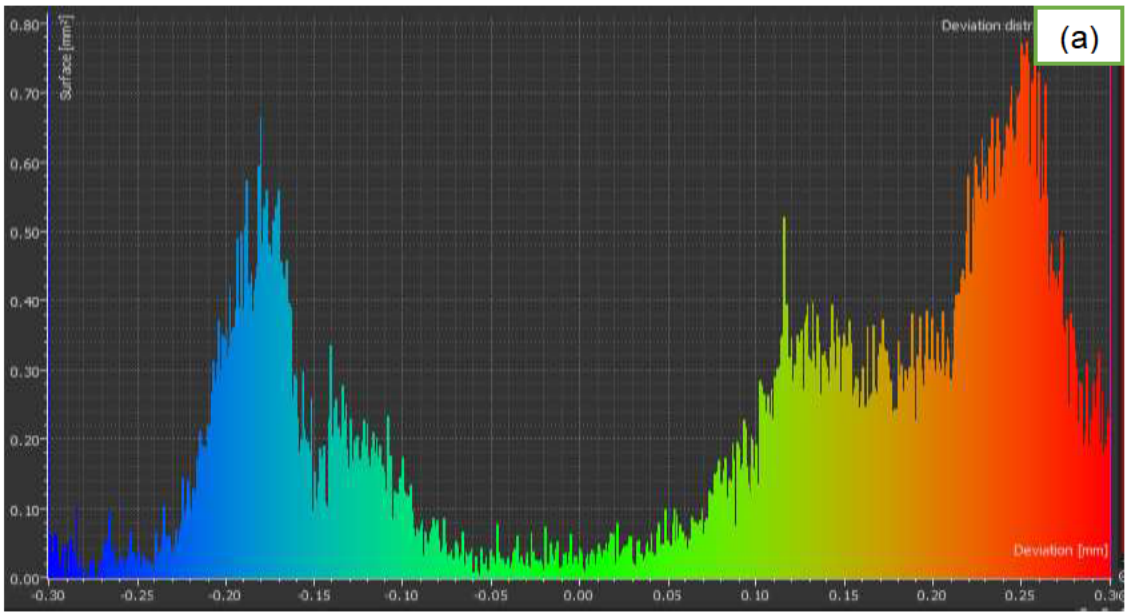

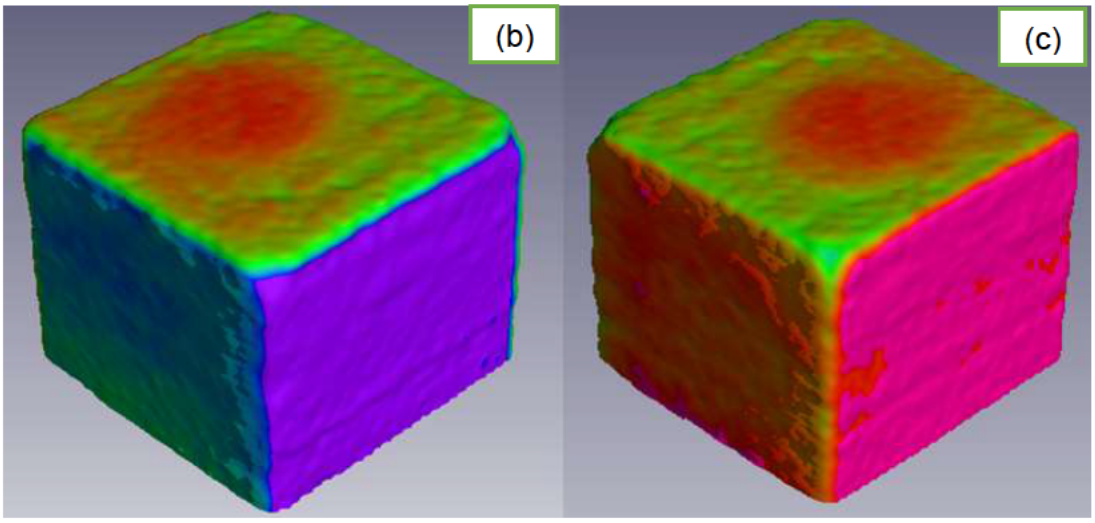


**Figure B. 6. Cube: (a) Deviation distribution, (b) top right view and top (c) left view**

## PrimeCast® results

### *Full volume*

The full volume comparison of the PrimeCast® pattern is predominantly green. Red is seen mostly towards the centre in the top view, while the bottom view shows blue at the centre. The surfaces towards the edges of the full volume in the top view are blue and in the bottom view are red. The top and bottom views show the opposite colours, that is to say, where it is blue at the top, it is red at the bottom, or vice versa, as seen in Figure B. 7. Cubes on the full volume indicate good accuracy and repeatability; the colours on all cubes are almost the same. The surrounding walls are predominantly green with hints of blue. The deviation distribution has a peak at the left and tails to the right. However, the peak is more towards the centre, that is at -0.05 mm. There is a small fraction of red that is distributed from 0.15 mm to 0.30 mm.

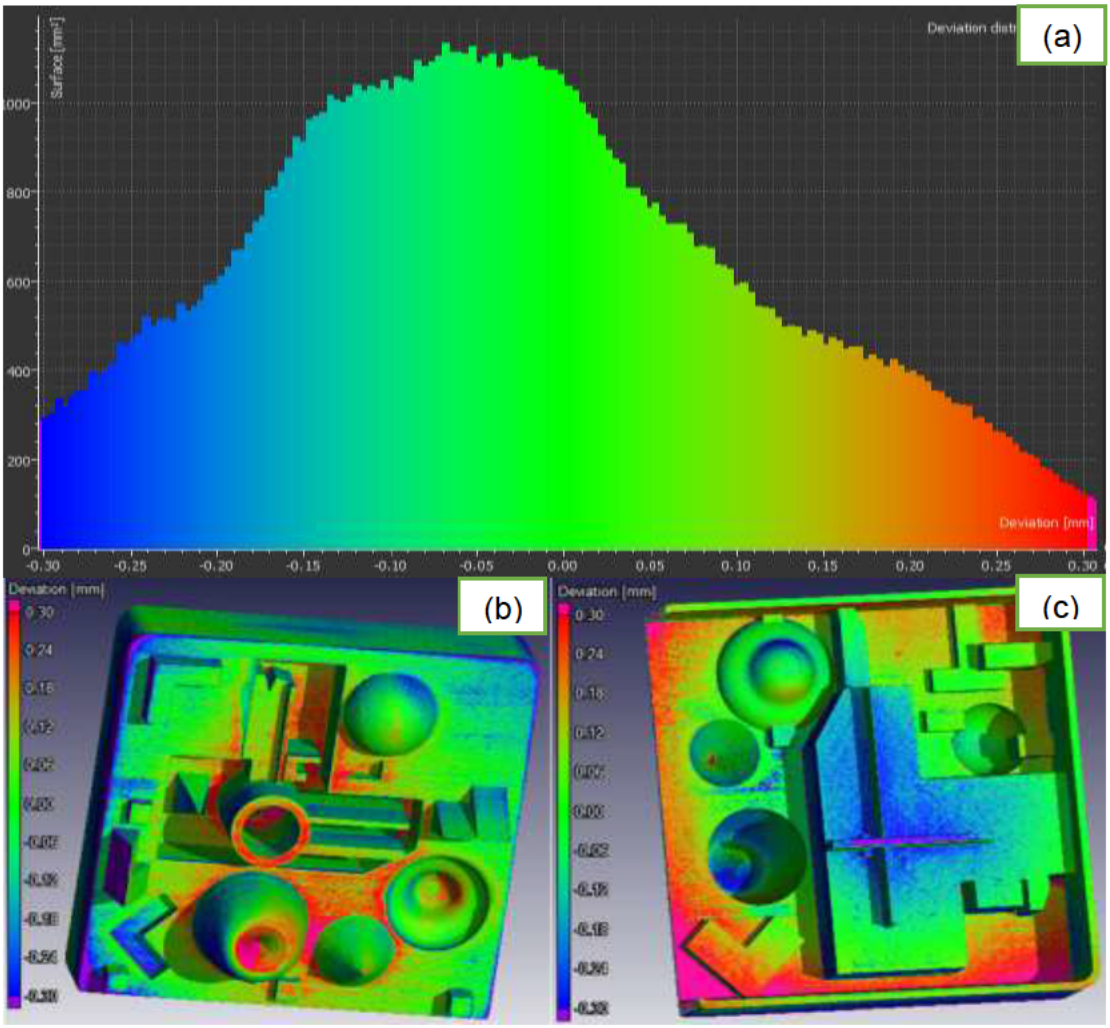


**Figure B. 7. Full volume: (a) Deviation distribution, (b) front view and (c) bottom view**

***Freeform (sinkhole)***

The non-constant sloping profile of the freeform (sinkhole) feature is predominantly green with a small fraction of blue followed by red. This shows excellent dimensional accuracy, as shown in Figure B. 8. The shape of the deviation distribution complies with a normal distribution with one peak and forms an approximate mirror image with respect to distribution. Green covers the largest area, indicating good dimensional accuracy.

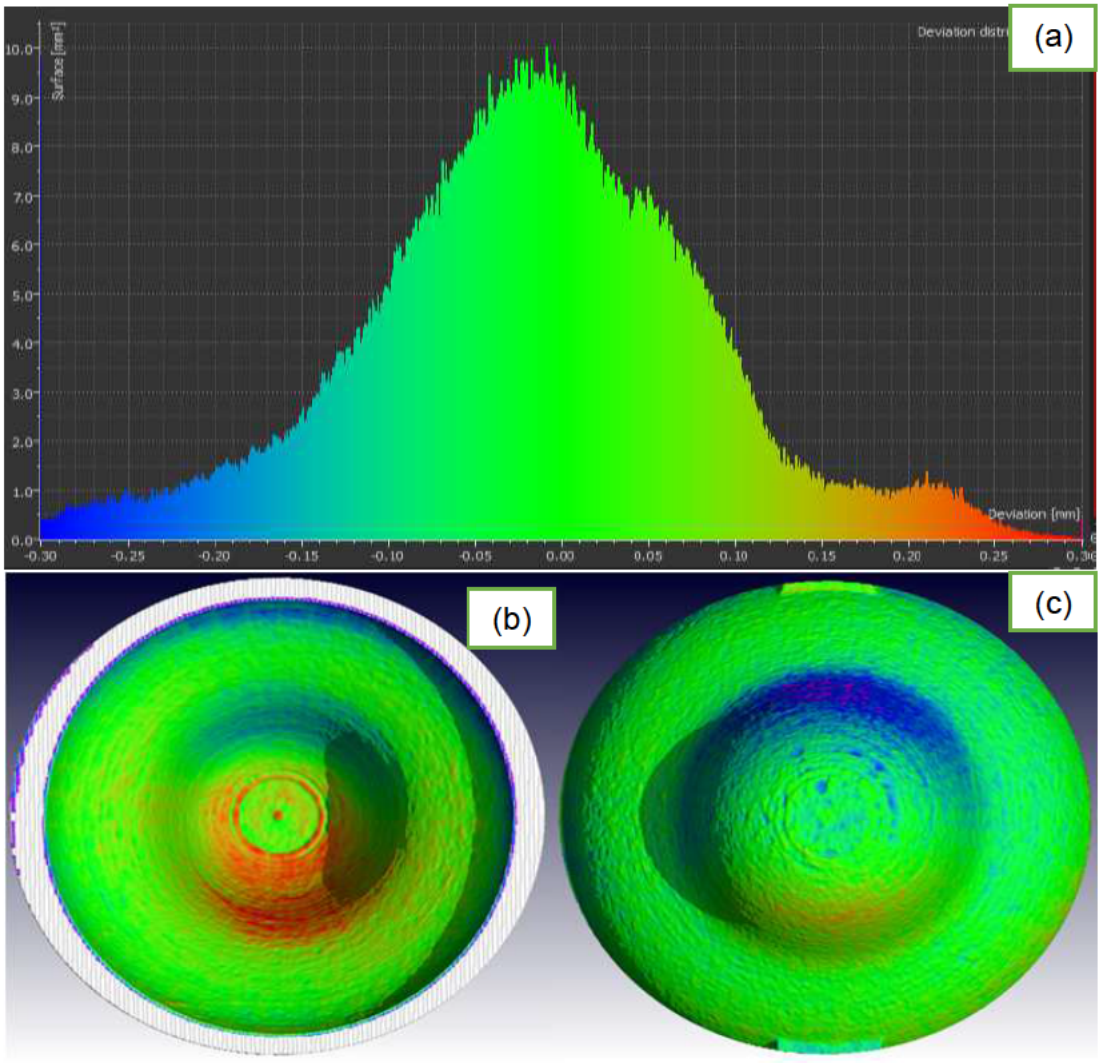


**Figure B. 8. Freeform (sinkhole): (a) Deviation distribution, (b) front view and (c) bottom view**

***Rectangular protrusion***

The top of the rectangular protrusion is predominantly green with touches of blue. The vertical inner sides are green and the vertical outer sides are fairly green and blue, as shown in Figure B. 9. The corners are blue, showing a small dimension. From the literature it was suggested that small radii should be made on the corners and edges as AM technologies experience challenges in producing sharp corners and edges. The deviation distribution shows many peaks that are not symmetrical. Green is spread from -0.15 mm to 0.1 mm and it covers the highest fraction of the surface area.

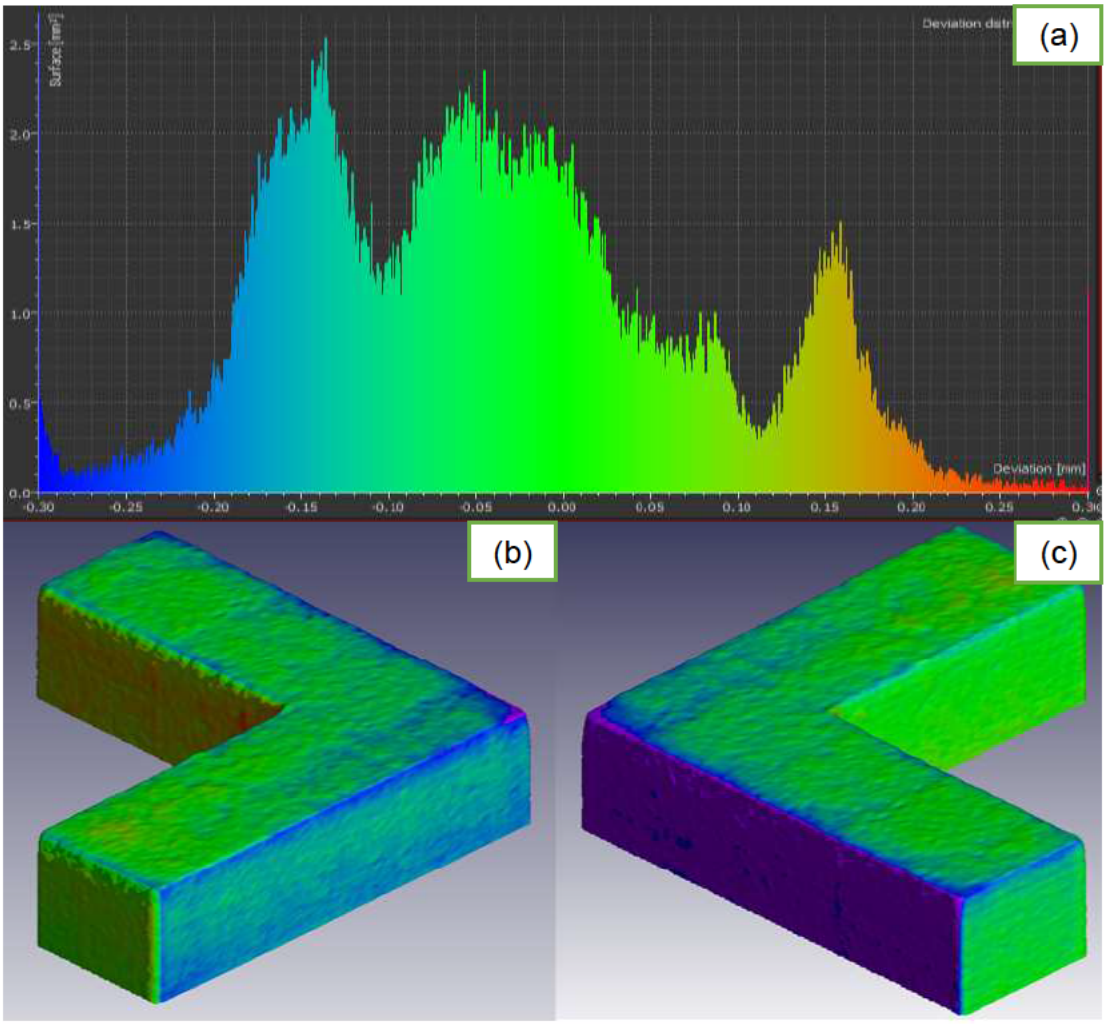


**Figure B. 9. Rectangular protrusion: (a) Deviation distribution, (b) top right view and (c) top left view**

***Freeform (Conical)***

Red is observed on the top surface of the freeform (conical) feature and the curved surface is dominated by green with a small portion of blue, as shown in Figure B. 10. The deviation distribution has two peaks and the shape is skewed to the right with a clear mode around -0.2 mm. In addition, it has another smaller peak around 0.05 mm. Red covers the smallest fraction of the surface area and is distributed from 0.2 mm to 0.30 mm.

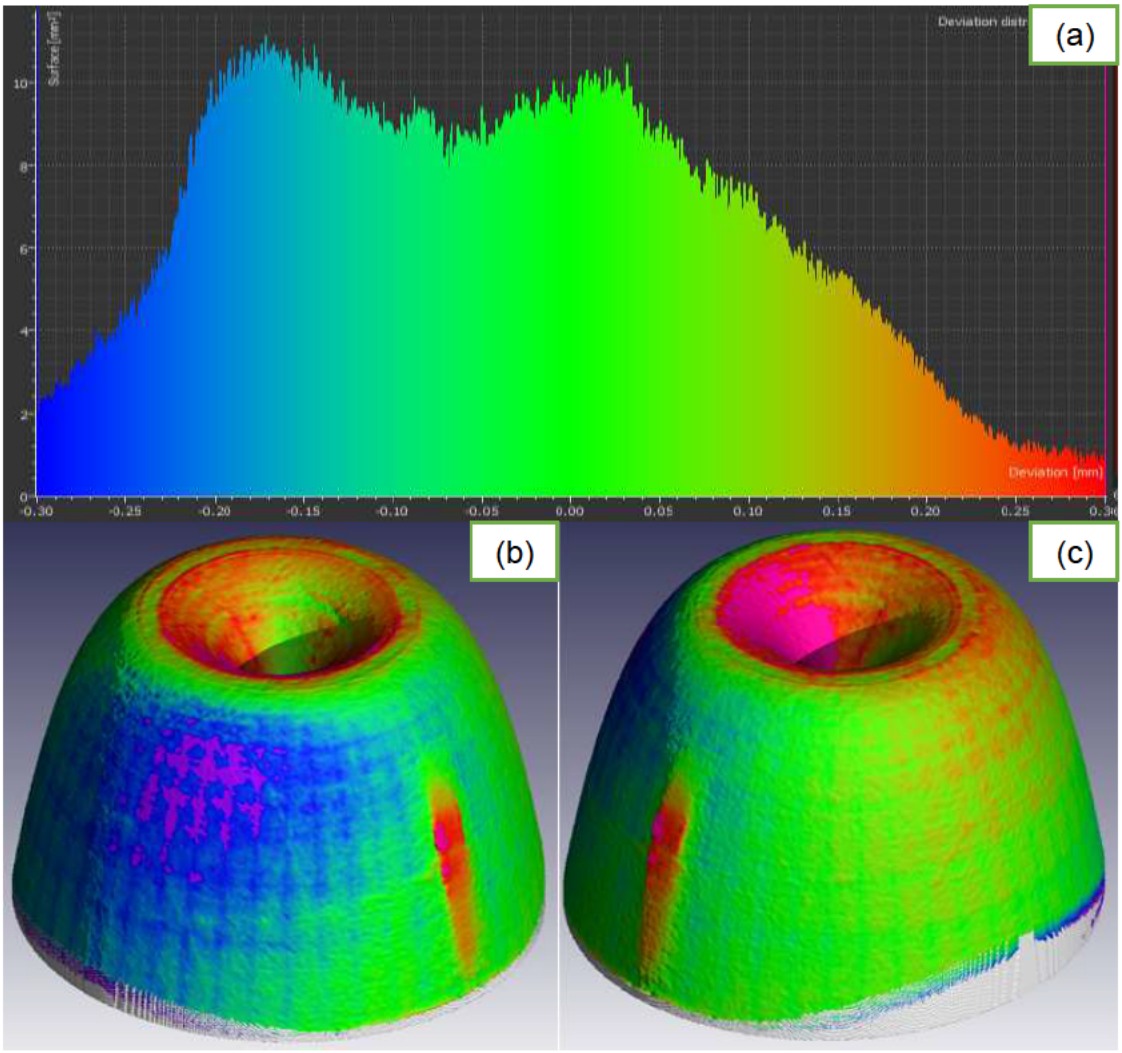


**Figure B. 10. Freeform (Conical): (a) Deviation distribution, (b) top right view and (c) top left view**

***Cone***

In Figure B. 11, the cone showed good dimensional accuracy with green in the constant sloping profile. Constant sloping profiles, taper, axial runout, radial runout and symmetry of the cone are well-replicated from the CAD model. The sharp edge of the cone is blue showing that the AM technology was not able to manufacture the sharp edge from the CAD model. The deviation distribution has a bell-shaped curve with a centre that much of the surface area clusters around. Symmetry is also seen from the deviation distribution.

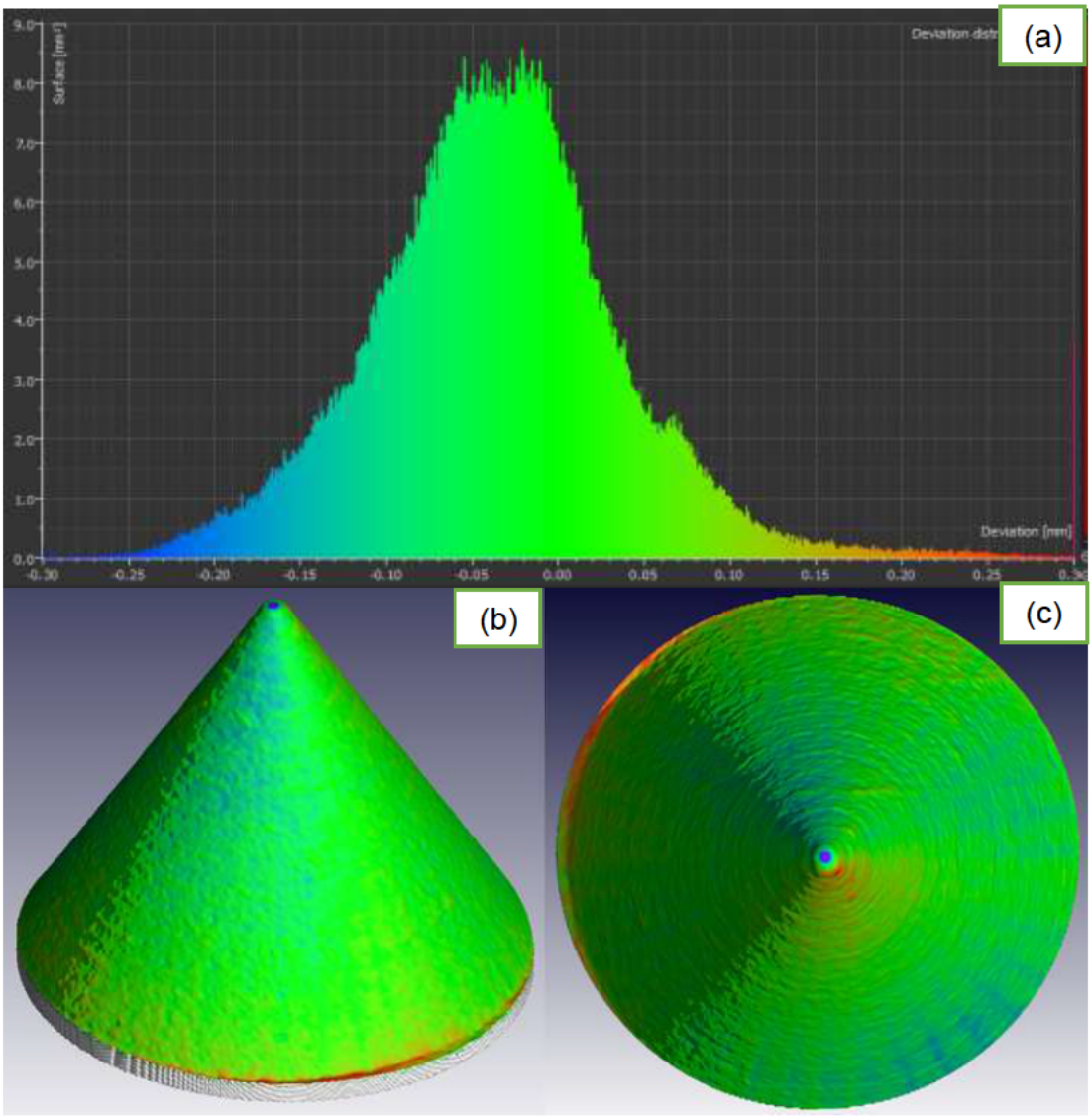


**Figure B. 11. Cone: (a) Deviation distribution, (b) top right view and (c) top view**

***Cube***

The cube has only two colours: green and blue. The cube shows best fit and smaller measurements, as shown in Figure B. 12. All corners and edges of the cube are blue while the flat surfaces are dominantly green. The corners and edges of the cubes were also sharp, as discussed earlier, with rectangular protrusion. The deviation distribution has multiple peaks with the right tail spreading up to 0.1 mm.

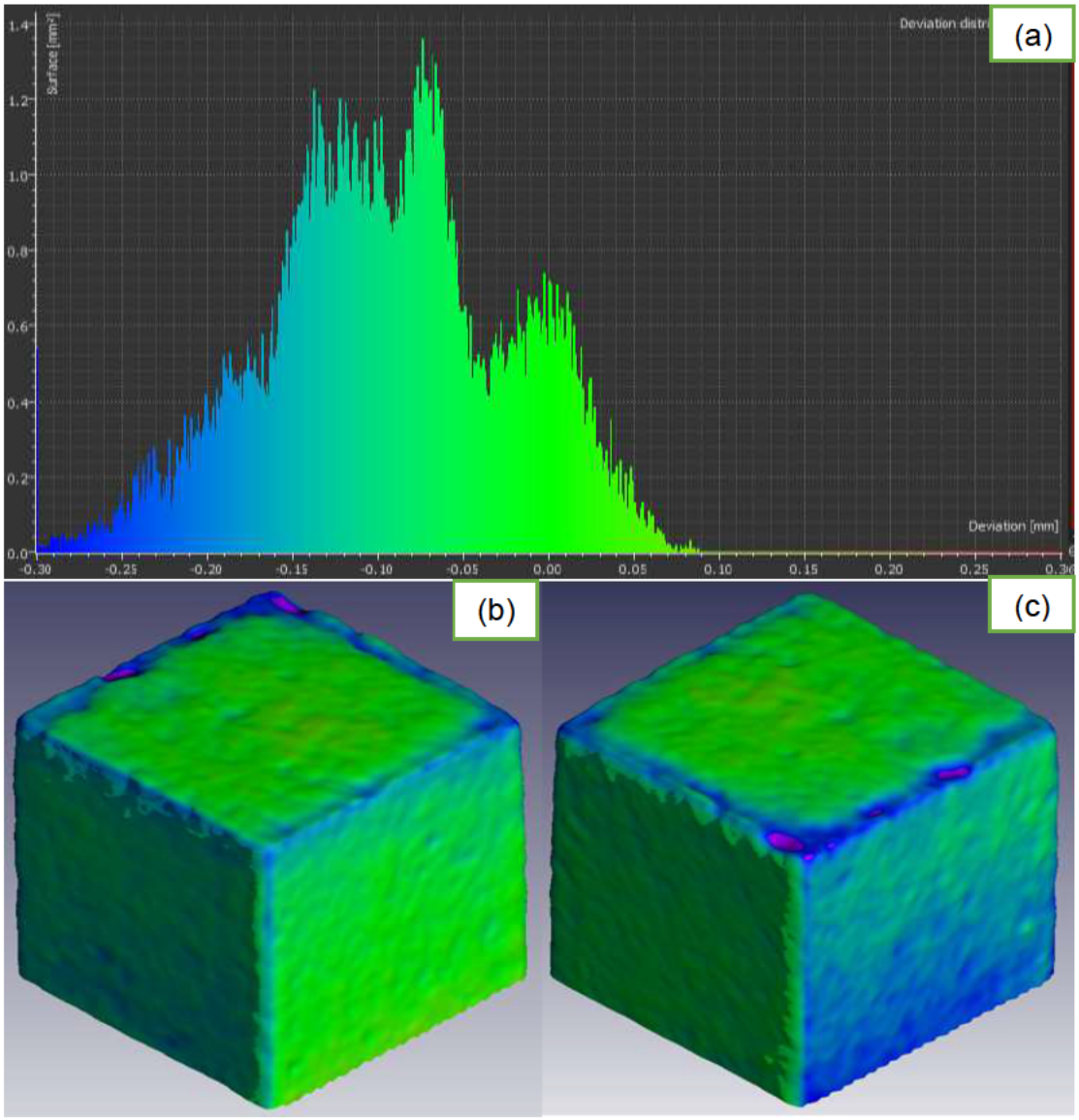


**Figure B. 12. Cube: (a) Deviation distribution, (b) top right view and (c) top left view**

## Comparison of PMMA and PrimeCast® patterns results

Figure B. 13 indicates the comparison between the two patterns. Top surfaces of both patterns are observed to have different colours. With PMMA, blue is prominent on most flat surfaces and green on the non-constant sloping profiles, such as the freeform (conical) feature. Most of the features on the diagonal of the PMMA pattern are blue. The PrimeCast® pattern is mostly green on flat surfaces with some traces of red, which is concentrated at the centre of the full volume. The far end, towards the corners of the part, is blue.

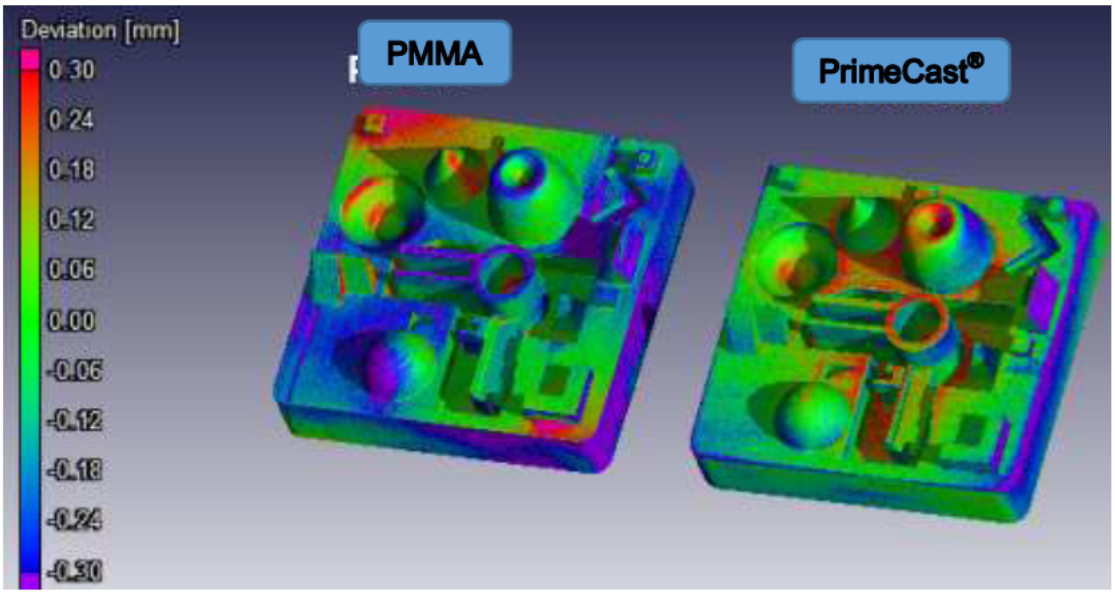


**Figure B. 13. Comparison of PrimeCast® and PMMA 3D CT images to CAD model (top view)**

Figure B. 14 shows the bottom view of the features of the patterns. The centre of the PMMA pattern is hinted with blue while red is seen on the surrounding walls. The centre of the PrimeCast® pattern is seen with drops of blue, but red on the far end of the pattern towards the corners.

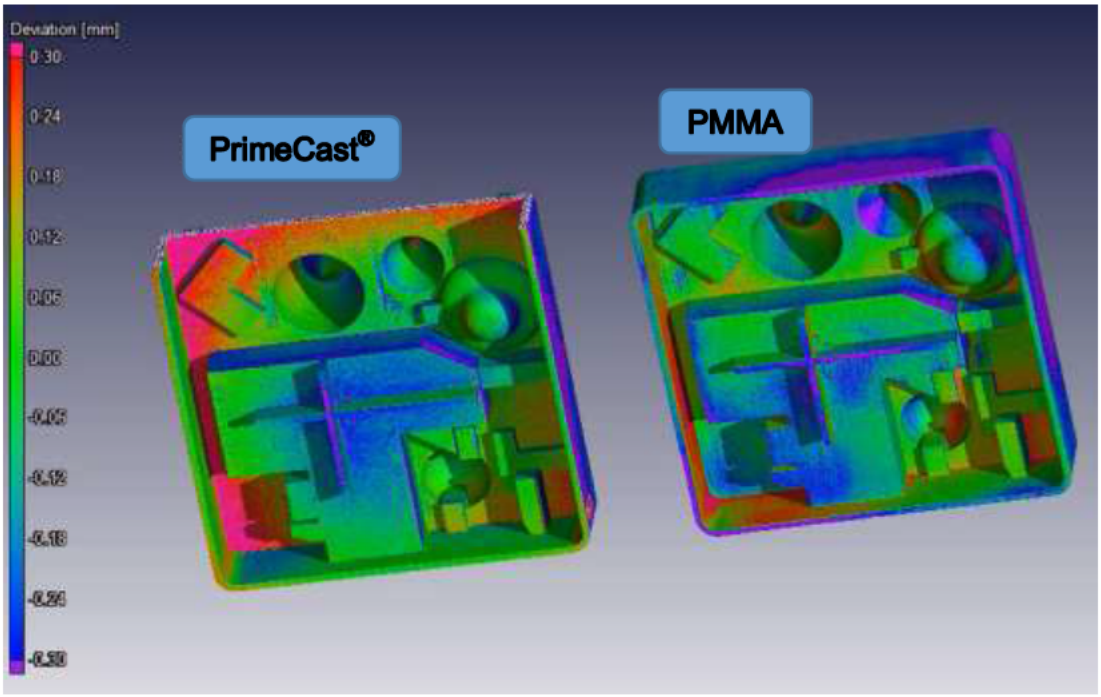


**Figure B. 14. Comparison of PrimeCast® and PMMA 3D CT images to CAD model (Bottom view)**

Specific features of each of the PrimeCast® and PMMA patterns were analysed and the results were tabulated in Table B. 1 below.

**Table B. 1. Comparison of different features of Primecast® and PMMA sacrificial patterns, from the tolerance range -0.3 mm to 0.3 mm**

| *Feature* | *Statistics* | *PMMA* | *PrimeCast®* |
|---|---|---|---|
| Cube | Mean (mm) | -0.13 | -0.09 |
| | Standard deviation (mm) | 0.18 | 0.07 |
| | Percentage (%) | 82.02 | 99.82 |
| Freeform (Conical) | Mean (mm) | -0.05 | -0.04 |
| | Standard deviation (mm) | 0.10 | 0.14 |
| | Percentage (%) | 98.57 | 99.10 |
| Cone | Mean (mm) | -0.02 | -0.04 |
| | Standard deviation (mm) | 0.15 | 0.07 |
| | Percentage (%) | 94.86 | 99.99 |
| Rectangular protrusion | Mean (mm) | 0.06 | -0.04 |
| | Standard deviation (mm) | 0.19 | 0.11 |
| | Percentage (%) | 87.65 | 83.17 |

| | | | |
|---|---|---|---|
| Freeform (Sinkhole) | Mean (mm) | 0.03 | 0.02 |
| | Standard deviation (mm) | 0.16 | 0.10 |
| | Percentage (%) | 94.18 | 99.71 |
| Full volume | Mean (mm) | -0.03 | -0.03 |
| | Standard deviation (mm) | 0.16 | 0.14 |
| | Percentage (%) | 90.15 | 92.53 |

On the PrimeCast® pattern, features such as the cone and freeform (sinkhole) have a good percentage based on the tolerances range specified, while features such as the freeform (conical) and rectangular protrusion have an average percentage. The PMMA pattern presents good percentages on the freeform (conical) feature, while the freeform (sinkhole) and cone have average percentages.

# Appendix C: Result of castings

## Results of the casting from PMMA sacrificial pattern

### *Full volume*

The minimum and maximum deviations were found to be -7.8 mm and 5.37 mm respectively. These deviations can be attributed to casting defects, such as a hole that was found where the gating was attached to the pattern. This can be seen in Figure C. 1 in the top view and inclusions due to bubbles that might have formed during mould making. For the analysis, the tolerances were therefore set at -1.5 mm to 1.5 mm for all the results for full volume.

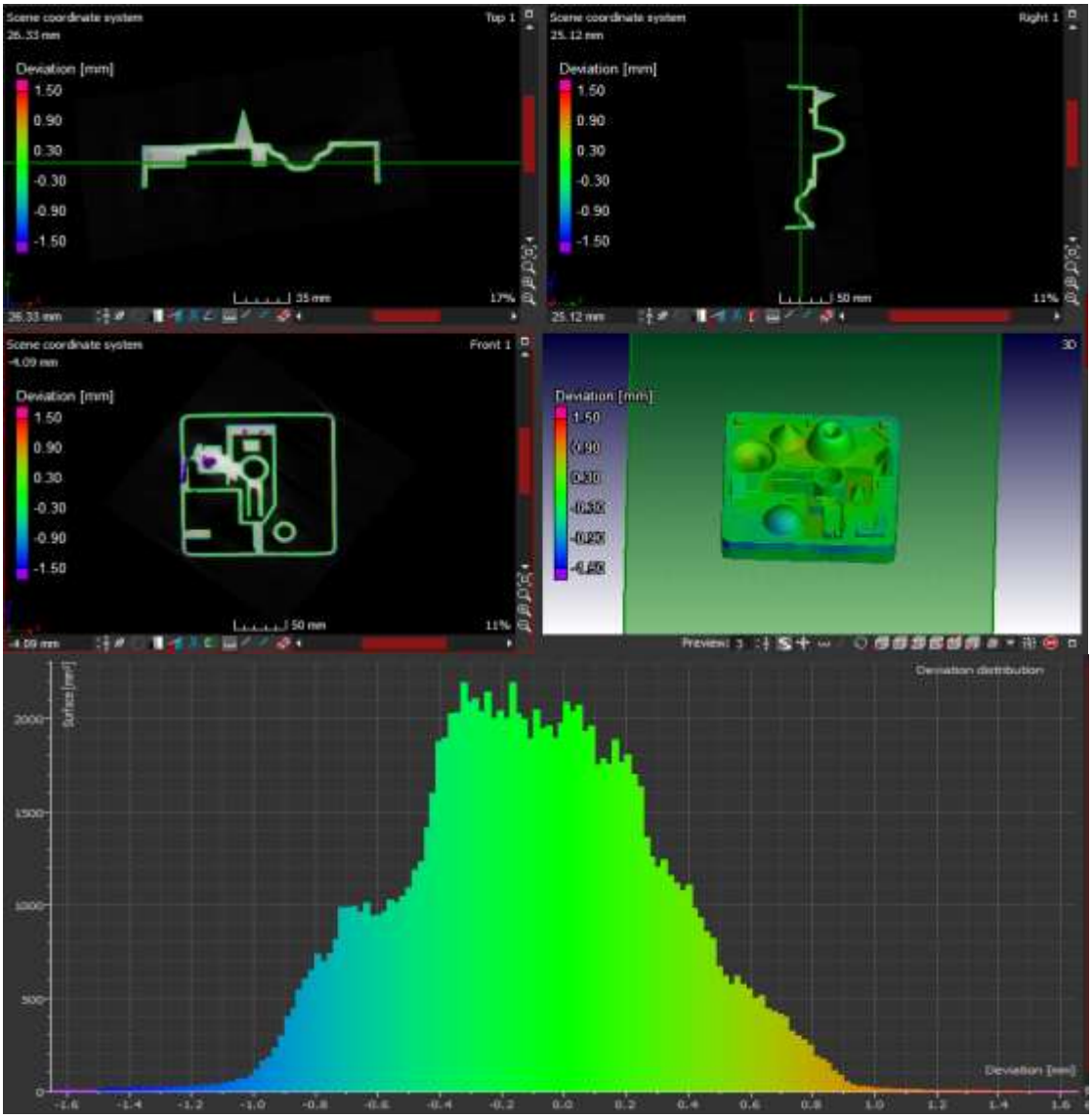


**Figure C. 1. Full volume**

Figure C. 1 shows top, right, front and 3D views of the full volume of the casting from the PMMA pattern. The scan comparison indicated predominantly green with small areas of blue and red. Blue is mostly seen on the corners of the full volume. The deviation distribution has a bell shape with the peak at the centre of the distribution. Green is distributed from -0.6 mm to 0.6 mm with 82.97% of the surface area. Blue is distributed on the left from –1.5 mm to 0.6 mm covering around 12.71% of the total area, while red covers only 4.34% and is distributed on the right from 0.6 mm to 1.5 mm.

***Rectangular protrusion***

Minimum and maximum deviation on the rectangular protrusion was found to be -0.78 mm and 1.47 mm, respectively. In Figure C. 2, the section views of the top, right, front as well as the 3D view are shown. The rectangular protrusion is blue on the flat surface, as seen on the 3D view, and predominantly green on the vertical inner surfaces. The outer vertical surfaces are blue with hints of red on the inner corner. The deviation distribution has four peaks and the two largest are on the left of the distribution. Green is distributed from -0.3 mm to 1.00 mm covering 35.70% of the total surface area. Blue covers 63.81% and ranges from -0.78 mm to -0.3 mm, while red covers the smallest area (0.5%) and distributed from 1.00 mm to 1.47 mm.

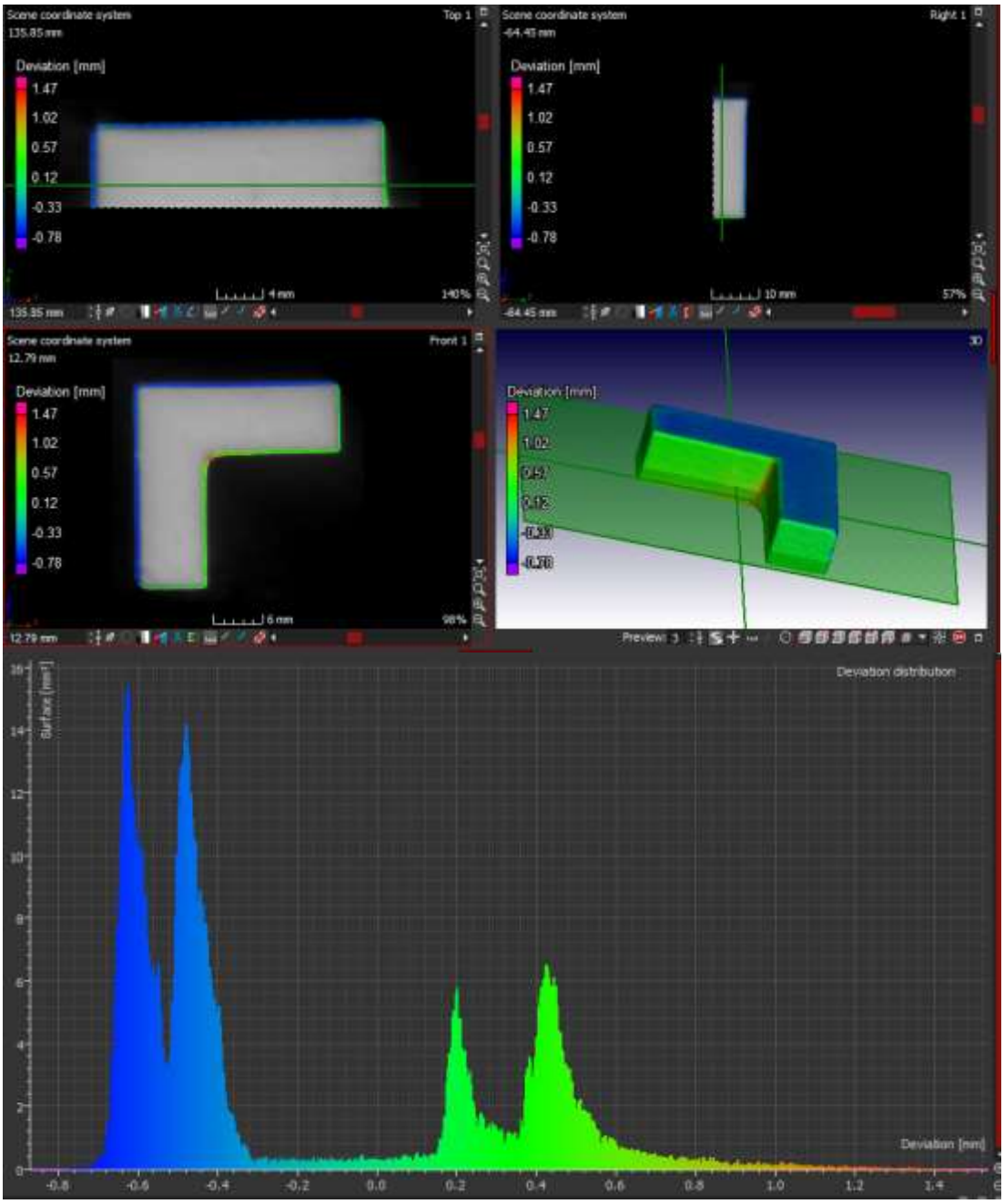


**Figure C. 2. Rectangular protrusion**

### *Cone*

The constantly sloping profile, taper, axial runout, radial runout and symmetry of the cone are well-replicated. The minimum and the maximum deviation of the cone was found to be -1.04 mm and 1.50 mm, respectively. Top and right section view in Figure C. 3 shows blue and red on the vertex of the cone. Hints of blue can also be seen both on the inner and outer surfaces of the constantly sloping profile. The deviation distribution shows a comb shape that

has many different peaks, with the highest peak on the left of the distribution. Green covers the biggest surface area (61.23%) and is distributed from -0.1 mm to 1.00 mm. Blue is distributed from -1.04 mm to -0.1 mm with 38.23% of the surface area, while red covers the remaining 0.12% and ranges from 1.00 mm to 1.5 mm on the distribution.

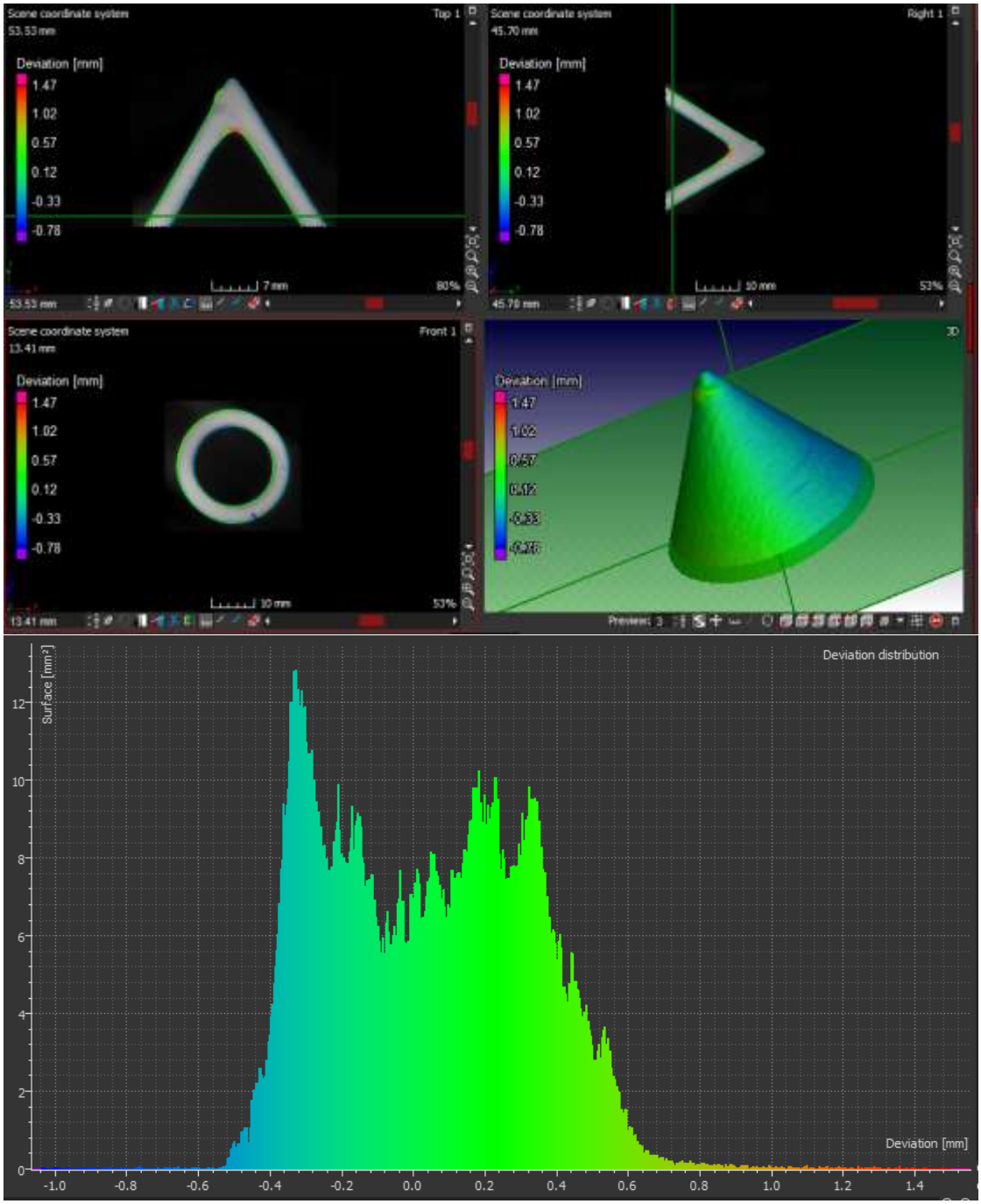


**Figure C. 3. Cone**

### *Cube*

The cube on the test geometry was used to measure straightness. The top surface was green while the vertical surfaces were blue and red on opposite sides, as shown in both top and front section view in Figure C. 4. Minimum and maximum deviations were -0.63 mm and 0.45 mm respectively. The deviation distribution has different peaks with the highest peak on the right of the distribution. Green covers the smallest fraction of the surface area (25.36%) and is distributed from -0.3 mm to 0.25 mm, 41.45% is covered with blue and is distributed from -0.63 mm to 0.3 mm while red covers 33.89% and ranges from 0.25 mm to 0.45 mm on the distribution.

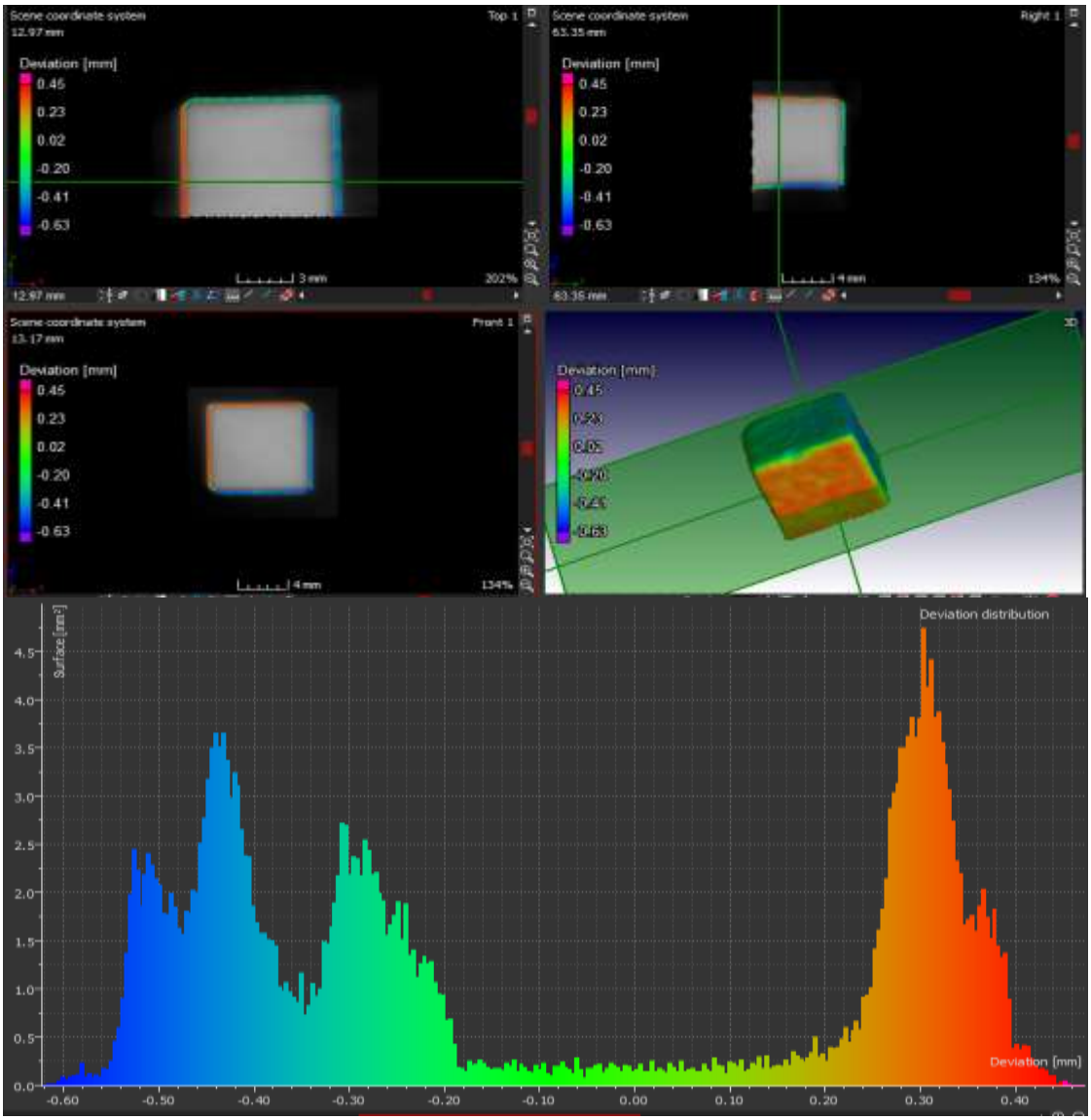


**Figure C. 4. Cube**

***Freeform (conical)***

Non-constant sloping profile axial runout, radial runout and symmetry were well-represented on the conical freeform feature, as it can be seen to be predominantly green. Red and blue are seen on the vertex of the conical freeform, as shown in the top and right section view in Figure C. 5. Traces of red can also be seen on the non-constantly sloping profile, and a hole, due to casting defects, is seen on the right section view. Minimum and maximum deviation was -1.48 mm and 0.95 mm, respectively. The deviation distribution shows a bell-like shape, with the peak at the centre of the distribution. Green covers the biggest fraction of the surface area, that is 96.94%, and is distributed from -0.8 mm to 0.4 mm on the distribution. Red and blue shares the remaining small fraction of the surface area, 2.78% and 0.33%, respectively.

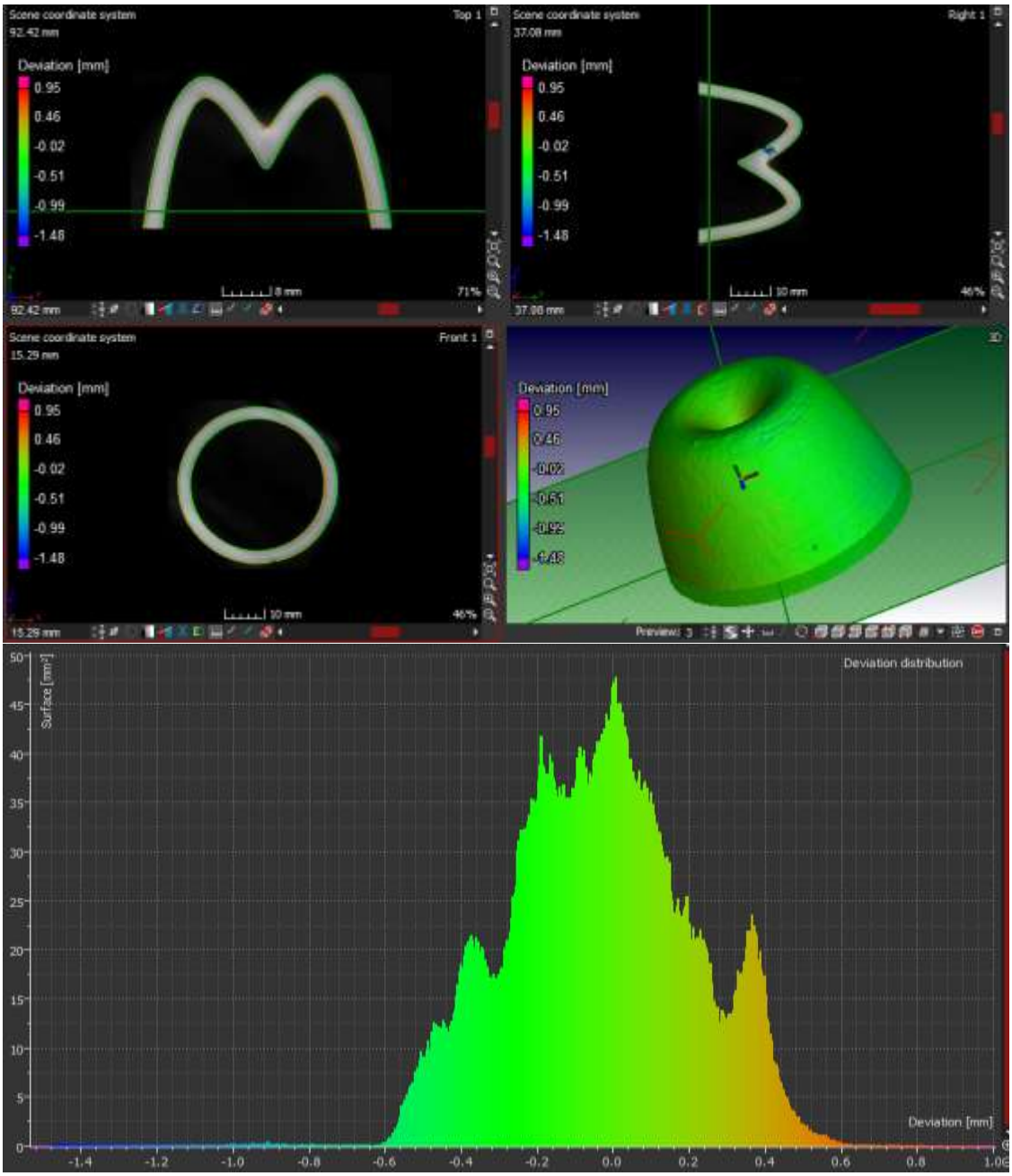


**Figure C. 5. Freeform (conical)**

***Freeform (sinkhole)***

Minimum and maximum deviation for the freeform sinkhole feature was -0.87 mm and 1.75 mm, respectively. The non-constant sloping profile is covered in green with hints of blue, as seen on the 3D view in Figure C. 6. below. A trace of red can be seen on the inside of the non-constant sloping feature, as indicated in the top, right and front section views. The deviation distribution has different peaks that are clustered towards the centre of the distribution.

Green is predominant with 70.56%, distributed from -0.4 mm to 0.3 mm, blue covers around 16.89%, ranging from -0.87 mm to -0.4 mm, while red covers 12.70%, and is spread from 0.3 mm to 0.75 mm on the distribution.

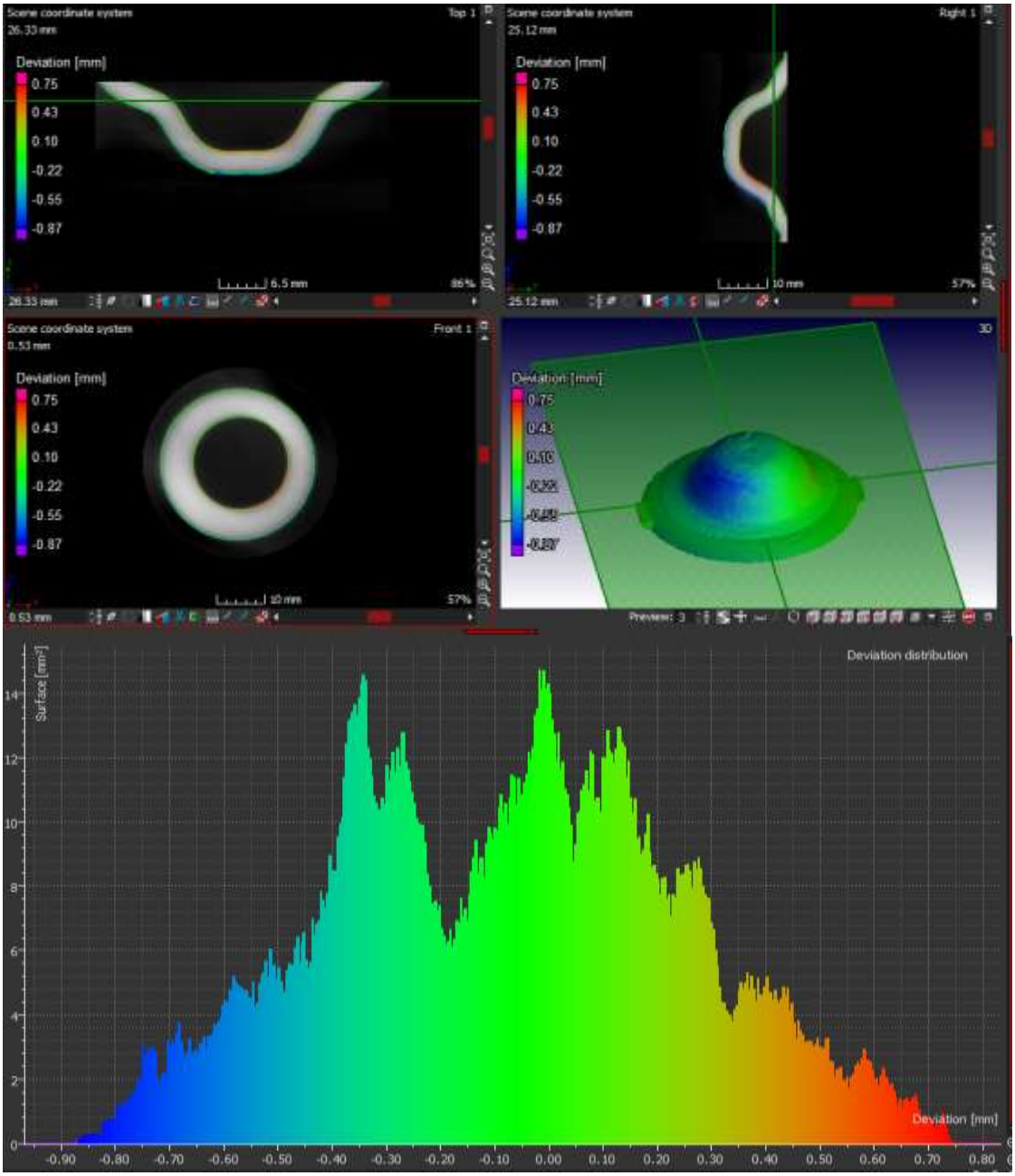


**Figure C. 6. Freeform (sinkhole)**

## Results of casting from a PrimeCast® sacrificial pattern

### *Full volume*

The full volume of casting from the PrimeCast® sacrificial pattern still has outliers with minimum and maximum deviation as -2.65 mm and 2.00 mm, respectively. As discussed in the previous section, these outliers were casting defects caused by entrapped air during mould making. The tolerance was then set from -1.5 mm to 1.5 mm, the full volume of casting from PrimeCast® pattern was covered with green with small areas of red and blue. The sliced and 3D views of the full volume are shown in Figure C. 7. From the top view it can be seen that the outermost area of the surrounding walls are blue. The deviation distribution has two peaks; the highest peak at the centre and the other peak at the left of the distribution. Green covers 63.72% of the surface area and is spread from -0.6 mm to 0.6 mm. Blue covers 22.27%, and is distributed from -1.5 mm and -0.6 mm, and finally, red covers the remaining 12.82%, and is dispersed from 0.6 mm to 1.5 mm of the distribution.

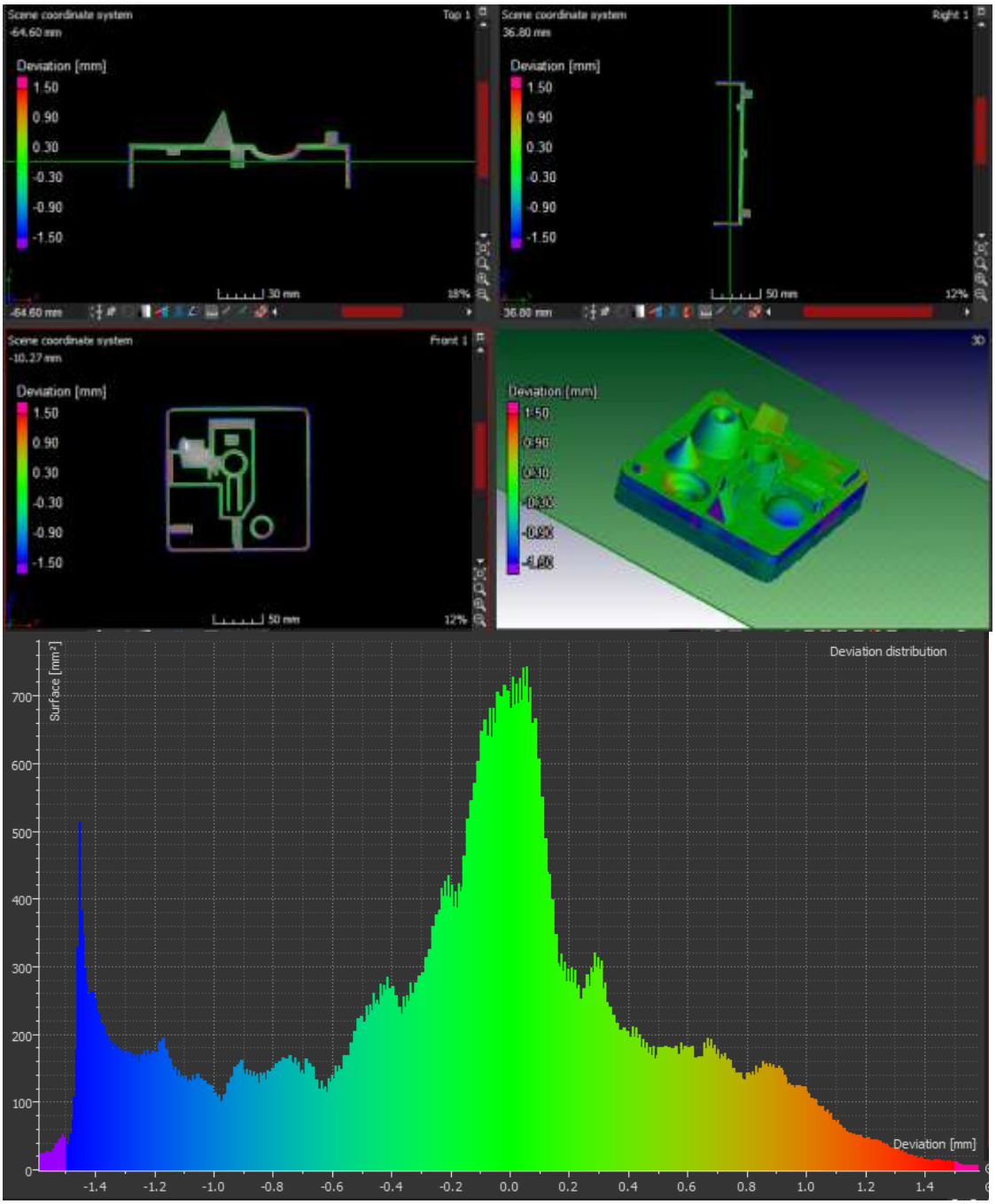


**Figure C. 7. Full volume**

### *Rectangular protrusion*

Minimum and maximum deviation of the rectangular protrusion was found to be -1.46 mm and 1.44 mm, respectively. This deviation is higher than was found in the PMMA results. In Figure C. 8, the section views of the top, right, front as well as the 3D view are shown. The rectangular protrusion is predominantly green with traces of blue and red. Green is mostly observed on

the flat horizontal surfaces of the rectangular protrusion while red and blue are on the vertical surfaces. The deviation distribution has many peaks with the largest on the centre of the distribution.

Green is distributed from -0.70 mm to 0.70 mm, covering 58.15% of the total surface area. Blue covers 30.32% and ranges from -1.46 mm to -0.7 mm, while red covers the smallest area (11.54%) and it is distributed from 0.8 mm to 1.44 mm. Although the rectangular protrusion from the PrimeCast® has a wide range of deviation, green covers a more significant fraction compared to that of the PMMA pattern.

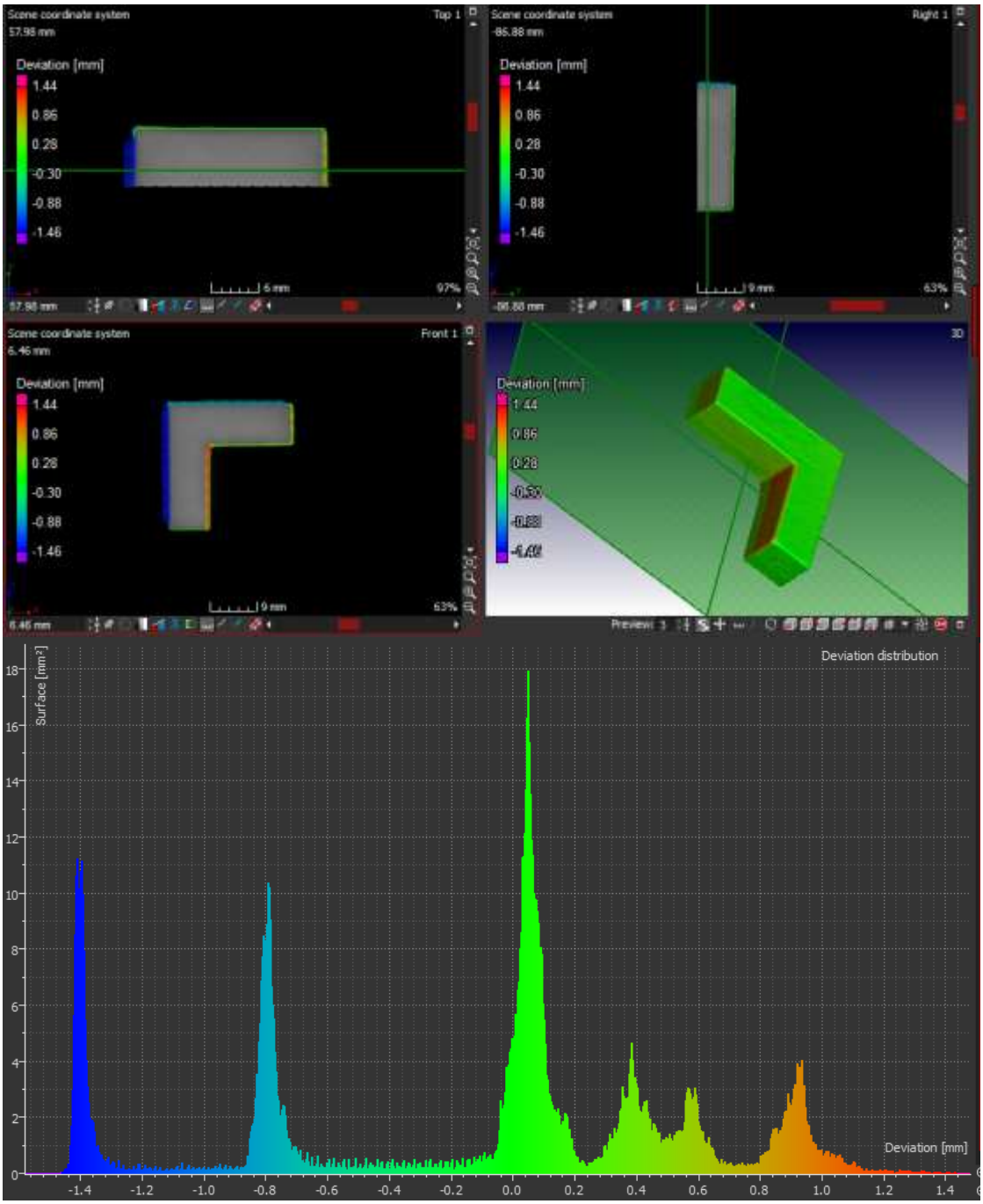


**Figure C. 8. Rectangular protrusion**

### *Cone*

The minimum and the maximum deviation of the cone was found to be -1.20 mm and 1.30 mm, respectively. Green is predominant on the outer surface of the constant sloping profile, as seen on the 3D view in Figure C. 9. Top and right section views display traces of blue and red on the inner and outer surfaces of the constantly sloping profile. The deviation distribution shows

many different peaks, with the highest peak on the right of the distribution. Green covers the biggest surface area (59.98%) and is distributed from -0.60 mm to 0.65 mm. Blue is distributed from -1.20 mm to -0.60 mm with 30.11% of the surface area, while red covers the remaining 10.34% and ranges from 0.65 mm to 1.30 mm on the distribution.

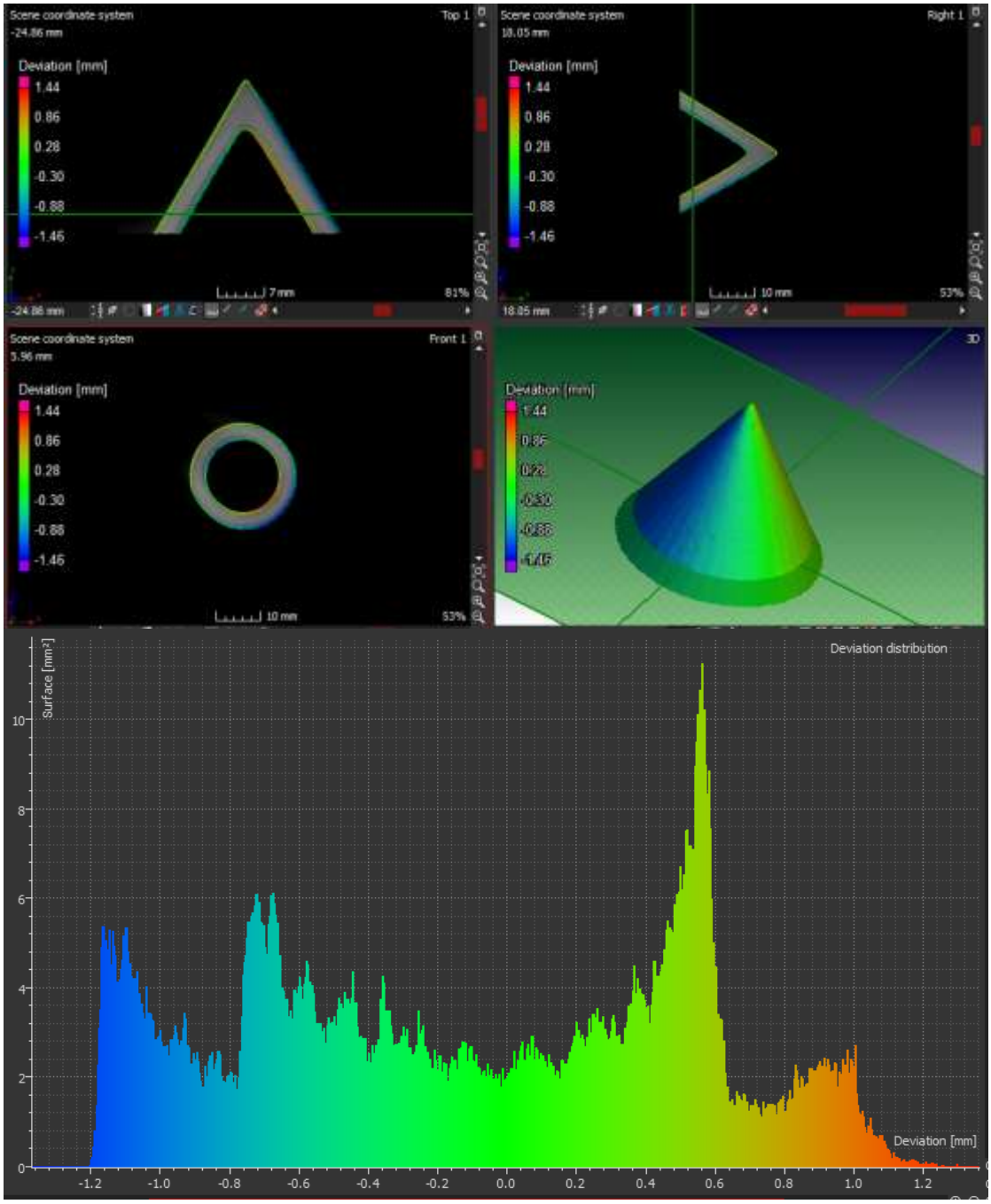


**Figure C. 9. Cone**

***Cube***

The straightness on the top surface of the cube was well-represented with green, as seen in Figure C. 10, and the vertical surfaces were blue and red on opposite sides, as shown in both top and front section views. Minimum and maximum deviations were -1.62 mm and 1.29 mm, respectively. The deviation distribution has different peaks, two on both the left and right and one in the centre. Green covers 29.10% of the surface area and is distributed from -0.75 mm to 0.60 mm, 29.21% is covered in blue and spread from -1.62 mm to -0.75 mm. The largest area (41.72%) is enclosed in red and is distributed from 0.6 mm to 1.29 mm.

The cube of the casting from the PrimeCast® pattern has a higher deviation distribution when compared to the casting from PMMA pattern, but with a better accuracy looking at the percentage covered by green.

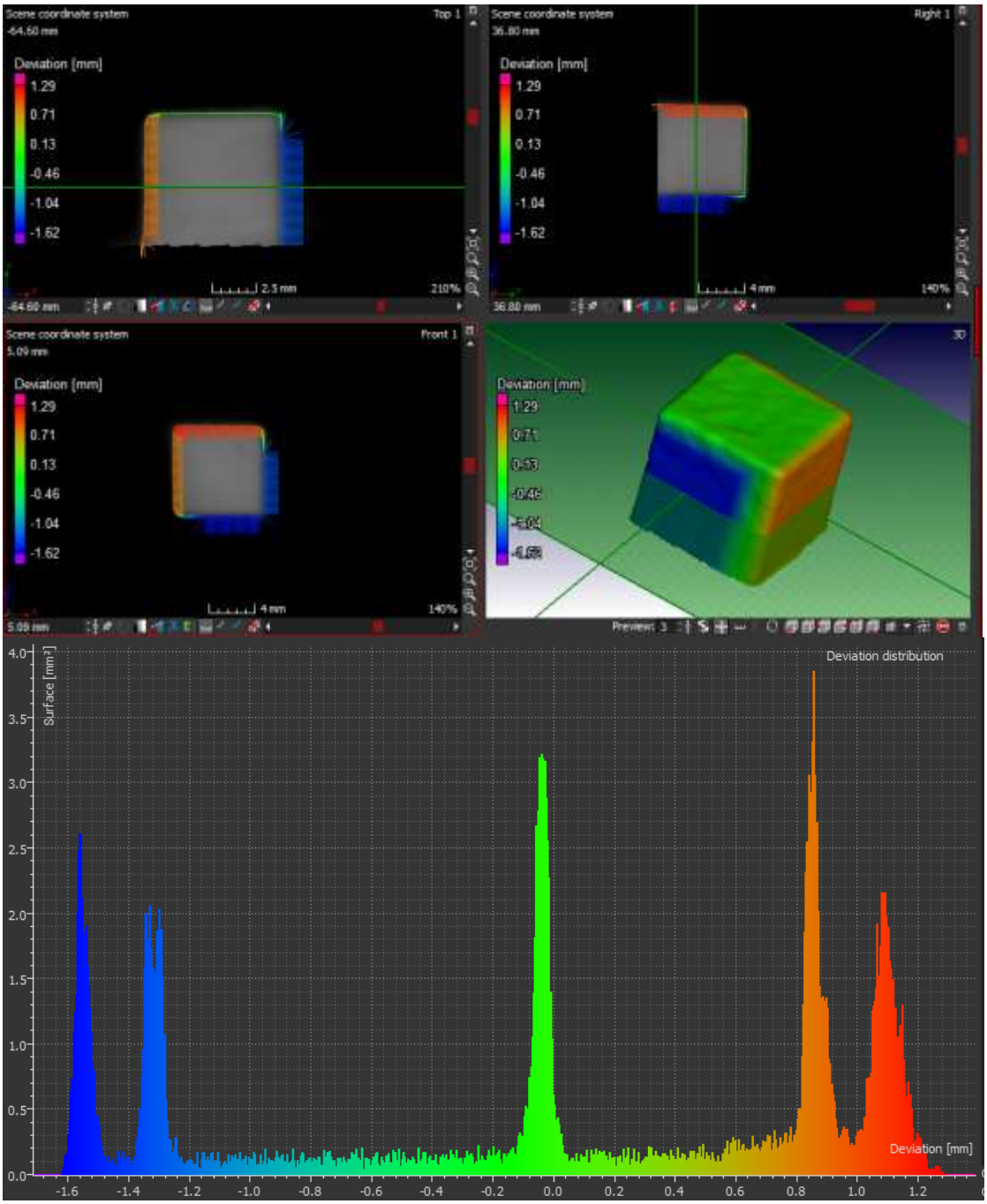


**Figure C. 10. Cube**

### *Freeform (conical)*

Minimum and maximum deviation of the freeform (conical) was -1.01 mm and 1.14 mm respectively. From Figure C. 11, it can be seen that green dominates on the surface of the non-constantly sloping profile with traces of blue in the outer surface and red in the inner surface. The deviation distribution shows an irregular shape with the highest peak at the centre of the distribution. Green covers 71.76% of the surface area and is spread from -0.6 mm to 0.6 mm, while blue covers 19.69% with the range from -1.01 mm to -0.6 mm, and finally, red covers 9.00% and is distributed from 0.60 mm to 1.14 mm.

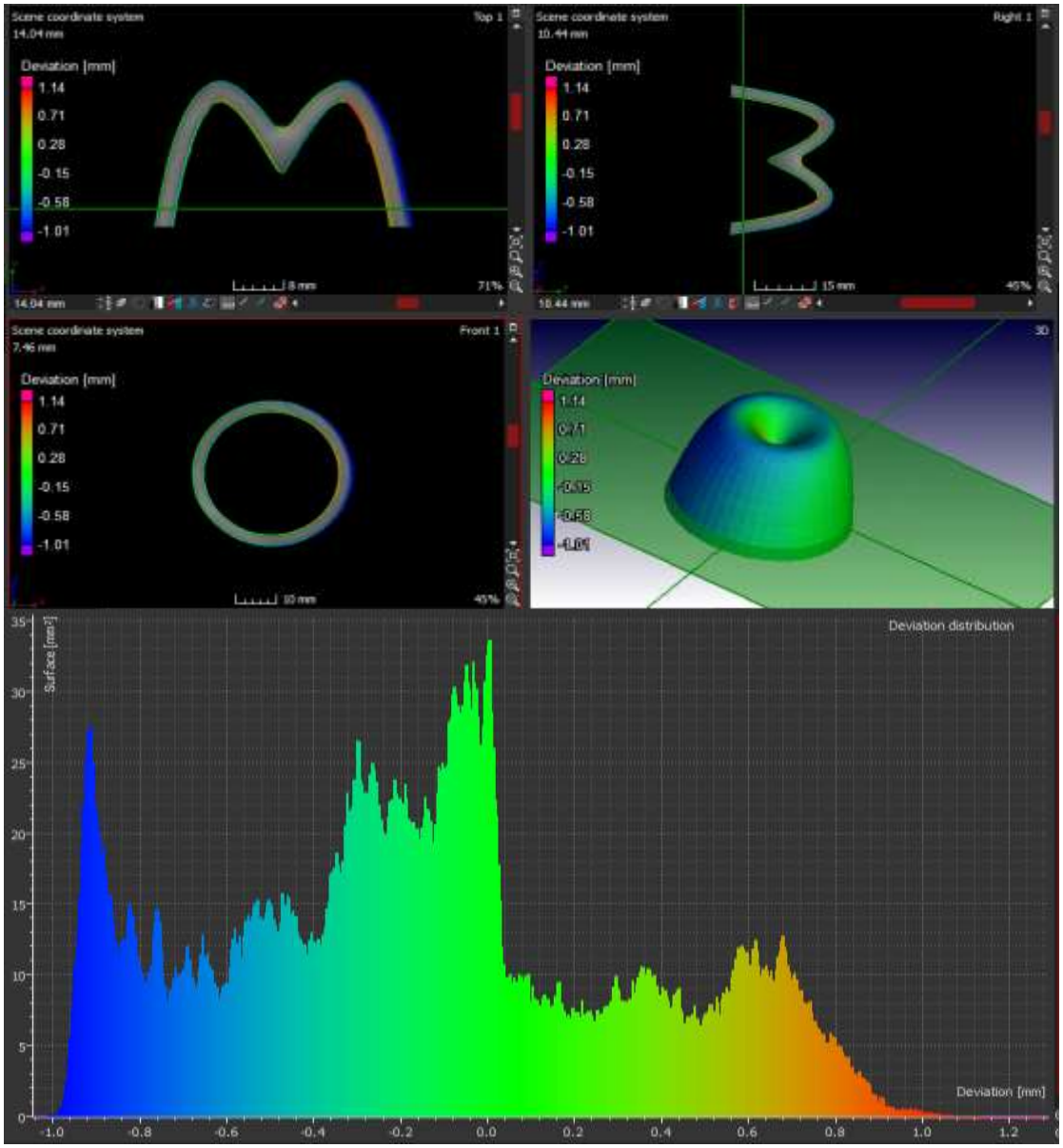


**Figure C. 11. Freeform (conical)**

***Freeform (sinkhole)***

The minimum and maximum deviation for the freeform (sinkhole) was -1.51 mm and 1.46 mm, respectively. The non-constant sloping profile is covered in green with hints of blue, as seen on the 3D view in Figure C. 12. below. A trace of red is seen on the inside of the non-constant slope, as indicated in the top, right and front section views. The deviation distribution has different peaks that are clustered towards the centre of the distribution. Green is dominant with 66.60%, and is distributed from -0.60 mm to 0.80 mm. Blue covers around 24.63% and ranges from -1.51 mm to -0.6 mm, while red covers 8.92%, and is spread from 0.80 mm to 1.46 mm on the distribution.

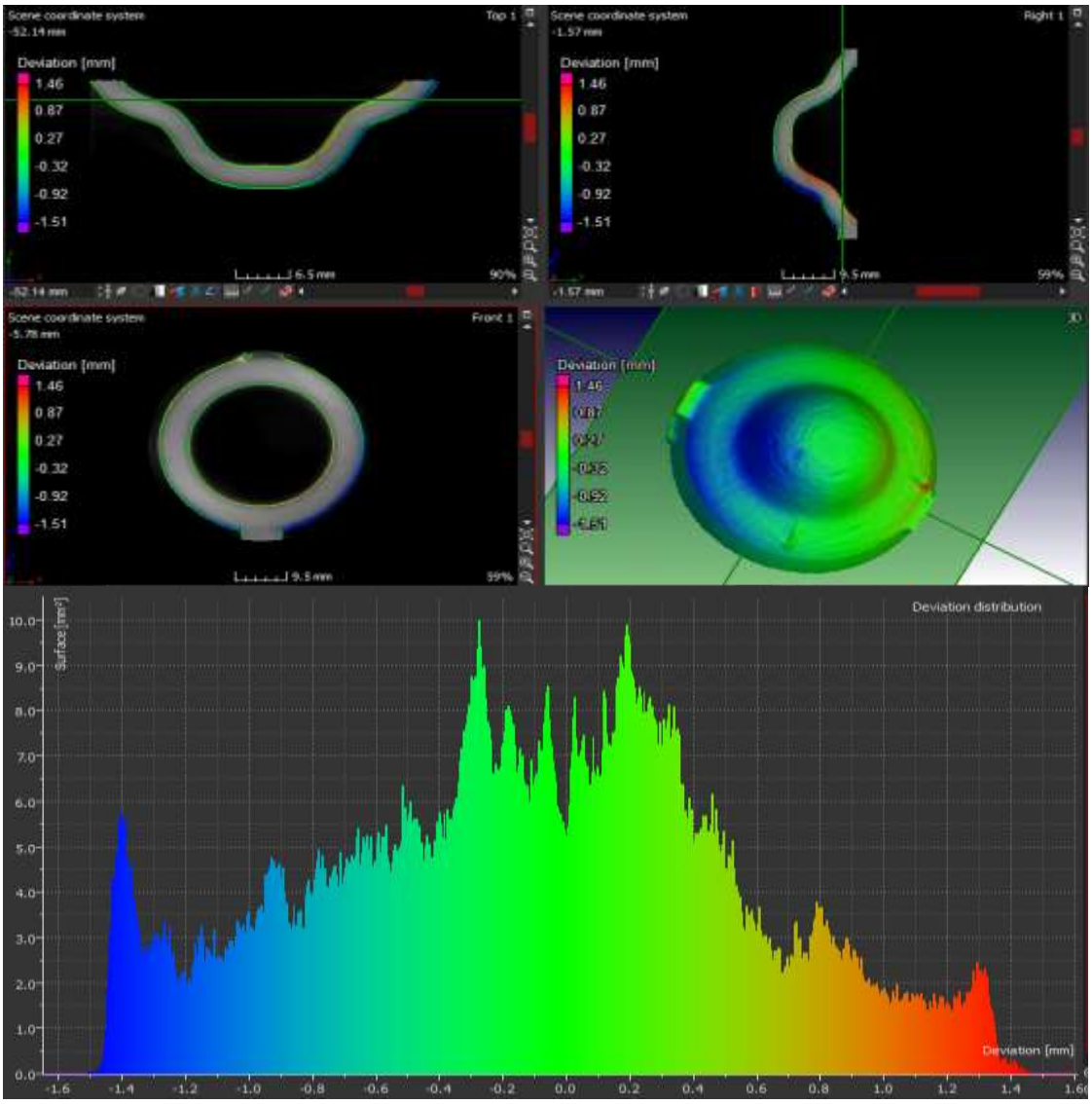


**Figure C. 12. Freeform (sinkhole)**

## Comparison of castings from PMMA and PrimeCast® patterns results

An analysis was done on five selected features from each casting, which were cube, rectangular protrusion, cone, freeform (conical) and freeform (sinkhole), as well as for the full volume of a casting. The analysis results for these features are tabulated in Table C. 1, which also gives the minimum and maximum deviation, the mean and the standard deviation.

**Table C. 1. Analysis from five selected feature of the castings**

| **Full volume** | | | | |
|---|---|---|---|---|
| ***Castings*** | ***Left (mm)*** | ***Right (mm)*** | ***Mean (mm)*** | ***Deviation (mm)*** |
| **PMMA1** | -1.50 | 1.50 | -0.14 | 0.45 |
| **PMMA2** | -1.50 | 1.50 | -0.11 | 0.40 |
| **PC1** | -1.50 | 1.50 | -0.14 | 0.65 |
| **PC2** | -1.50 | 1.50 | -0.11 | 0.67 |
| **Cube** | | | | |
| **PMMA1** | -0.75 | 0.53 | -0.15 | 0.45 |
| **PMMA2** | -0.63 | 0.45 | -0.11 | 0.34 |
| **PC1** | -1.62 | 1.29 | -0.01 | 0.98 |
| **PC2** | -1.77 | 1.54 | -0.02 | 1.12 |
| **Rectangular protrusion** | | | | |
| **PMMA1** | -1.76 | 1.63 | -0.63 | 0.69 |
| **PMMA2** | -0.78 | 1.47 | -0.21 | 0.46 |
| **PC1** | -1.46 | 1.44 | -0.13 | 0.71 |
| **PC2** | -1.46 | 1.38 | -0.15 | 0.65 |
| **Cone** | | | | |
| **PMMA1** | -1.39 | 1.21 | 0.02 | 0.41 |
| **PMMA2** | -1.04 | 1.50 | 0.04 | 0.29 |
| **PC1** | -1.20 | 1.30 | -0.12 | 0.64 |
| **PC2** | -1.48 | 1.98 | -0.07 | 0.79 |
| **Freeform (conical)** | | | | |
| **PMMA1** | -1.49 | 1.03 | -0.15 | 0.34 |
| **PMMA2** | -1.48 | 0.98 | -0.04 | 0.25 |
| **PC1** | -1.01 | 1.14 | -0.15 | 0.47 |
| **PC2** | -1.47 | 1.22 | -0.11 | 0.52 |
| **Freeform (sinkhole)** | | | | |
| **PMMA1** | -1.44 | 0.98 | -0.04 | 0.40 |
| **PMMA2** | -0.87 | 0.75 | -0.08 | 0.33 |
| **PC1** | -1.51 | 1.46 | -0.12 | 0.66 |
| **PC2** | -1.49 | 1.64 | -0.01 | 0.71 |

When the tolerances were set at -1.5 mm to 1.5 mm for full volume, the surface area within this range of PMMA1 and PMMA2 was 99.21% and 98.77%, respectively. The similar surface area for PC1 and PC2 was 98.62% and 97.85%, respectively. The mean deviation value for PMMA1 and PC1 is the same (-0.14) and similarly, the mean deviation value for PMMA2 and PC2 (-0.11). However, their standard deviations are different. The standard deviation of PMMA1 and PMMA2 are smaller than that of PC1 and PC2. This means that PC1 and PC2 have more variability than PMMA1 and PMMA2, respectively. PMMA2 has the smallest standard deviation: its data values are most concentrated around the mean. With the cube, the tolerances range of the castings from the PMMA patterns was smaller compared to that of the PrimeCast® patterns.

# Appendix D: Dimensional accuracy of individual features on the patterns

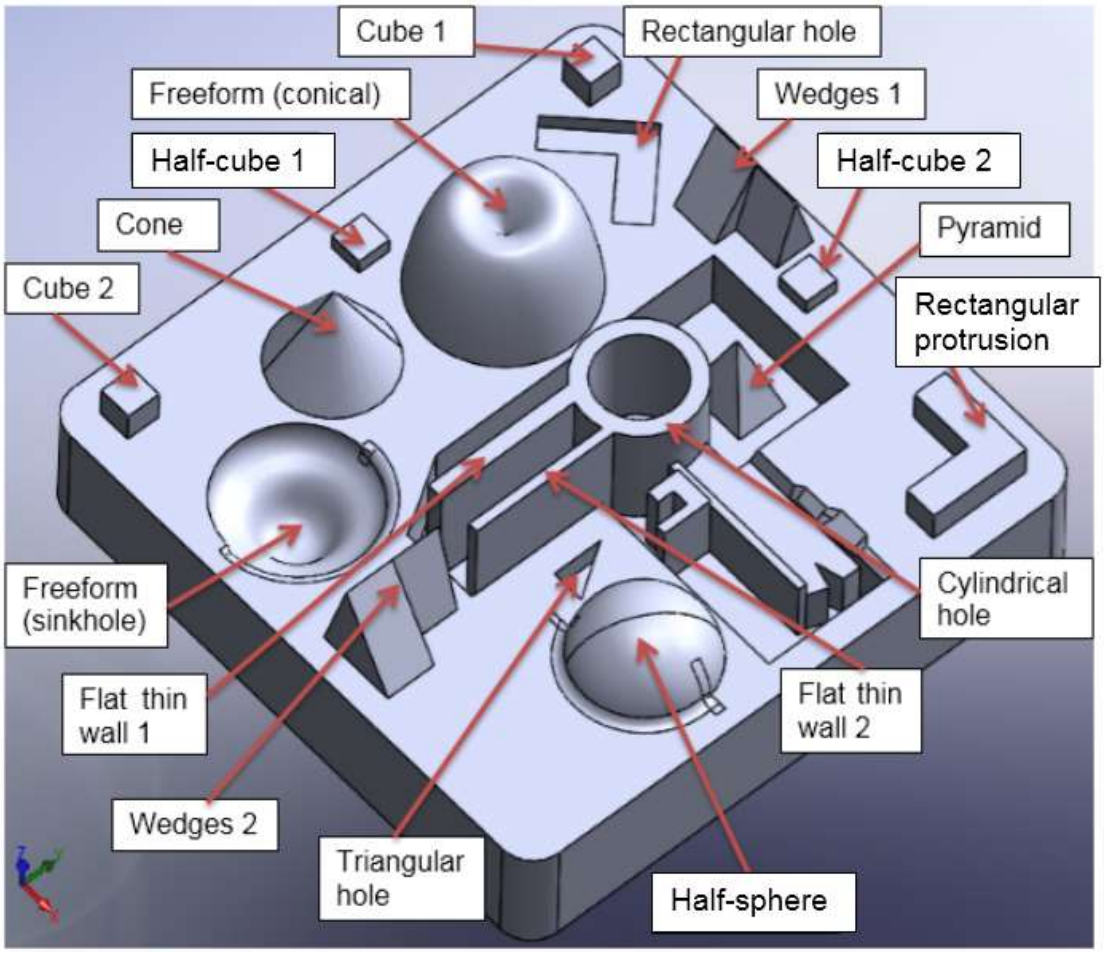


**Figure D. 1: Features on the standard part labelled for measurements**

## PMMA

**Table D. 1. Dimensional accuracy of each feature on the standard part**

| ***Feature*** | | ***Dimensions*** | | |
|---|---|---|---|---|
| | | ***CAD*** | ***PMMA*** | ***Difference*** |
| Cube 1 | X-axis | 8.42 mm | 8.46 mm | 0.04 mm |
| | Y-axis | 8.42 mm | 8.56 mm | 0.14 mm |
| | Z-axis | 8.42 mm | 8.36 mm | -0.06 mm |
| Cube 2 | X-axis | 8.42 mm | 8.24 mm | -0.18 mm |
| | Y-axis | 8.42 mm | 8.19 mm | -0.24 mm |
| | Z-axis | 8.42 mm | 8.38 mm | -0.04 mm |
| Half-cube 1 | X-axis | 8.42 mm | 8.65 mm | 0.23 mm |
| | Y-axis | 8.42 mm | 8.49 mm | 0.07 mm |
| | Z-axis | 4.21 mm | 4.01 mm | -0.20 mm |

| | | | | |
|---|---|---|---|---|
| Half-cube 2 | X-axis | 8.42 mm | 8.39 mm | -0.03 mm |
| | Y-axis | 8.42 mm | 8.32 mm | -0.10 mm |
| | Z-axis | 4.21 mm | 3.89 mm | -0.32 mm |
| Rectangular protrusion | X-axis | 25.25 mm | 25.88 mm | 0.63 mm |
| | Y-axis | 25.25 mm | 25.55 mm | 0.30 mm |
| | Z-axis | 8.42 mm | 8.18 mm | -0.24 mm |
| Pyramid | X-axis | 16.20 mm | 16.04mm | -0.16 mm |
| | Y-axis | 12.40 mm | 12.68 mm | 0.28 mm |
| | Z-axis | 23.30 mm | 22.88 mm | -0.42 mm |
| Half-sphere | Ø | 33.70 mm | 33.35 mm | -0.35 mm |
| | Thickness | 3.30 mm | 3.22 mm | -0.08 mm |
| Cone | Ø | 25.30 mm | 25.48 mm | 0.18 mm |
| | Z-axis | 28.35 mm | 28.30 mm | -0.05 mm |
| Freeform (conical) | Ø | 36.00 mm | 35.77 mm | -0.23 mm |
| | Z-axis | 27.65.mm | 27.52 mm | -0.13 mm |
| Freeform (sinkhole) | Ø | 37.00 mm | 37.84 mm | -0.84 mm |
| | Z-axis | 20.30 mm | 20.03 mm | -0.17 mm |
| Wedges 1 | X-axis | 19.22 mm | 19.12 mm | -0.10 mm |
| | Y-axis | 25.25 mm | 25.28 mm | 0.03 mm |
| | Angle | 74.95º | 74.82º | -0.13º |
| Wedges 2 | X-axis | 25.25 mm | 25.16 mm | -0.09 mm |
| | Y-axis | 15.50 mm | 15.27 mm | -0.23 mm |
| | Angle | 74.95º | 74.63º | -0.32º |
| Rectangular hole | X-axis | 25.25 mm | 25.58 mm | 0.33 mm |
| | Y-axis | 25.25 mm | 25.37 mm | 0.12 mm |
| | Z-axis | 4.20 mm | 4.11 mm | -0.09 mm |
| Cylindrical hole/ Hollow cylinder | $Ø_{Inner}$ | 21.00 mm | 21.19 mm | 0.19 mm |
| | $Ø_{Outer}$ | 29.40 mm | 29.22 mm | -0.18 mm |
| | Z-axis | 29.45 mm | 29.68 mm | 0.23 mm |
| Triangular hole | X-axis | 8.40 mm | 8.27 mm | -0.13 mm |
| | Y-axis | 12.60 mm | 12.47 mm | -0.13 mm |
| | Z-axis | 5.60 mm | 5.78 mm | 0.18 mm |
| Flat thin wall 1 | X-axis | 4.20 mm | 4.42 mm | 0.22 mm |
| | Y-axis | 36.30 mm | 36.57 mm | 0.27 mm |
| | Z-axis | 29.45 mm | 29.38 mm | -0.07 mm |
| Flat thin wall 2 | X-axis | 2.50 mm | 2.37 mm | -0.13 mm |
| | Y-axis | 36.45 mm | 36.42 mm | -0.03 mm |
| | Z-axis | 29.45 mm | 29.67 mm | 0.22 mm |
| Square base | X-axis | 151.50 mm | 151.05 mm | -0.45 mm |
| | Y-axis | 151.50 mm | 151.23 mm | -0.27 mm |
| | Z-axis | 29.46 mm | 29.41 mm | -0.05 mm |

## PrimeCast®

**Table D. 2. Dimensional accuracy of each feature on the standard part**

| *Feature* | | *Dimensions* | | |
|---|---|---|---|---|
| | | *CAD* | *PrimeCast®* | *Difference* |
| Cube 1 | X-axis | 8.42 mm | 8.33 mm | -0.09 mm |
| | Y-axis | 8.42 mm | 8.60 mm | 0.18 mm |
| | Z-axis | 8.42 mm | 8.39 mm | -0.03 mm |
| Cube 2 | X-axis | 8.42 mm | 8.30 mm | -0.12 mm |
| | Y-axis | 8.42 mm | 8.18 mm | -0.25 mm |
| | Z-axis | 8.42 mm | 8.37 mm | -0.05 mm |
| Half-cube 1 | X-axis | 8.42 mm | 8.65 mm | 0.23 mm |
| | Y-axis | 8.42 mm | 8.59 mm | 0.17 mm |
| | Z-axis | 4.21 mm | 3.84 mm | -0.37 mm |
| Half-cube 2 | X-axis | 8.42 mm | 8.39 mm | -0.03 mm |
| | Y-axis | 8.42 mm | 8.22 mm | -0.20 mm |
| | Z-axis | 4.21 mm | 3.92 mm | -0.29 mm |
| Rectangular protrusion | X-axis | 25.25 mm | 24.98 mm | -0.27 mm |
| | Y-axis | 25.25 mm | 24.95 mm | -0.30 mm |
| | Z-axis | 8.42 mm | 8.33 mm | -0.09 mm |
| Pyramid | X-axis | 16.50 mm | 16.68 mm | 0.18 mm |
| | Y-axis | 12.36 mm | 12.58 mm | 0.22 mm |
| | Z-axis | 23.30 mm | 23.49 mm | 0.19 mm |
| Half-sphere | Ø | 34.50 mm | 34.65 mm | 0.15 mm |
| | Thickness | 4.30 mm | 4.18 mm | -0.12 mm |
| Cone | Ø | 29.00 mm | 29.27 mm | 0.27 mm |
| | Z-axis | 28.35 mm | 28.30 mm | 0.05 mm |
| Freeform (conical) | Ø | 36.00 mm | 36.18 mm | 0.18 mm |
| | Z-axis | 27.65.mm | 27.89 mm | 0.24 mm |
| Freeform (sinkhole) | Ø | 35.80 mm | 35.74 mm | -0.06 mm |
| | Z-axis | 20.30 mm | 20.09 mm | -0.21 mm |
| Wedges 1 | X-axis | 19.22 mm | 18.89 mm | -0.33 mm |
| | Y-axis | 25.25 mm | 25.38 mm | 0.13 mm |
| | Angle | 74.95º | 74.87º | -0.08º |
| Wedges 2 | X-axis | 25.25 mm | 24.93 mm | -0.32 mm |
| | Y-axis | 15.50 mm | 15.17 mm | -0.33 mm |
| | Angle | 74.95º | 74.56º | -0.39º |
| Rectangular hole | X-axis | 25.25 mm | 24.95 mm | -0.30 mm |
| | Y-axis | 25.25 mm | 24.88 mm | -0.37 mm |
| | Z-axis | 4.20 mm | 4.29 mm | 0.09 mm |
| Cylindrical hole/ Hollow cylinder | $Ø_{Inner}$ | 29.42 mm | 29.54 mm | -0.12 mm |
| | $Ø_{Outer}$ | 21.00 mm | 21.29 mm | 0.29 mm |
| | Z-axis | 29.45 mm | 29.59 mm | 0.14 mm |
| Triangular hole | X-axis | 8.40 mm | 8.53 mm | 0.13 mm |
| | Y-axis | 12.60 mm | 12.78 mm | 0.18 mm |
| | Z-axis | 5.60 mm | 5.71 mm | 0.11 mm |
| Flat thin wall 1 | X-axis | 4.20 mm | 4.33 mm | 0.13 mm |

| | | | | |
|---|---|---|---|---|
| | Y-axis | 36.30 mm | 36.13 mm | -0.17 mm |
| | Z-axis | 29.45 mm | 29.27 mm | -0.18 mm |
| Flat thin wall 2 | X-axis | 2.50 mm | 2.77 mm | 0.27 mm |
| | Y-axis | 36.45 mm | 36.37 mm | -0.08 mm |
| | Z-axis | 29.45 mm | 29.33 mm | -0.12 mm |
| Square base | X-axis | 151.50 mm | 151.05 mm | -0.45 mm |
| | Y-axis | 151.50 mm | 151.66 mm | 0.16 mm |
| | Z-axis | 29.46 mm | 29.17 mm | -0.29 mm |

# Appendix E: Dimensional accuracy of individual features on the castings

## PMMA

**Table E. 1. Dimensional accuracy of each feature on the standard part**

| *Feature* | | *Dimensions* | | |
|---|---|---|---|---|
| | | *CAD* | *PMMA* | *Difference* |
| Cube 1 | X-axis | 8.42 mm | 8.33 mm | -0.09 mm |
| | Y-axis | 8.42 mm | 8.60 mm | 0.18 mm |
| | Z-axis | 8.42 mm | 8.39 mm | -0.03 mm |
| Cube 2 | X-axis | 8.42 mm | 8.30 mm | -0.12 mm |
| | Y-axis | 8.42 mm | 8.18 mm | -0.25 mm |
| | Z-axis | 8.42 mm | 8.37 mm | -0.05 mm |
| Half-cube 1 | X-axis | 8.42 mm | 8.85 mm | 0.43 mm |
| | Y-axis | 8.42 mm | 8.59 mm | 0.17 mm |
| | Z-axis | 4.21 mm | 3.84 mm | -0.37 mm |
| Half-cube 2 | X-axis | 8.42 mm | 8.39 mm | -0.03 mm |
| | Y-axis | 8.42 mm | 8.22 mm | -0.20 mm |
| | Z-axis | 4.21 mm | 3.79 mm | -0.42 mm |
| Rectangular protrusion | X-axis | 25.25 mm | 24.88 mm | -0.37 mm |
| | Y-axis | 25.25 mm | 24.85 mm | -0.40 mm |
| | Z-axis | 8.42 mm | 7.94 mm | -0.48 mm |
| Pyramid | X-axis | 16.50 mm | 17.05 mm | 0.55 mm |
| | Y-axis | 12.36 mm | 12.88 mm | 0.52 mm |
| | Z-axis | 23.30 mm | 21.88 mm | -1.42 mm |
| Half-sphere | Ø | 34.50 mm | 34.65 mm | 0.15 mm |
| | Thickness | 3.30 mm | 3.18 mm | -0.12 mm |
| Cone | Ø | 25.30 mm | 24.37 mm | -0.93 mm |
| | Z-axis | 28.35 mm | 27.30 mm | -1.05 mm |
| Freeform (conical) | Ø | 36.00 mm | 35.26 mm | -0.74 mm |
| | Z-axis | 27.65 mm | 28.02 mm | 0.37 mm |
| Freeform (sinkhole) | Ø | 37.00 mm | 36.84 mm | -0.16 mm |
| | Z-axis | 20.30 mm | 19.95 mm | -0.35 mm |
| Wedges 1 | X-axis | 19.22 mm | 19.99 mm | 0.77 mm |
| | Y-axis | 25.25 mm | 25.38 mm | 0.13 mm |
| | Angle | 74.95º | 74.77º | -0.16º |
| Wedges 2 | X-axis | 25.25 mm | 25.31 mm | 0.06 mm |
| | Y-axis | 15.50 mm | 14.47 mm | -1.03 mm |
| | Angle | 74.95º | 74.10º | -0.85º |
| Rectangular hole | X-axis | 25.25 mm | 24.95 mm | -0.30 mm |
| | Y-axis | 25.25 mm | 25.88 mm | 0.55 mm |
| | Z-axis | 4.20 mm | 4.09 mm | -0.11 mm |
| Cylindrical hole/ Hollow cylinder | $Ø_{Inner}$ | 29.42 mm | 29.91 mm | 0.49 mm |
| | $Ø_{Outer}$ | 21.00 mm | 21.29 mm | 0.29 mm |

| | | | | |
|---|---|---|---|---|
| | Z-axis | 29.45 mm | 28.68 mm | -0.77 mm |
| Triangular hole | X-axis | 8.40 mm | 8.06 mm | -0.34 mm |
| | Y-axis | 12.60 mm | 11.67 mm | -0.92 mm |
| | Z-axis | 5.60 mm | 5.90 mm | 0.30 mm |
| Flat thin wall 1 | X-axis | 4.20 mm | 3.17 mm | -1.03 mm |
| | Y-axis | 36.30 mm | 37.29 mm | 1.02 mm |
| | Z-axis | 29.45 mm | 28.50 mm | -0.95 mm |
| Flat thin wall 2 | X-axis | 2.50 mm | 2.34 mm | -0.16 mm |
| | Y-axis | 36.45 mm | 36.37 mm | -0.08 mm |
| | Z-axis | 29.45 mm | 27.65 mm | -1.80 mm |
| Square base | X-axis | 151.50 mm | 150.05 mm | -1.45 mm |
| | Y-axis | 151.50 mm | 151.66 mm | 0.16 mm |
| | Z-axis | 29.46 mm | 28.43 mm | -1.03 mm |

**PrimeCast®**

**Table E. 2. Dimensional accuracy of each feature on the standard part**

| ***Feature*** | | ***Dimensions*** | | |
|---|---|---|---|---|
| | | ***CAD*** | ***PrimeCast®*** | ***Difference*** |
| Cube 1 | X-axis | 8.42 mm | 7.98 mm | -0.44 mm |
| | Y-axis | 8.42 mm | 7.95 mm | -0.47 mm |
| | Z-axis | 8.42 mm | 8.60 mm | 0.18 mm |
| Cube 2 | X-axis | 8.42 mm | 8.68 mm | 0.26 mm |
| | Y-axis | 8.42 mm | 7.96 mm | -0.46 mm |
| | Z-axis | 8.42 mm | 7.98 mm | -0.44 mm |
| Half-cube 1 | X-axis | 8.42 mm | 8.98 mm | 0.56 mm |
| | Y-axis | 8.42 mm | 7.95 mm | -0.47 mm |
| | Z-axis | 4.21 mm | 4.59 mm | 0.38 mm |
| Half-cube 2 | X-axis | 8.42 mm | 8.96 mm | 0.54 mm |
| | Y-axis | 8.42 mm | 8.01 mm | -0.41 mm |
| | Z-axis | 4.21 mm | 3.98 mm | -0.23 mm |
| Rectangular protrusion | X-axis | 25.25 mm | 24.55 mm | -0.70 mm |
| | Y-axis | 25.25 mm | 24.62 mm | -0.63 mm |
| | Z-axis | 8.42 mm | 7.62 mm | -0.80 mm |
| Pyramid | X-axis | 16.50 mm | 16.60 mm | 0.10 mm |
| | Y-axis | 12.36 mm | 12.68 mm | 0.28 mm |
| | Z-axis | 23.30 mm | 22.77 mm | -0.53 mm |
| Half-sphere | Ø | 34.50 mm | 34.87 mm | 0.37 mm |
| | Thickness | 3.30 mm | 3.01 mm | -0.29 mm |
| Cone | Ø | 25.30 mm | 24.63 mm | -0.67 mm |
| | Z-axis | 28.35 mm | 27.40 mm | -0.95 mm |
| Freeform (conical) | Ø | 36.00 mm | 36.79 mm | 0.79 mm |
| | Z-axis | 27.65 mm | 27.51 mm | -0.14 mm |
| Freeform (sinkhole) | Ø | 37.00 mm | 37.66 mm | 0.66 mm |
| | Z-axis | 20.30 mm | 20.00 mm | -0.30 mm |
| Wedges 1 | X-axis | 19.22 mm | 19.45 mm | 0.23 mm |

| | | | | |
|---|---|---|---|---|
| | Y-axis | 25.25 mm | 24.35 mm | -0.90 mm |
| | Angle | 74.93º | 73.14º | 1.79º |
| Wedges 2 | X-axis | 25.25 mm | 25.12 mm | -0.13 mm |
| | Y-axis | 15.50 mm | 14.46 mm | -1.04 mm |
| | Angle | 76.10º | 75.22º | 0.88º |
| Rectangular hole | X-axis | 25.25 mm | 25.38 mm | 0.33 mm |
| | Y-axis | 25.25 mm | 25.73 mm | 0.48 mm |
| | Z-axis | 4.20 mm | 3.95 mm | -0.25 mm |
| Cylindrical hole/ Hollow cylinder | $Ø_{Inner}$ | 21.00 mm | 20.77 mm | -0.23 mm |
| | $Ø_{Outer}$ | 29.42 mm | 28.45 mm | -0.97 mm |
| | Z-axis | 29.45 mm | 29.76 mm | 0.31 mm |
| Triangular hole | X-axis | 8.40 mm | 8.04 mm | -0.38 mm |
| | Y-axis | 12.60 mm | 11.97 mm | -0.63 mm |
| | Z-axis | 5.60 mm | 5.92 mm | 0.32 mm |
| Flat thin wall 1 | X-axis | 4.20 mm | 3.69 mm | -0.51 mm |
| | Y-axis | 36.30 mm | 37.28 mm | 1.02 mm |
| | Z-axis | 29.45 mm | 29.11 mm | -0.34 mm |
| Flat thin wall 2 | X-axis | 2.50 mm | 2.02 mm | -0.48 mm |
| | Y-axis | 36.45 mm | 36.94 mm | 0.49 mm |
| | Z-axis | 29.45 mm | 29.93 mm | 0.48 mm |
| Square base | X-axis | 151.50 mm | 148.88 mm | -2.62 mm |
| | Y-axis | 151.50 mm | 149.08 mm | -2.42 mm |
| | Z-axis | 29.46 mm | 28.67 mm | -0.79 mm |

# Appendix G

## PMMA1

| Settings for Analysis 1 (Nominal/actual comparison of PMMA1 [filtered]) | |
|---|---|
| Actual object | PMMA1 [filtered] |
| Nominal object | Mesh 1 |
| Max. distance [mm] | 10.00 |
| Precision | Standard |
| Swap sign of deviation | Off |
| Consider surface orientation | Off |
| Compensate for mesh problems | Off |
| Memory optimized | On |
| Deviation interval [mm] | n/a |
| Interval mode | n/a |
| Min. surface [mm²] | n/a |
| Show components only | Off |
| Tolerancing | Disabled |

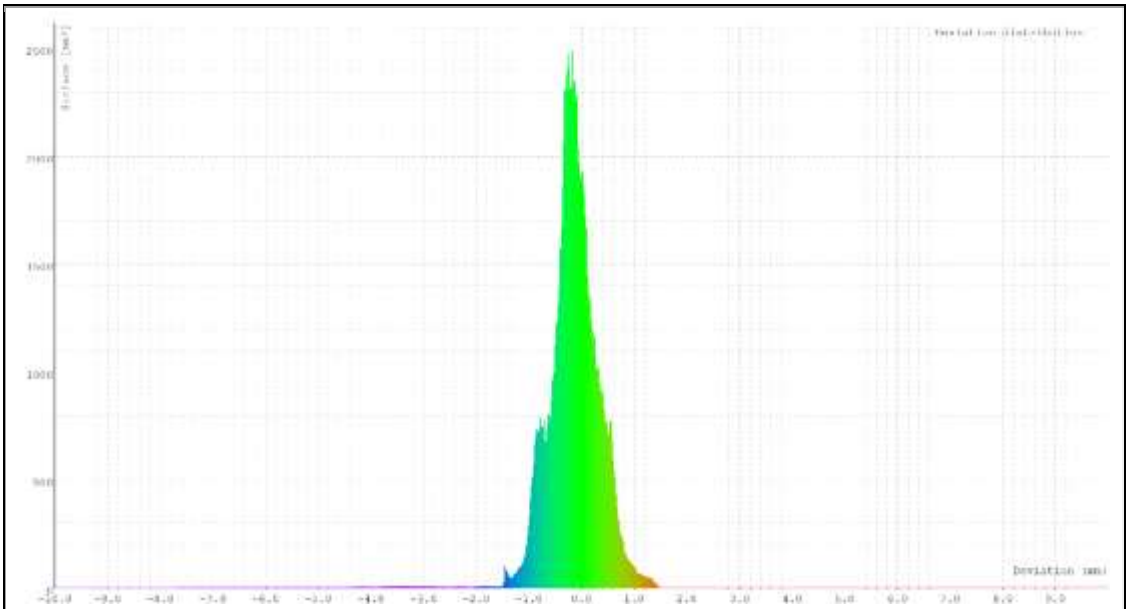

| | |
|---|---|
| Min. deviation [mm] | -8.20 |
| Max. deviation [mm] | 1.77 |

**Figure G. 1. Deviation distribution**

| Cumulation | Absolute |
|---|---|
| Cumulated absolute 90% [mm] | 0.81 |
| Cumulated absolute 95% [mm] | 0.96 |
| Cumulated absolute 98% [mm] | 1.23 |

**Figure G. 2. Cumulated deviation distribution**

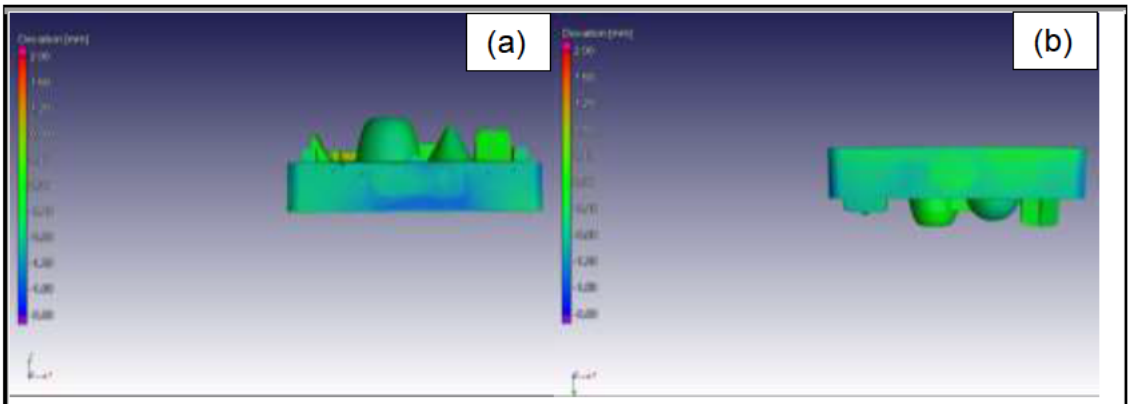


**Figure G. 3. 3D images: (a) top and (b) bottom**

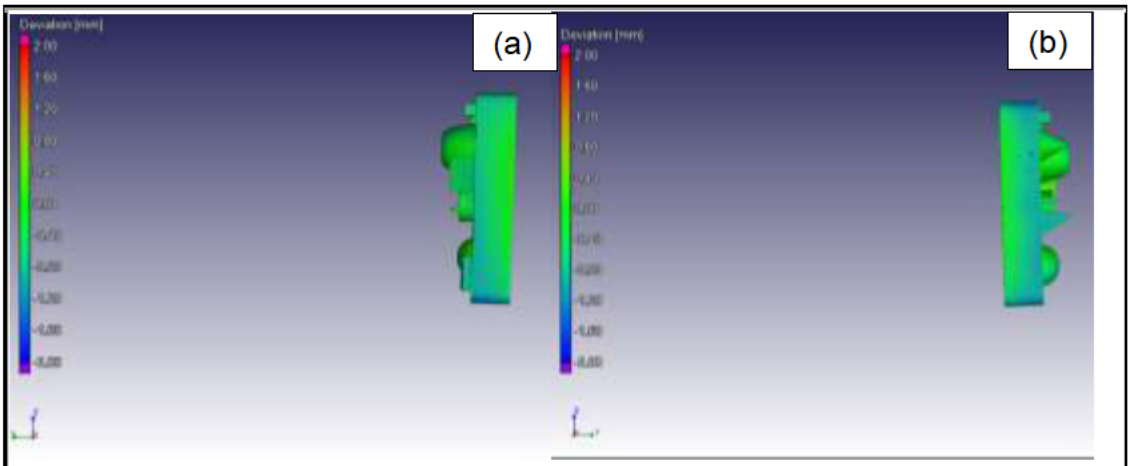


**Figure G. 4. 3D images: (a) left and (b) right**

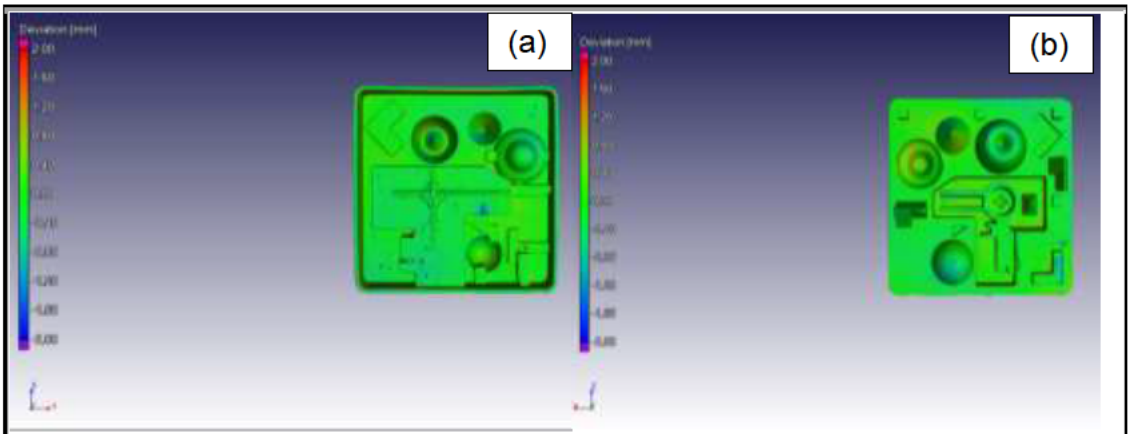


Figure G. 5. 3D images: (a) front and (b) back

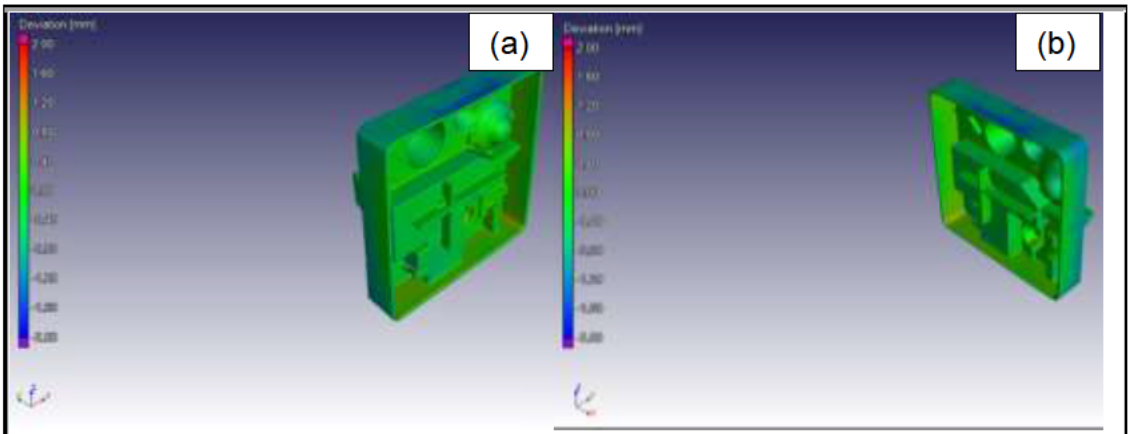


Figure G. 6. 3D images: (a) top-left-front and (b) top-front-right

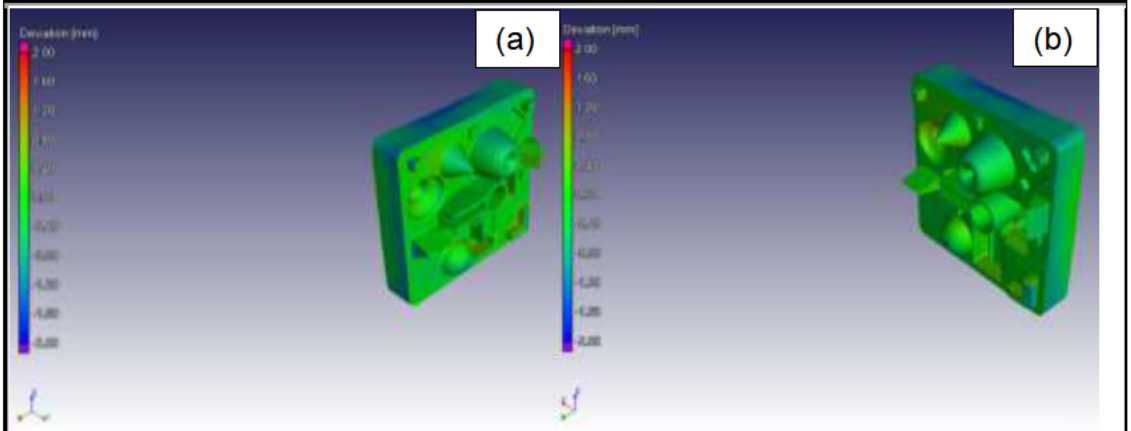


Figure G. 7. 3D images: (a) top-right-back and (b) top-back-left

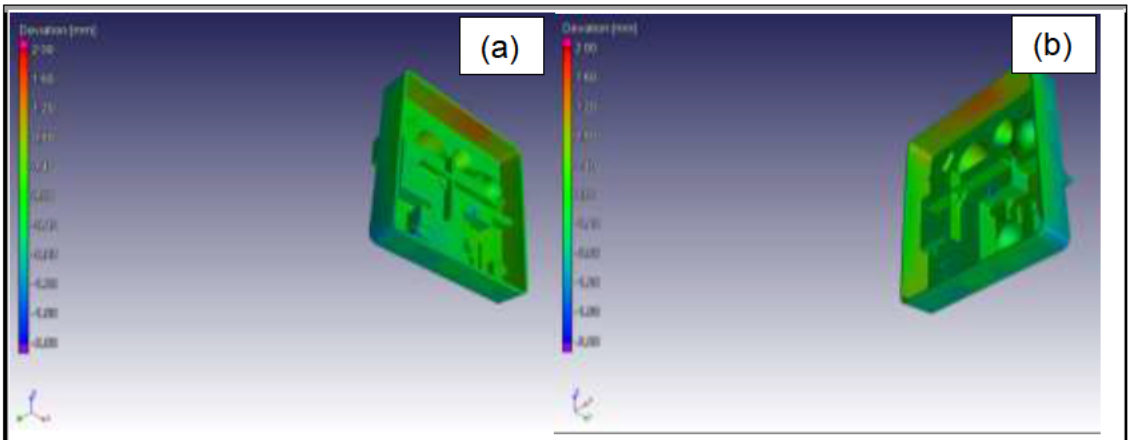


Figure G. 8. 3D images: (a) bottom-left-front and (b) bottom-front-right

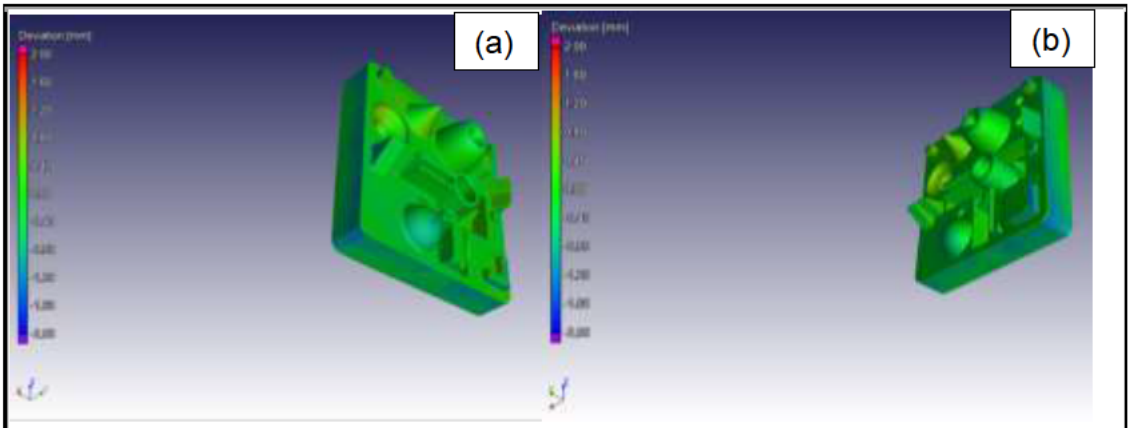


Figure G. 9. 3D images: (a) bottom-right-back and (b) bottom-back-left

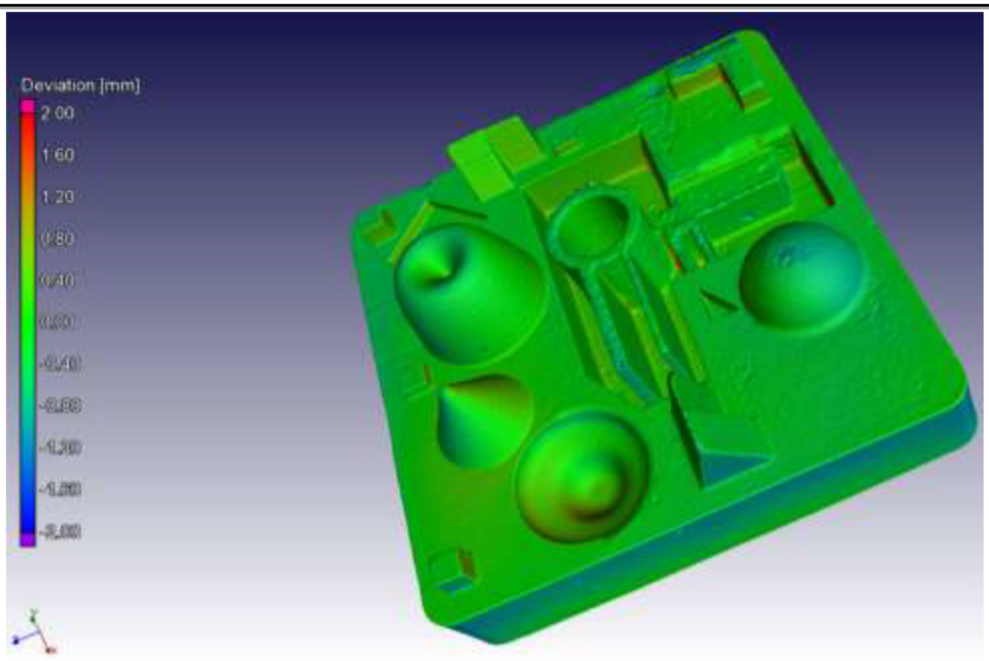


Figure G. 10. 3D image: current camera settings

## PMMA2

| Settings for Analysis 1 (Nominal/actual comparison of PMMA2 [filtered]) | |
|---|---|
| Actual object | PMMA2 [filtered] |
| Nominal object | Mesh 1 |
| Max. distance [mm] | 10.00 |
| Precision | Standard |
| Swap sign of deviation | Off |
| Consider surface orientation | Off |
| Compensate for mesh problems | Off |
| Memory optimized | On |
| Deviation interval [mm] | n/a |
| Interval mode | n/a |
| Min. surface [mm²] | n/a |
| Show components only | Off |
| Tolerancing | Disabled |

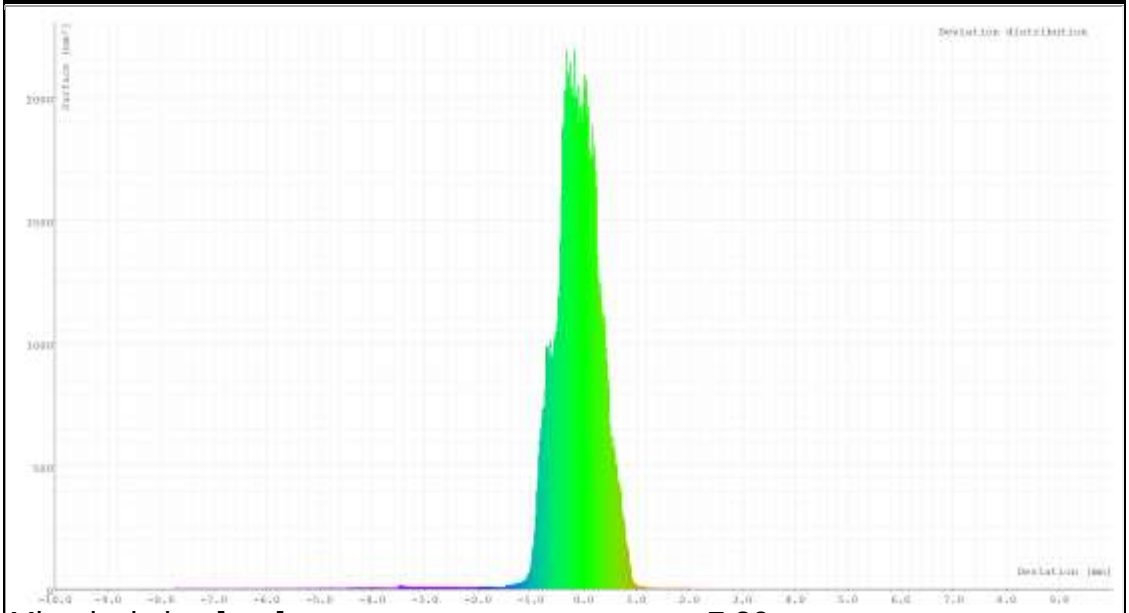

| | |
|---|---|
| Min. deviation [mm] | -7.80 |
| Max. deviation [mm] | 5.37 |

**Figure G. 11. Deviation distribution**

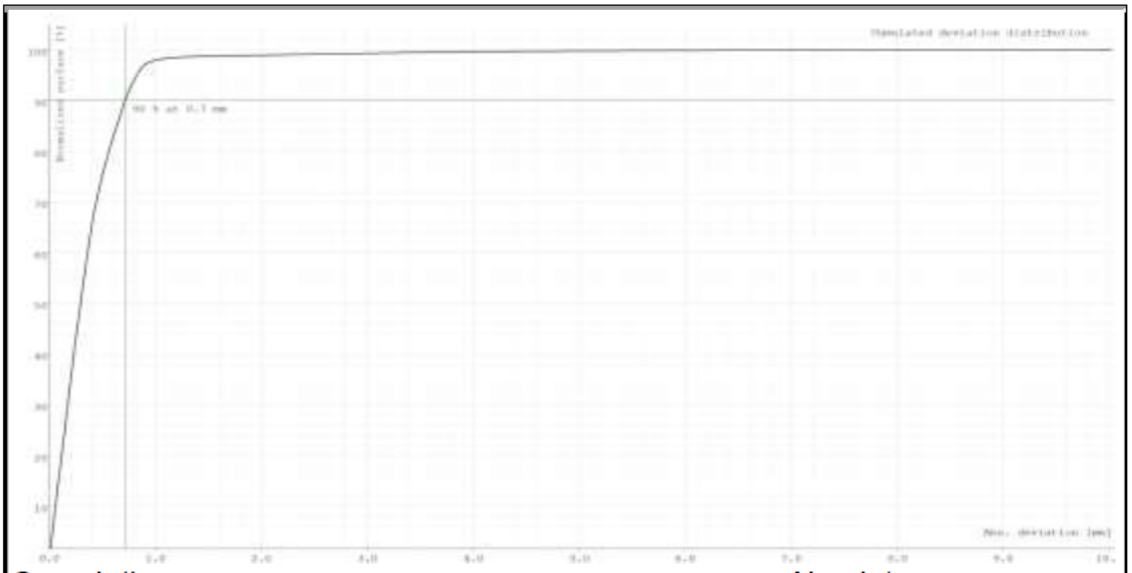

| Cumulation | Absolute |
|---|---|
| Cumulated absolute 90% [mm] | 0.71 |
| Cumulated absolute 95% [mm] | 0.82 |
| Cumulated absolute 98% [mm] | 1.01 |

**Figure G. 12. Cumulated deviation distribution**

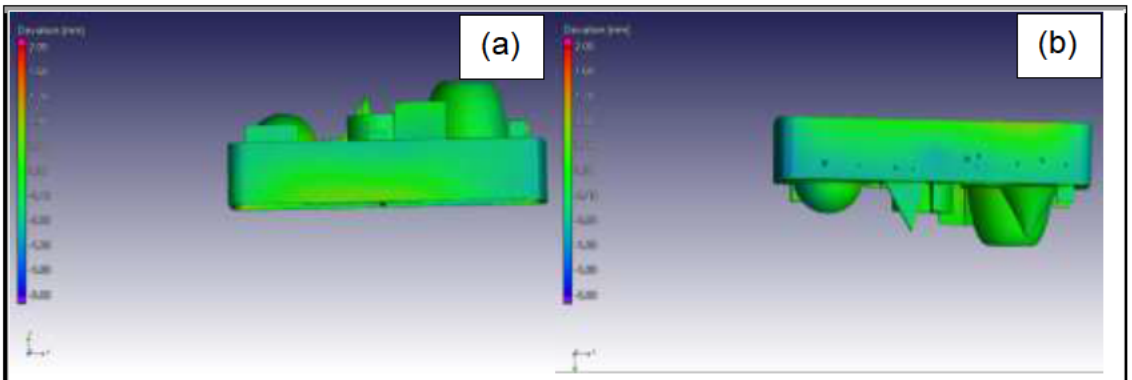


**Figure G. 13. 3D images: (a) top and (b) bottom**

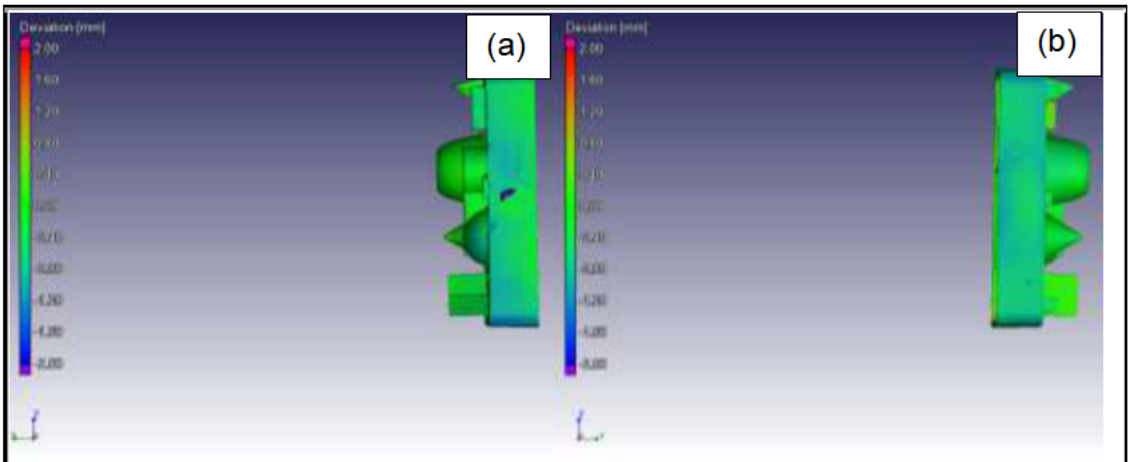


**Figure G. 14. 3D images: (a) left and (b) right**

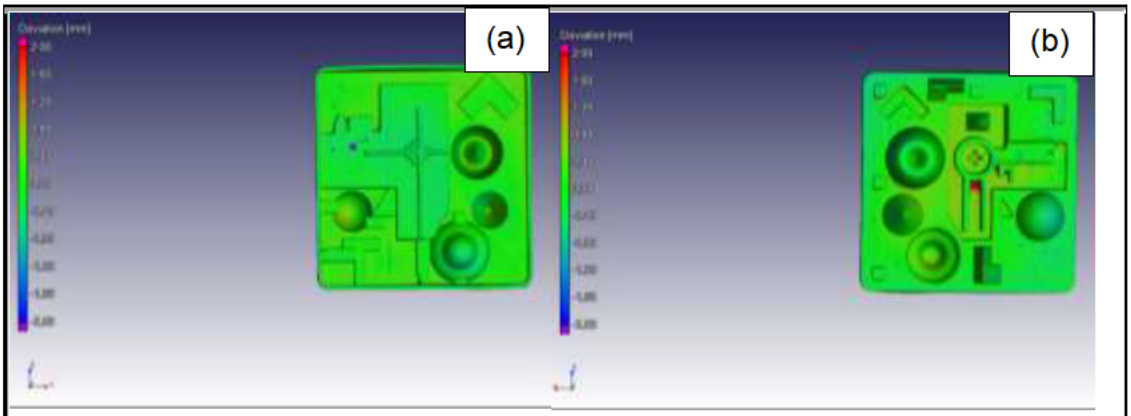


**Figure G. 15. 3D images: (a) front and (b) back**

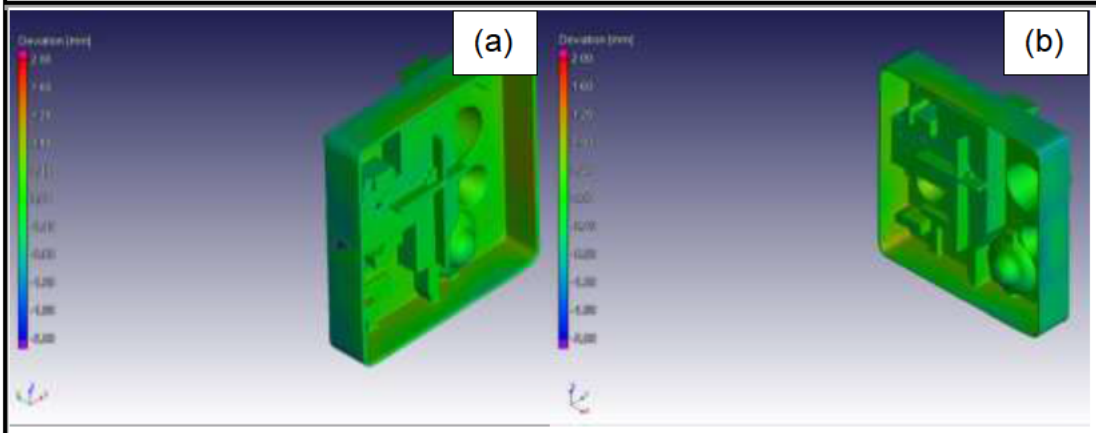


**Figure G. 16. 3D images: (a) top-left-front and (b) top-front-right**

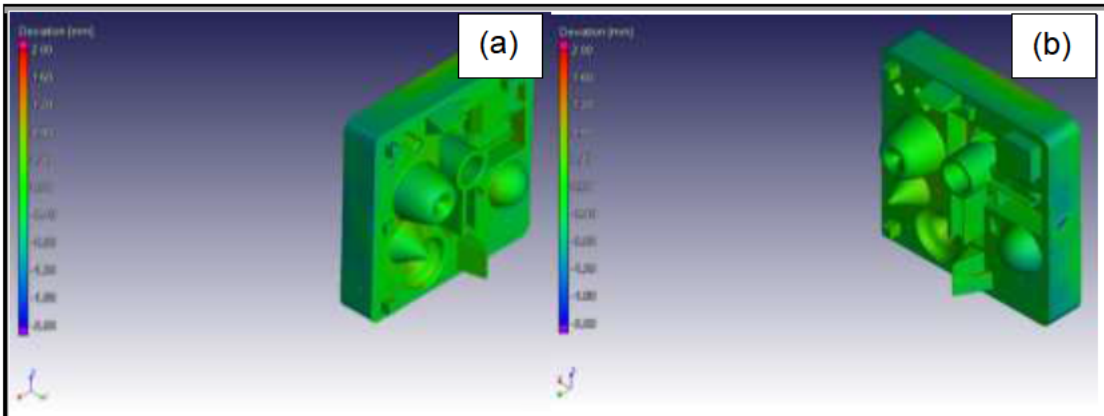


**Figure G. 17. 3D images: (a) top-right-back and (b) top-back-left**

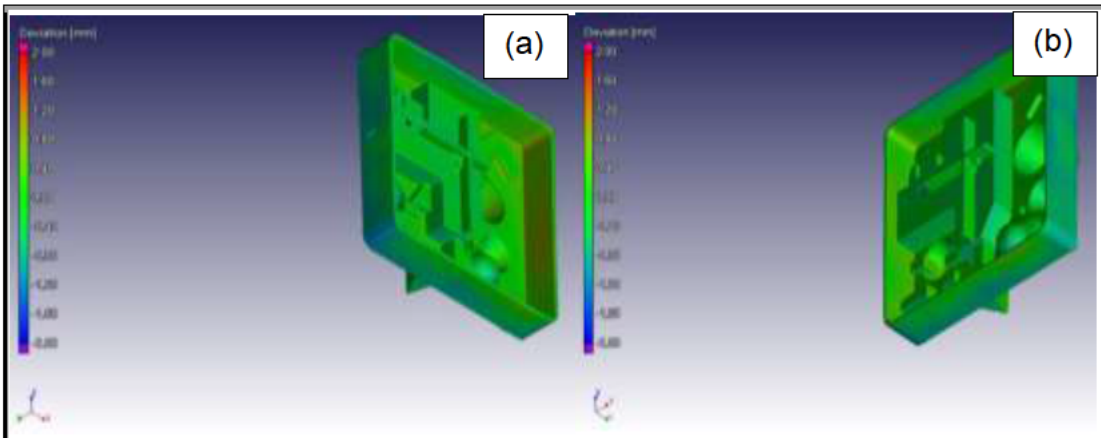


Figure G. 18. 3D images: (a) bottom-left-front and (b) bottom-front-right

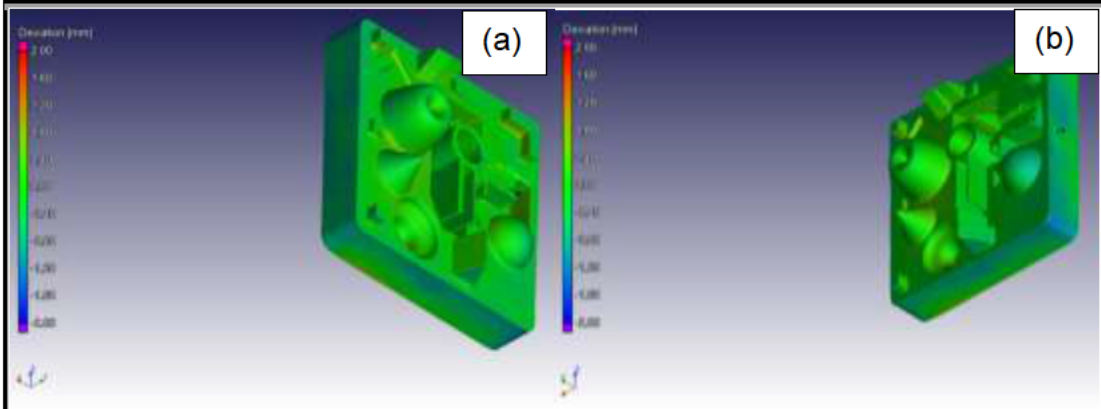


Figure G. 19. 3D images: (a) bottom-right-back and (b) bottom-back-left

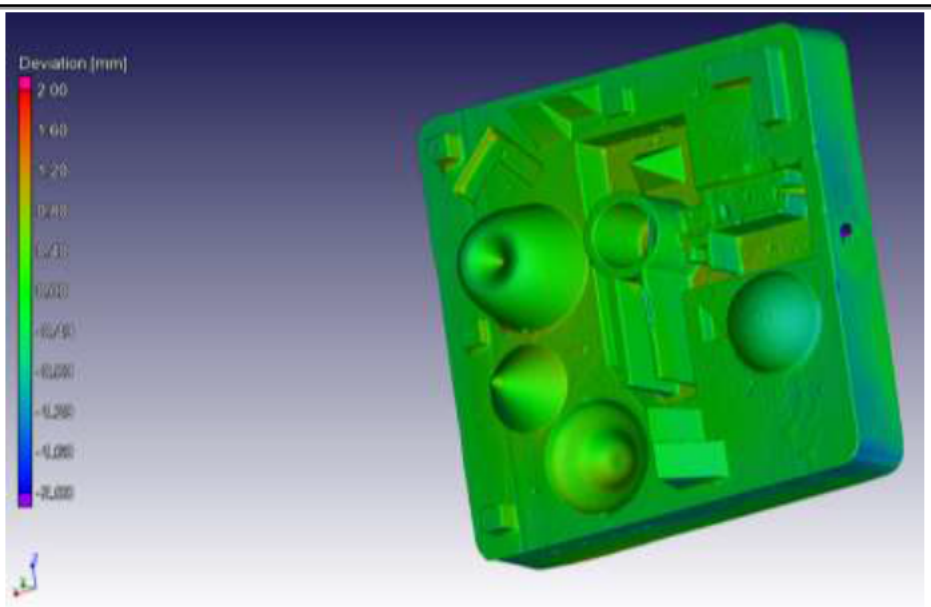


Figure G. 20. 3D image: current camera settings

## PC1

| Settings for Analysis 1 (Nominal/actual comparison of PC 1[filtered]) | |
|---|---|
| Actual object | PC1 [filtered] |
| Nominal object | Mesh 1 |
| Max. distance [mm] | 3.00 |
| Precision | Standard |
| Swap sign of deviation | Off |
| Consider surface orientation | Off |
| Compensate for mesh problems | Off |
| Memory optimized | On |
| Deviation interval [mm] | n/a |
| Interval mode | n/a |
| Min. surface [mm²] | n/a |
| Show components | Off |
| Tolerancing | Disabled |

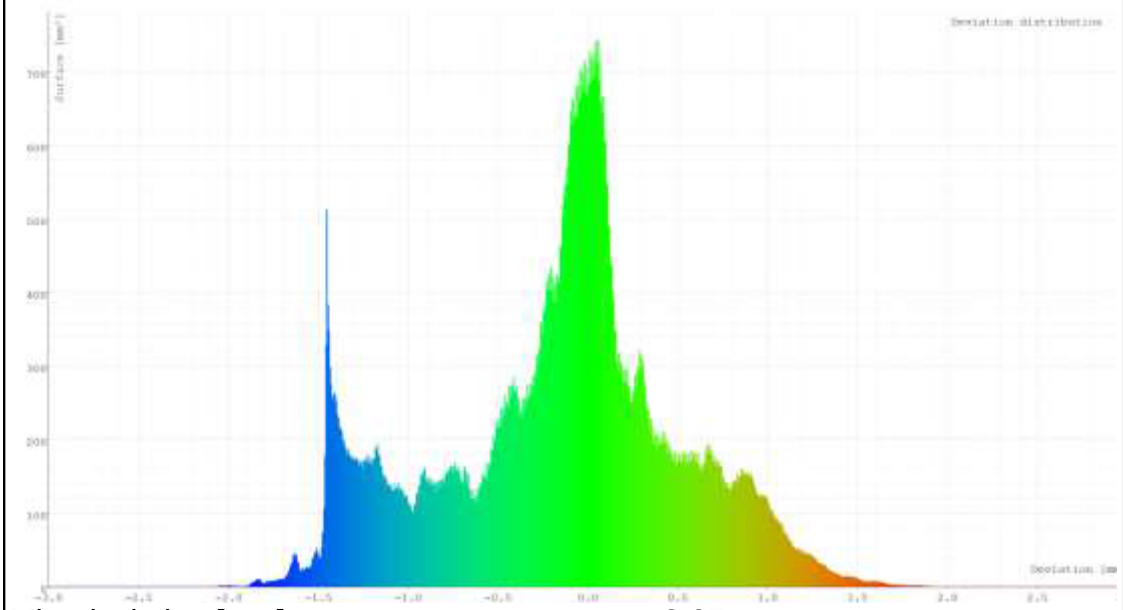

| | |
|---|---|
| Min. deviation [mm] | -2.65 |
| Max. deviation [mm] | 2.00 |

**Figure G. 21. Deviation histogram**

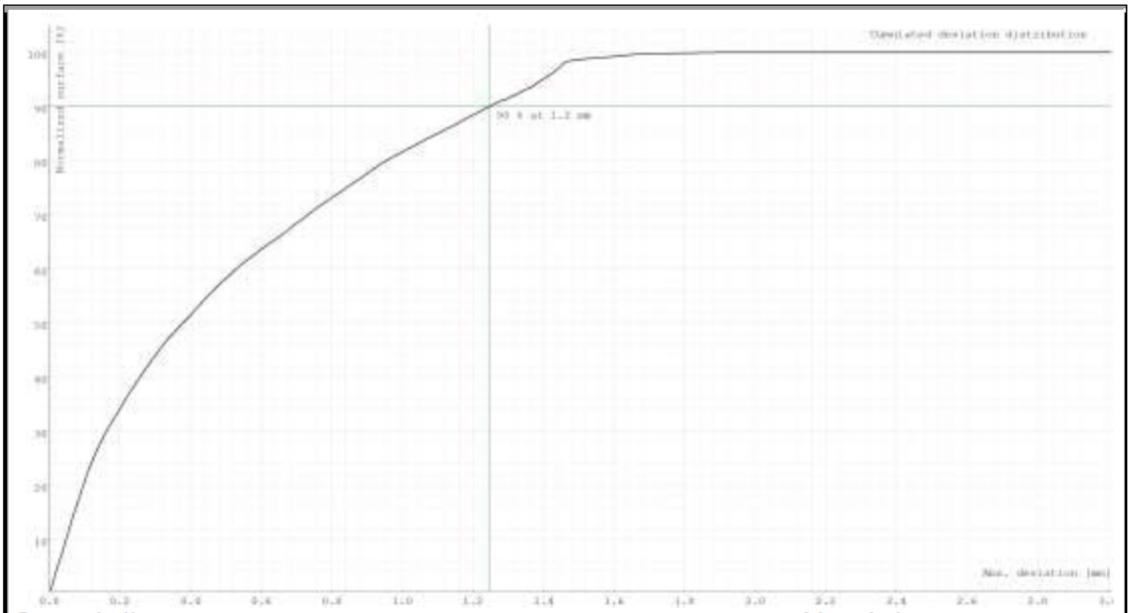

| Cumulation | Absolute |
|---|---|
| Cumulated absolute 90% [mm] | 1.25 |
| Cumulated absolute 95% [mm] | 1.40 |
| Cumulated absolute 98% [mm] | 1.46 |

**Figure G. 22. Cumulated deviation distribution**

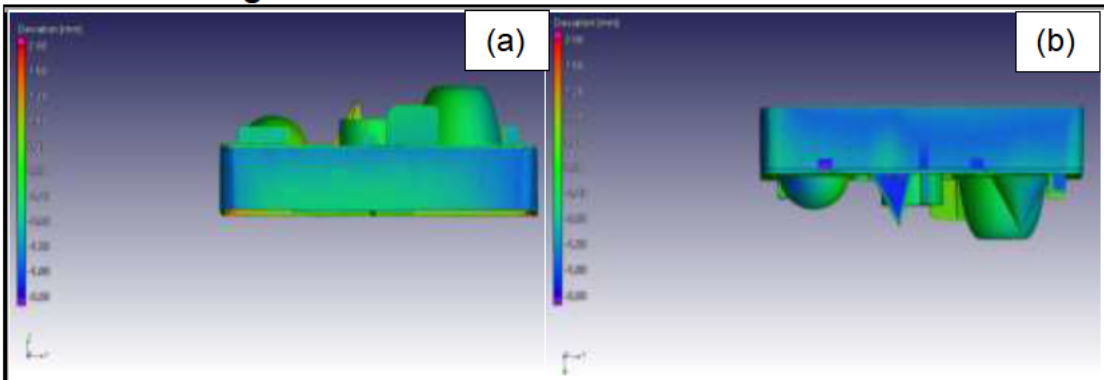


**Figure G. 23. 3D images: (a) top and (b) bottom**

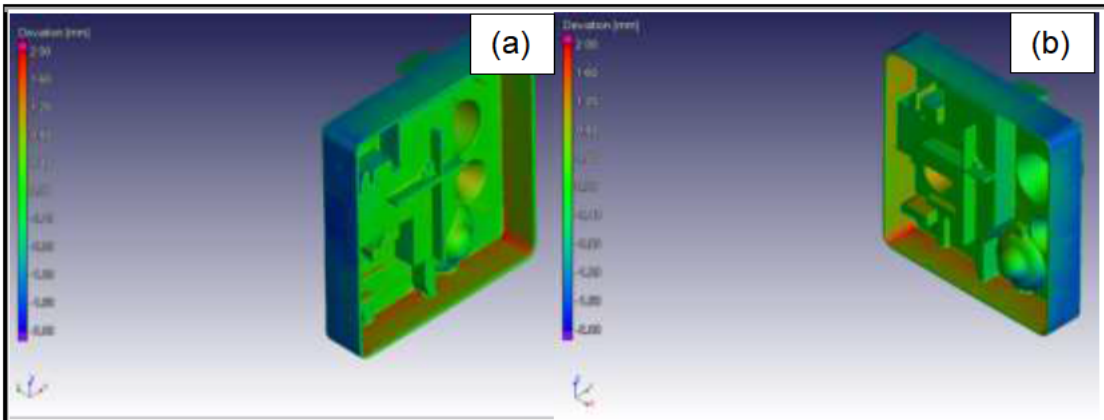


**Figure G. 24. 3D images: (a) top-left-front and (b) top-front-right**

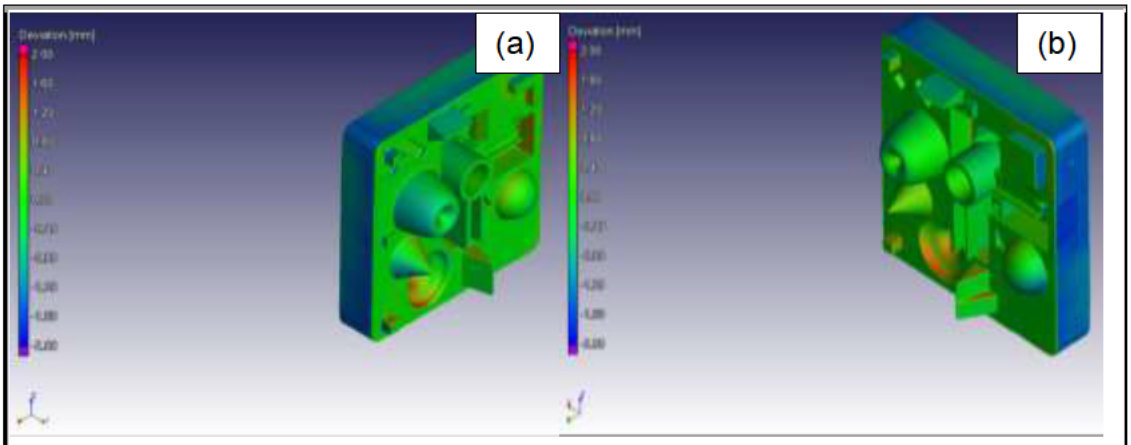


Figure G. 25. 3D images: (a) top-left-back and (b) top-back left

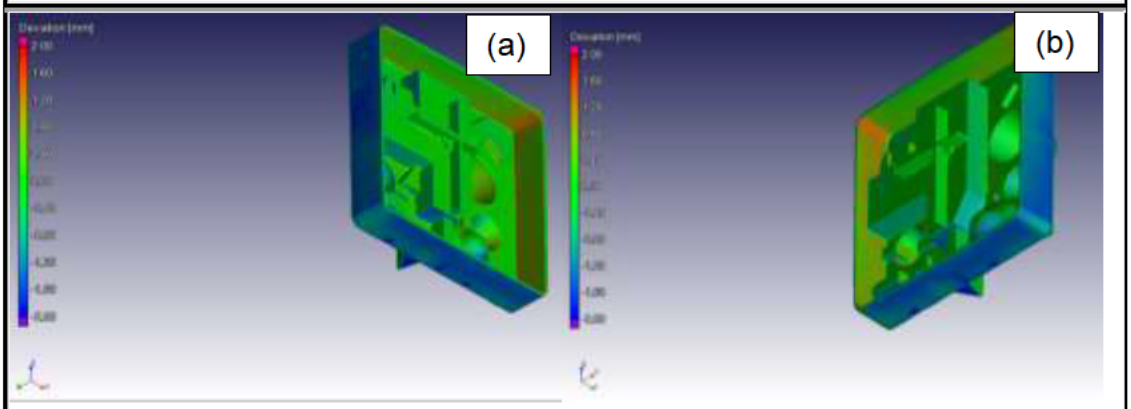


Figure G. 26. 3D images: (a) bottom-left-front and (b) bottom-front-right

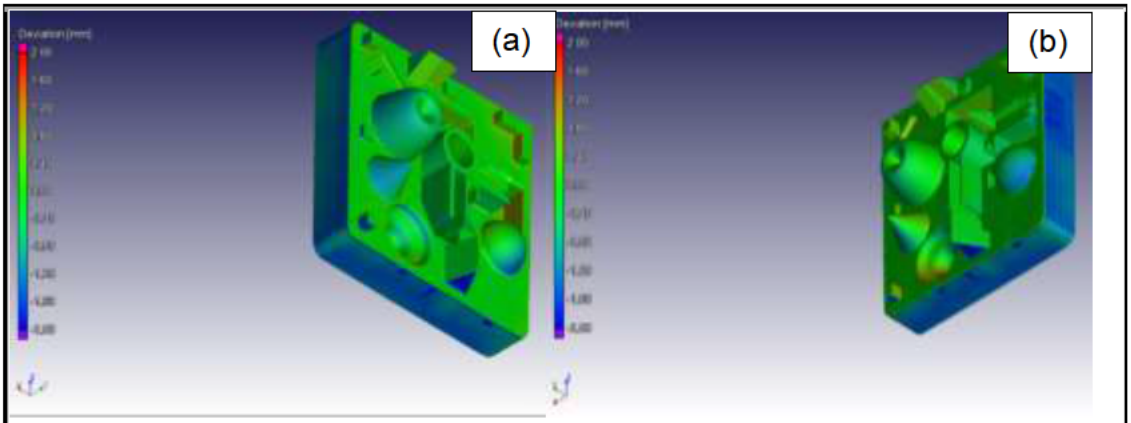


Figure G. 27. 3D images: (a) bottom-right-back and (b) bottom-back-left

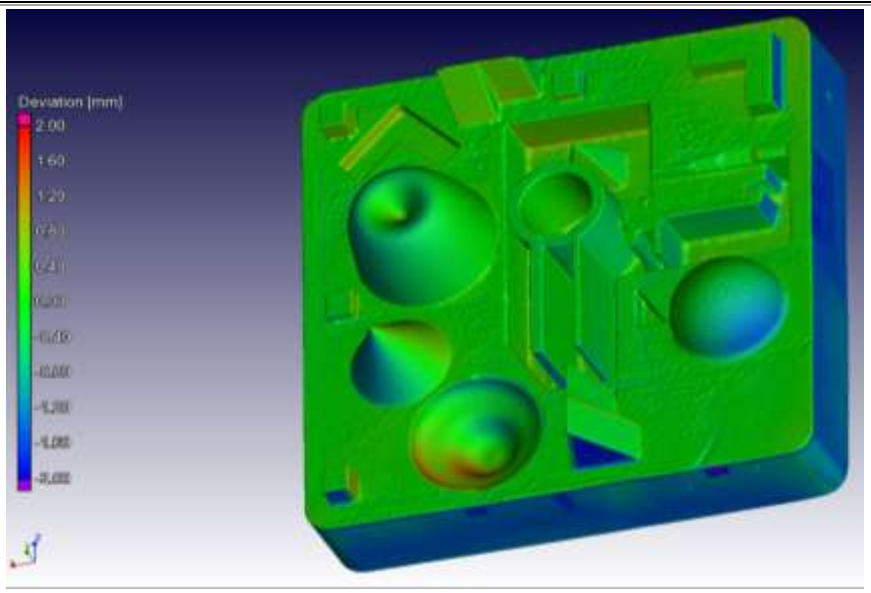


**Figure G. 28. 3D image: current camera settings**

## PC2

| **Settings for Analysis 1 (Nominal/actual comparison of PC2 [filtered])** | |
|---|---|
| Actual object | PC2 [filtered] |
| Nominal object | Mesh 1 |
| Max. distance [mm] | 3.00 |
| Precision | Standard |
| Swap sign of deviation | Off |
| Consider surface orientation | Off |
| Compensate for mesh problems | Off |
| Memory optimized | On |
| Deviation interval [mm] | n/a |
| Interval mode | n/a |
| Min. surface [mm²] | n/a |
| Show components only | Off |
| Tolerancing | Disabled |

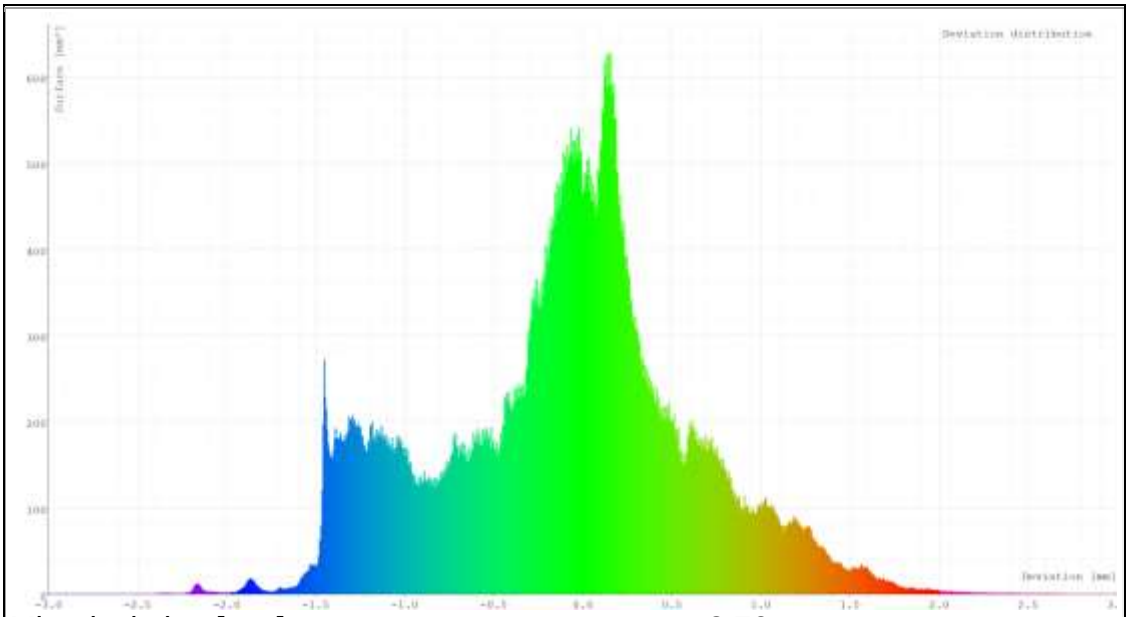

| | |
|---|---|
| Min. deviation [mm] | -2.70 |
| Max. deviation [mm] | 2.75 |

**Figure G. 29. Deviation histrogram**

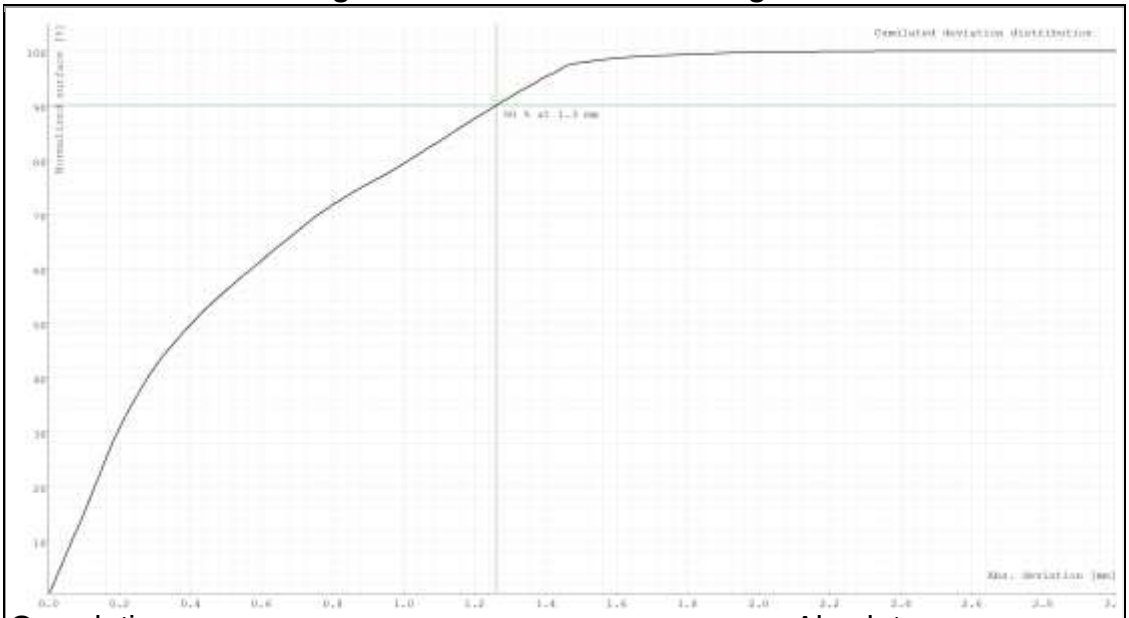

| | |
|---|---|
| Cumulation | Absolute |
| Cumulated absolute 90% [mm] | 1.26 |
| Cumulated absolute 95% [mm] | 1.39 |
| Cumulated absolute 98% [mm] | 1.52 |

**Figure G. 30. Cumulated deviation distribution**

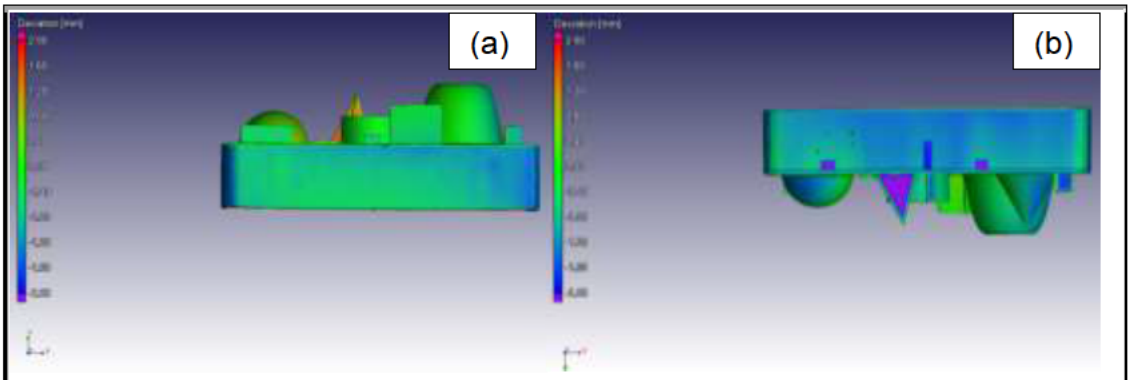


**Figure G. 31. 3D images: (a) top (a) and (b) bottom**

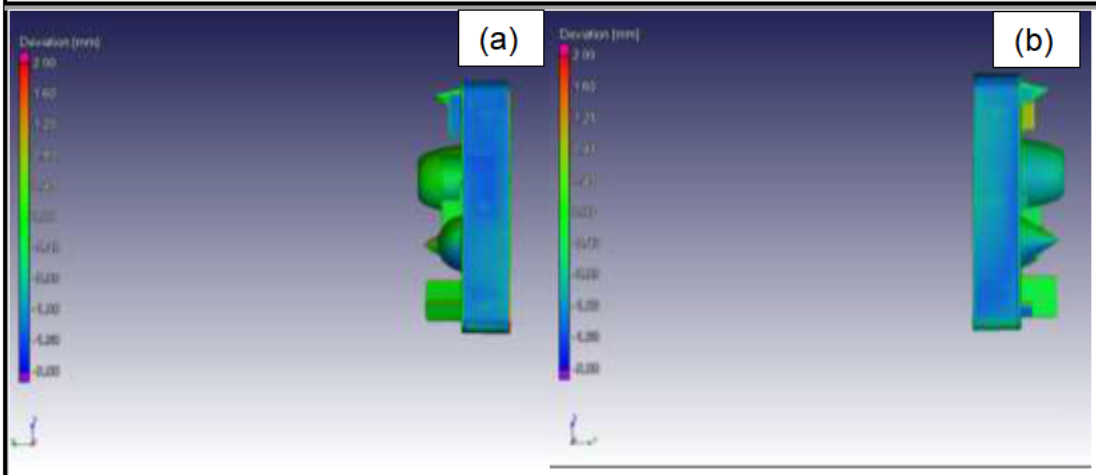


**Figure G. 32. 3D images: (a) left and (b) right**

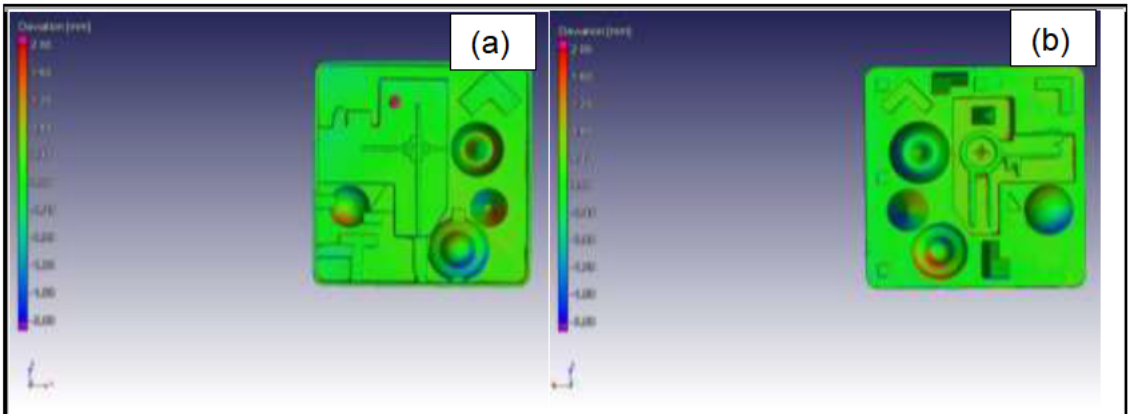


**Figure G. 33. 3D images: (a) front and (b) back**

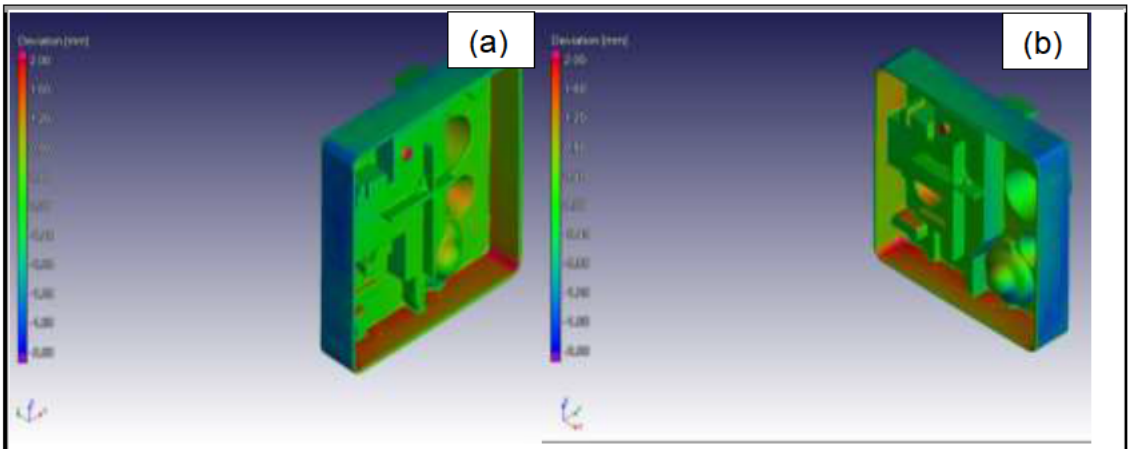


Figure G. 34. 3D images: (a) top-left-front and (b) top-front-right

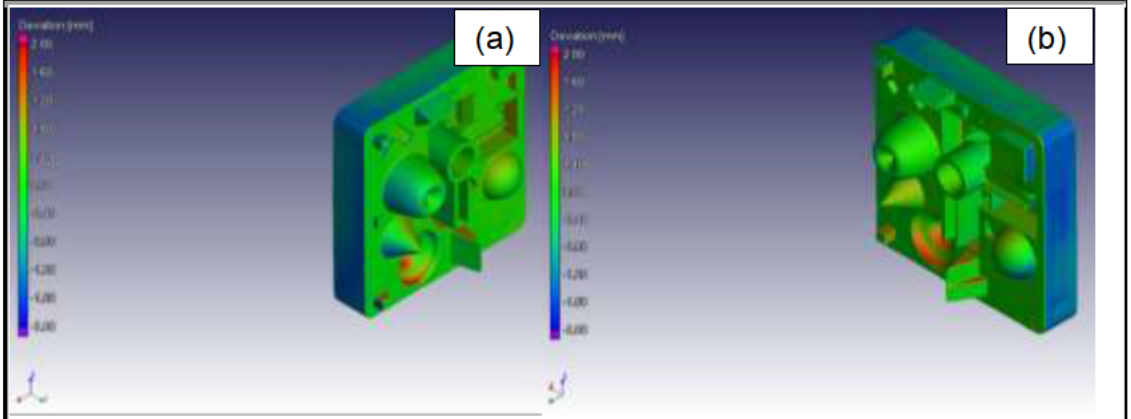


Figure G. 35. 3D images: (a) top-right-back and (b) top-back-left

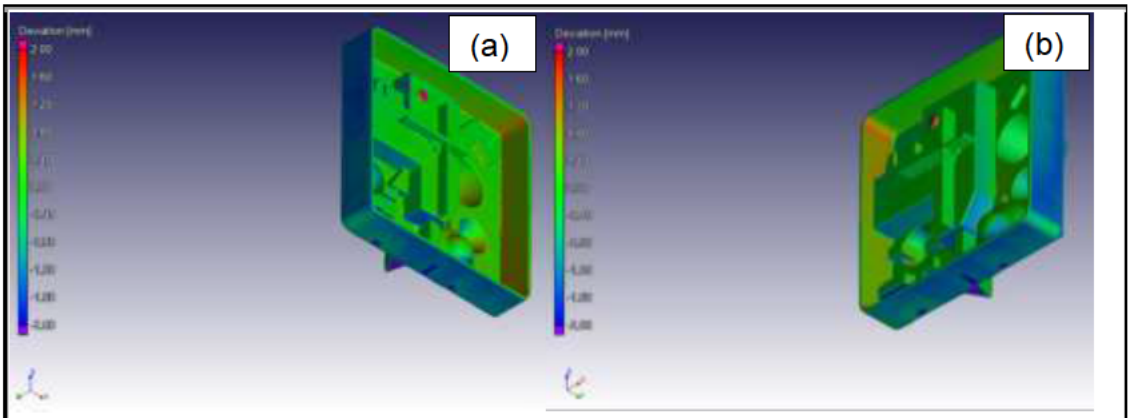


Figure G. 36. 3D images: (a) bottom-left-front and (b) bottom-front-right

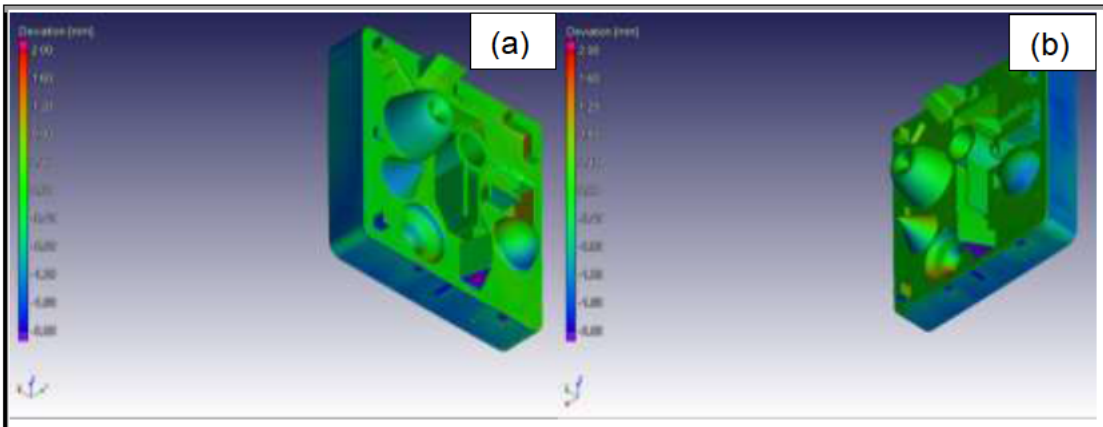


Figure G. 37. 3D images: (a) bottom-right-back and (b) bottom-back-left

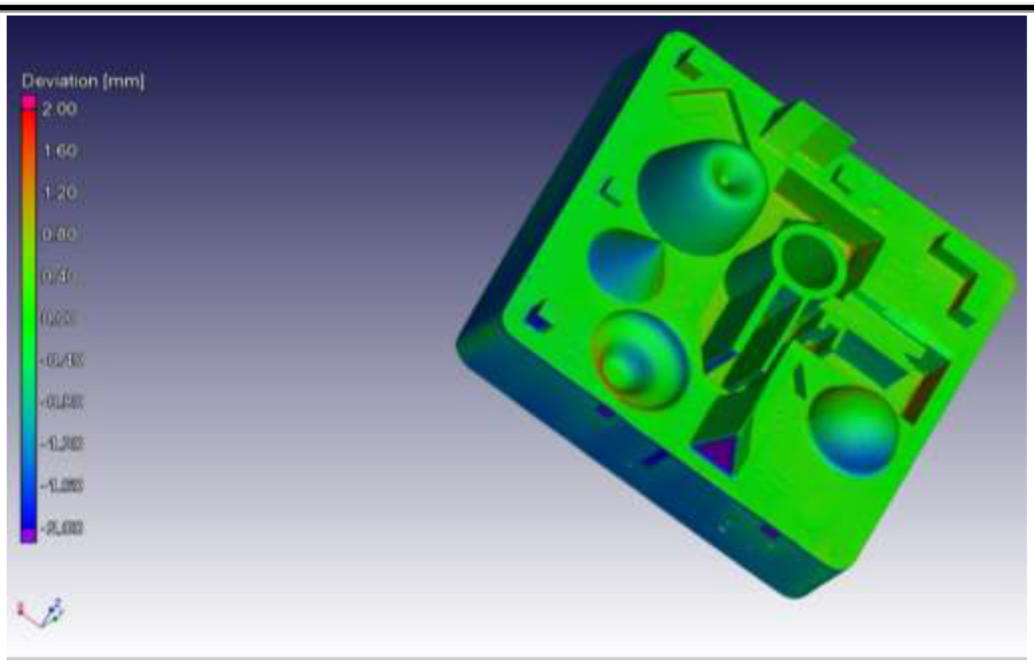


Figure G. 38. 3D images: Current camera settings